A Two-Ion Balance for High Precision Mass Spectrometry

by

Simon Rainville

Submitted to the Department of Physics
in partial fulfillment of the requirements for the degree of

Doctor of Philosophy

at the

MASSACHUSETTS INSTITUTE OF TECHNOLOGY

June 2003

Author .....
Department of Physics
May 16, 2003

Certified by .....
David E. Pritchard
Cecil and Ida Green Professor of Physics
Thesis Supervisor

Accepted by .....
Thomas J. Greytak
Professor of Physics, Associated Department Head for Education

A Two-Ion Balance

for High Precision Mass Spectrometry

by

Simon Rainville

Submitted to the Department of Physics
on May 16, 2003, in partial fulfillment of the
requirements for the degree of
Doctor of Philosophy

Abstract

This thesis describes the demonstration of a new technique that allows masses to be compared with fractional uncertainty at or below 1×10^{-11}, an order of magnitude improvement over our previous results. By confining two different ions in a Penning trap we can now *simultaneously* measure the ratio of their two cyclotron frequencies, making our mass comparisons insensitive to many sources of fluctuations (e.g. of the magnetic field).

To minimize the systematic error associated with the Coulomb interaction between the two ions, we keep them about 1 mm apart from each other, on a common magnetron orbit. We have developed novel techniques to measure and control all three normal modes of motion of each ion, including the two strongly coupled magnetron modes. With the help of a new computer control system we have characterized the electric field anharmonicities and magnetic field inhomogeneities to an unprecedented level of precision. This allows us to optimize the trap so that our measurement of the cyclotron frequency ratio is to first order insensitive to the field imperfections.

Using the ions $^{13}C_2H_2{}^+$ and $^{14}N_2{}^+$, we performed many tests of our understanding of the ions dynamics and of the various sources of errors in this technique. From these we conclude that there should be no systematic error in our measurements at the level of 5×10^{-12}. Thus we feel confident reporting a value for the mass ratio of these ions with an uncertainty of 10^{-11}.

In this thesis, we also report measurements of the two mass ratios $m[^{33}S^+]/m[^{32}SH^+]$ and $m[^{29}Si^+]/m[^{28}SiH^+]$ with a relative uncertainty of less than 10^{-11}, which makes them the best known mass ratios to date. These can be combined with precise measurements of high-energy gamma-rays to provide a direct test of the relation $E = mc^2$. This is a test of special relativity which does not rely on the assumption of a preferred reference frame. The uncertainty on the atomic mass of ^{29}Si is also reduced by about an order of magnitude.

Thesis Supervisor: David E. Pritchard
Title: Cecil and Ida Green Professor of Physics

Acknowledgments

Thanks to the many people who have surrounded me, my graduate career has been a fantastic life experience.

First, I am indebted to many staff members in the Physics department and the Research Laboratory of Electronics for their help with the many things outside the laboratory that had to be done. Their ever-present smiles created a welcoming environment in which I really enjoyed working. Tan-Quy Tran, Peggy Berkovitz, Pat Solakoff, Maxine Samuels, Maureen Howard, Lorraine Simmons, Gerry Power, Al McGurl, ... thank you all!

Carol Costa was always there with her words of encouragement and friendly reminders. She happily shared with me her extensive experience on many aspects of the life at MIT, and generously took on her shoulders all of the administrative load she possibly could. Thank you for everything Carol !

One way or another, everybody in the Atomic, Molecular and Optical Physics group has contributed to my happiness. Even though I did not interact regularly with Dan Kleppner and Wolfgang Ketterle, I always felt their support and interest in our work. I also have many good memories of nice summer evenings spent on the softball field playing for the "Balldrivers" with fellow atomic physicists. In studying for classes and qualifying exams, I developed great friendships with Stephen Moss, Tony Roberts and Shin Inouye, which extended far beyond the classroom (sailing and windsurfing on the Charles river, playing basketball, sharing great dinners, ...). Thank you all!

In the lab, I have had the pleasure to interact with many undergraduates (Roland, Baruch, Sidney, Josh, Miranda, and Nisha) and Claudiu Stan who spent his first year as a graduate student with us. It has also been a privilege to collaborate over the last year with Edmund Myers from FSU. I want to thank him especially for his amazing dedication to continue our work and his critical reading of this thesis.

I think James and I have realized the dreams of several previous members of the MIT ICR group. But without their dedication and excellent work, we would never have had the chance to work on such a wonderful apparatus. In particular, I want to mention Michael Bradley and Trey Porto with whom I had the pleasure to work during my early years at MIT. They taught me most of what I know about the ICR apparatus and the importance of perseverance. They also left behind an apparatus in top shape. Mike, Trey, you did not have the chance to harvest all the fruits of your work, but I want to share with you all our success. Thank you very much!

I have also been very happy to work with David Pritchard, my supervisor. His managing style, which fosters independence and critical thinking has fitted well with my own personality. I have learned very many things from Dave: a lot of physics obviously, but also the importance of looking at the data and thinking about what they mean. The impressive breadth of topics we discussed in group meetings (or on his sailboat) has definitely broadened my view of the world. I am also very thankful for the confidence he has shown in me

all along. Thank you Dave for everything.

The most positive aspect of my graduate career has been my interaction with James. I am extremely grateful to have had the chance to work during my entire graduate career with such a talented physicist and outstanding person. James is always committed to excellent work; he is the most creative thinker I have ever met, and an inexhaustible source of new ideas. I have always been impressed by his ability to tackle a problem and, after filling a pad of paper with math, give me a nice intuitive physical explanation of the solution. On the personal level, James is a very curious, open and respectful person. I have enjoyed every discussions we had, every basketball games we played, and every trip we took together. Debbie, his wife, has also been a great source of support during the last few years, and Catherine and I are looking forward to a life-long friendship with them. James, Debbie, thank you for being there.

I also want to use this occasion to acknowledge the people who made me who I am. My mother Lucille, my father Bertrand and my brother Luc gave me the curiosity and passion that made it possible for me to begin this task, and the patience and perseverance to complete it successfully. Despite the distance, I have always felt their support, their presence, and their love. I also thank my other family Rita, Eugène, Mélanie, Yves, and Marc-André for sharing their lives with me and adding more colors to the palette of my life. Thank you. I love you.

Finally, my beloved wife Catherine deserves by deepest gratitude. She was always by my side along this tortuous road, patiently giving me perspective in the difficult times and making the happy moments even happier. Her Faith inspires me confidence, her love shatters every boundaries. She makes me want to be a better person, and gives meaning to my life. Catherine, thank you for being my best friend and the love of my life.

This work was supported by the National Science Foundation (NSF), the Joint Services Electronics Program (JSEP) and a Precision Measurement Grant from the National Institute of Standards and Technology (NIST). I appreciate the support of two fellowships (master and doctorate) from the Fonds pour la formation de chercheur et l'aide à la recherche (FCAR).

To Catherine, Bertrand, Lucille and Luc
with all my love.

Contents

List of Figures

List of Tables

Chapter 1

Introduction

In the 1980's, the ability to confine single ions in a Penning trap was a revolution in mass spectrometry that allowed the first mass comparisons with relative accuracies below 10^{-9}. Over the past 20 years, the MIT ion trap experiment has established itself as the leader in the field of precision mass measurements. Its unique phase coherent approach to the comparison of single ion cyclotron frequencies has proven extremely powerful and versatile. The group has produced a table of the masses of 14 stable isotopes ranging from the masses of the proton and neutron to the mass of ^{133}Cs, all with relative accuracies near or below 1×10^{-10}. The approach of comparing molecular ions has opened the possibility of performing many redundant measurements, which have earned the confidence of the metrology community in the reported values. Besides generally improving our knowledge of a very fundamental property of matter (by one to three orders of magnitude), some of the measured masses lead to important applications in fundamental physics and metrology, including:

- a recalibration of the current γ-ray wavelength standard,
- an atomic definition of the kilogram,
- a new determination of the fine structure constant,
- several reference ions used in mass spectrometry of radioactive isotopes.

The topic of this thesis is the demonstration of a new technique that has improved the accuracy of our measurements by an order of magnitude. By simultaneously confining two different ions in our Penning Trap, we have been able to directly compare their cyclotron frequencies with a fractional accuracy of 1×10^{-11} or better.

Our demonstration of the two-ion technique is the culmination of the work of many people. The idea of simultaneously confining two different ions in our trap was explored shortly after the very first single ion measurement by our group. In 1989, Deborah Kuchnir, an undergraduate working with Eric Cornell, described in her B.Sc. thesis the first observation of the signals of two ions in the same trap [1]. However due to the lack of control of the ions'

trajectories, they could not perform a precision mass comparison. Because of the technical difficulties associated with the two-ion technique, the idea was put on hold by the next few graduate students while the single-ion technique was improved and used to build the "MIT mass table". In 1994, Michael Bradley and Fred Palmer (post-doc) tried to implement the two-ion technique again, but the apparatus developed a helium leak and they had to build a completely new apparatus. The transition from an rf to a dc SQUID happened at that time. I joined the MIT ICR Lab a few months before the new apparatus was first cooled down and a new post-doc, Trey Porto, joined the lab (Summer 1996).

1.1 My career at MIT

The first couple of years of my career at MIT were spent learning the ropes of the ICR experiment from Mike and Trey, while taking classes and qualifying exams. During this period, the apparatus was unfortunately cursed with feedback and noise pickup problems. It required about a year and half before single ions could be trapped again. I then learned how to measure mass ratios by actively participating in the measurement of the masses of the alkali ^{133}Cs, ^{87}Rb, ^{85}Rb, and ^{23}Na for a new determination of the fine structure constant α. In the Spring 1999, Mike had all the data he needed and handed the experiment to James Thompson and I. (James had joined the group as a graduate student a year after me). The first thing we decided to do was to increase the coupling between the coil of our detector and the dc SQUID. Unfortunately, the coil broke in the process, and we had to spend the summer making a new one. It was well worth the trouble however since a lot of our subsequent work really benefited from the increased coupling. During the Fall of 1999, it became apparent that progress would be very difficult with the existing computer control system and so I started developing a new one. A few months later, the new data acquisition system was used to demonstrate electronic refrigeration of our detector. Unfortunately, despite many months of efforts we never succeeded in using parametric amplification to directly show that the ion's temperature was reduced. We nevertheless used the improved signal-to-noise that electronic refrigeration provided us to precisely measure the relativistic shift of Ne^{++} and Ne^{+++}, thereby obtaining a 3 % calibration of the absolute amplitude of motion of the ion (a large improvement compared to the factor of two uncertainty we previously had).

By the end of the Summer 2000, we were ready to tackle the two-ion technique challenge. Initially, we had to automate the ion-making process and develop many new techniques to load a pair of different ions in the trap and roughly park them in a favorable orbit. In February 2001, we made the very first simultaneous comparison of the cyclotron frequencies of two ions ! The measured cyclotron frequency difference was completely insensitive to magnetic field fluctuations, as expected, and this immediately provided a gain in precision of at least an order of magnitude. However, the data exhibited sudden large jumps every

6-10 hours. It took us over a year to develop the many novel diagnostic tools and the quantitative understanding of the trap and the two-ion dynamics that allowed us to identify the source of these jumps. When we finally discovered that it was the polarization force on CO^+ that was responsible for the observed jumps, we immediately turned to a different pair ($^{13}C_2H_2{}^+/^{14}N_2{}^+$) that did not have this problem. During the Summer-Fall 2002, we then studied the systematic errors associated with the two-ion technique and demonstrated accuracy as well as precision. Finally, in December '02 and January '03, we used our newly developed techniques to measure two mass ratios with a precision below 10^{-11} for a direct test of the famous relationship $E = mc^2$.

This thesis is an attempt to present the progress we have made in the past four years. Since this work is an extension of the single-ion alternating measurement technique that was used for all the previous measurements from this group, the reader is urged to consult the seven excellent Ph.D. theses that have covered extensively the details of that technique: Robert Flanagan (1987), Robert Weisskoff (1989), Eric Cornell (1990), Kevin Boyce (1992), Vasant Natarajan (1993), Frank DiFilippo (1994), and Michael Bradley (2000). In Chapter 2, after a brief outline of our experimental apparatus and basic techniques, we will describe various experimental advances which are the foundations of what follows: the new computer data acquisition system, a demonstration of electronic refrigeration, a precise calibration of the amplitude of an ion's motion in the trap, and a precise characterization of our trapping fields. Chapter 3 will present an overview of the two-ion technique and outline many aspects of the technique that will be described in detail elsewhere. Then, the simultaneous measurement procedure is described in Chap. 4, and all the sources of errors associated with it are discussed in Chap. 5. Having demonstrated accuracy as well as precision with the two-ion technique, we present in Chap. 6 our measurements of two mass ratios involving sulfur and silicon isotopes that open the door to a new test of special relativity.

First, a word about notation. We need to stress a few conventions here to make things absolutely clear. We refer to the two trapped ions as 'ion 0' and 'ion 1'. Ion 0 is *always* the heavier one. For compactness, we use the subscript 2 for quantities that refer to the difference between ion 1 and ion 0. For example $\omega_{ct2} \equiv \omega_{ct1} - \omega_{ct0}$. We realize this convention is not as transparent as more standard alternatives such as $\Delta\omega_{ct}$ or ω_{ct10}, but the problem is that we will refer a lot to this difference frequency and we wanted a compact symbol for it. We will also need to refer to the shift of the difference frequency which can then simply be written as $\Delta\omega_{ct2}$ (as opposed to $\Delta\Delta\omega_{ct}$!). Finally, this convention keeps the theoretical discussion here parallel to the experimental reality of the computer control system and data analysis machinery. There, this notation arose naturally since boolean convert easily into 0's and 1's, and the next element of an array is 2.

Unless specified otherwise, all the quantities in the expressions given in this thesis should be expressed in SI units. Finally, all the voltages on trap electrodes (V_r, V_{gr}) are taken to be positive numbers.

Chapter 2

Experimental Techniques

To make the presentation self-contained, we begin with a brief tour of our apparatus, pointing out along the way the basic concepts of the physics of an ion in a Penning trap, and the key experimental techniques on which everything else will be built. We will then describe various experimental techniques (and results) that have played a crucial role in the two-ion technique (discussed in the rest of the thesis).

The vast majority of the equipment we used for the two-ion technique was in place when I joined the laboratory[†]. One of the things that is completely new however is the computer control system of the experiment and the data analysis software we developed over the past few years. In Section 2.2, we will describe how these have brought the ICR Lab into the modern age of automation and mass data production. Then follows a short section on electronic refrigeration. I wish this technique had played a more prominent role in the data we took, but it is one of the few projects that, despite all our efforts, did not work as well as we had hoped. (But we still think that the electronic refrigeration technique is one of the most promising solutions to the problem of cyclotron amplitude fluctuations discussed in Sect. 5.6.1.) However, we did use the improved signal-to-noise provided by electronic refrigeration for calibrating the amplitude of the orbits of our ions in the trap by measuring relativistic shifts of Ne^{++} and Ne^{+++} as described in Sect. 2.4. One of the key things that the new level of automation of the apparatus has allowed us to do is to map very carefully the frequencies of an ion in the trap as a function of its cyclotron and magnetron radii. Section 2.5 will describe these measurements, which have provided us with unprecedented knowledge of the imperfections in our trapping electric and magnetic fields, which in turn have played a crucial role in our ability to control systematic errors in the two-ion technique. This chapter will conclude with two short sections on our progress towards building a double-trap system and the observed dependence of our detector frequency on atmospheric pressure.

[†]In fact, that is why we started working on the two-ion technique as opposed to building the double-trap.

2.1 The MIT Penning Trap Mass Spectrometer

A schematic diagram of the MIT ICR[‡] apparatus is shown in Fig. 2-1. The experimental dewar shown in the figure, a couple of racks of electronics and frequency synthesizers, and a computer is basically all there is to this machine. The experiment is performed inside a superconducting magnet from Oxford Instruments with an 8.8 cm warm bore. The custom-made extension dewar serves the purpose of introducing liquid helium into this region and of cooling our SQUID detector to 4 K while keeping it away from the strong magnetic field region where it could not operate.

Our magnet generates a very uniform magnetic field $\vec{B} = B_0\,\hat{z}$, where $B_0 = 8.5\,\mathrm{T}$. Were an ion placed in that field it would revolve around the field lines at the "free-space" cyclotron frequency

$$\omega_\mathrm{c} = \frac{qB_0}{m}\,, \tag{2.1}$$

where q and m are the charge and mass of the ion. The basic principle behind all very precise mass spectrometers is to compare the cyclotron frequency of two ions in the same magnetic field; the ratio of the cyclotron frequencies is then the inverse ratio of the masses (if they have equal charges). To allow for the long observation time needed to precisely measure ω_c, the ions are held in a Penning trap which consists of the strong uniform magnetic field (to confine the ions radially) and a weak quadrupole electric field (to confine the ion along $\hat{z}$). The electric field is generated by a set of hyperbolic electrodes shown in Fig. 2-2. To trap positive ions, we apply a voltage $-V_\mathrm{r}$ on the ring electrode (with respect to the endcaps). The potential is then given by

$$\Phi(z,\rho) = V_\mathrm{r}\,\frac{z^2-\rho^2/2}{2d^2} \qquad \text{where} \qquad d^2 = \frac{z_{(0)}^2}{2} + \frac{\rho_{(0)}^2}{4}\,. \tag{2.2}$$

In our trap, $z_{(0)} = 0.600\,\mathrm{cm}$ and $\rho_{(0)} = 0.696\,\mathrm{cm}$ so that $d = 0.549\,\mathrm{cm}$ (see Fig. 2-2).

The potential above is what would be generated by perfectly hyperbolic electrodes extending to infinity. Because of the truncation of the electrodes and the presence of charge patches, this potential is only valid near the center of the trap. In order to minimize the lowest order non-quadrupole electric field component (C_4) (see Appendix A), another set of electrodes, called guard rings, are located on the hyperbolic asymptotes and are adjusted to approximately half the voltage on the ring electrode. The dc voltage applied to the guard ring V_gr therefore allows us to control the level of anharmonicity of the trap. At rf frequencies, the guard rings are split in order to provide dipole drives and quadrupole mode couplings for the radial modes (see Sect. 2.1.2). The electrode surfaces are coated with graphite (Aerodag) to minimize charge patches.

In an ideal Penning trap, the motion of the ion is described by three normal modes:

[‡]ICR stands for Ion Cyclotron Resonance. It is somewhat of a misnomer for our experiment since our measurement technique does not involve fitting any resonance.

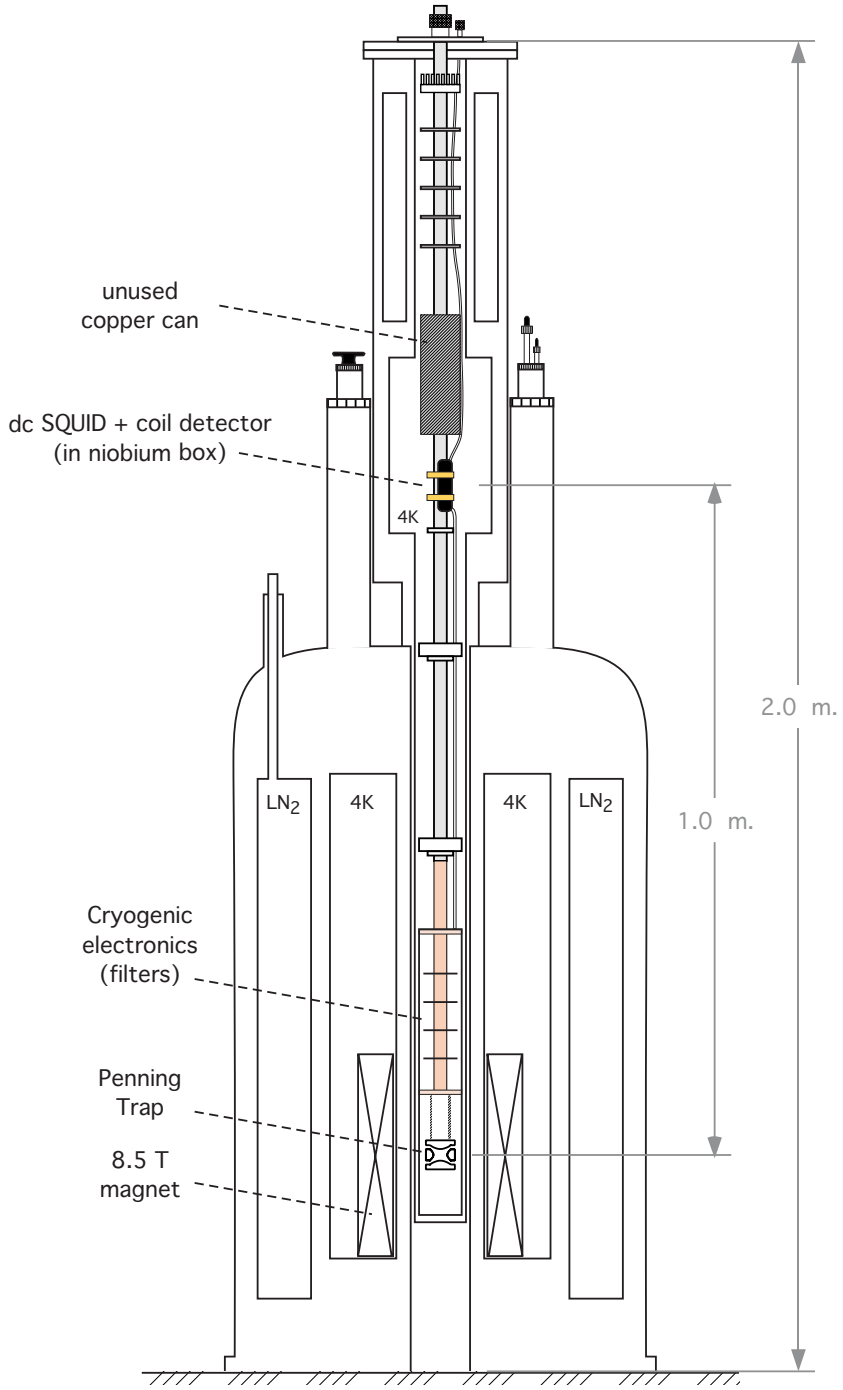

Figure 2-1: Schematic of the ion mass spectrometer at MIT. The superconducting magnet produces a stable 8.5 T magnetic field. The image current induced in the endcap by the ion's axial motion is detected using a dc SQUID. The trap, the magnet and the SQUID are at liquid helium temperature (4 K)

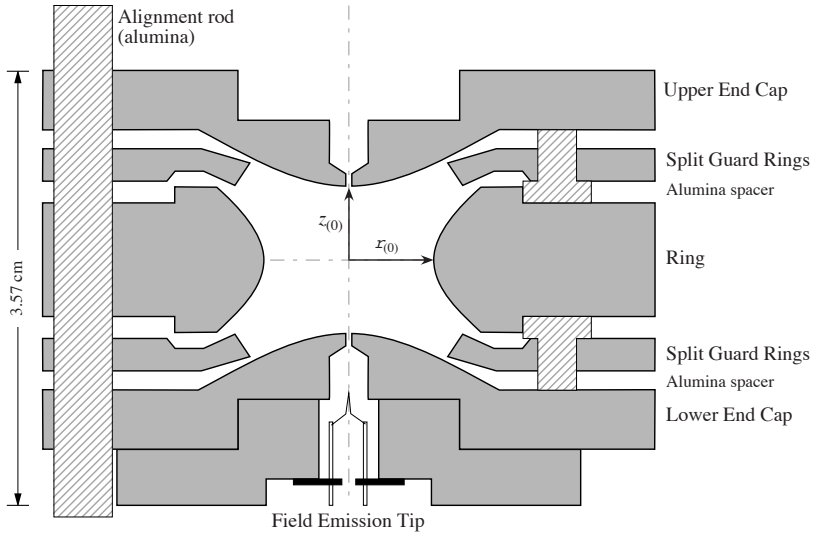

Figure 2-2: Cross section of our orthogonally compensated hyperbolic Penning Trap. The copper electrodes are hyperbolae of rotation and form the equipotentials of a weak quadrupole electric field. By adjusting the voltage applied to the guard ring electrodes located on the hyperbolic asymptotes we have control over the lowest order non-quadrupole electric field component. The electrode surfaces are covered with a thin layer of graphite (Aerodag) to minimize charge patches. The characteristic size of the trap $d = 0.549\,\mathrm{cm}$ (defined by Eq. 2.2).

an oscillation along $\hat{z}$ that we call the axial motion, and two radial modes called the cyclotron and magnetron motions. The frequencies of these modes are obtained by solving the equations of motion, assuming that all three modes behave like harmonic oscillators, i. e., guessing the forms $z = z_0\Re\{\mathrm{e}^{i\omega_z t}\}$ and $\vec{\rho} = \vec{\rho}_0\Re\{\mathrm{e}^{i\omega t}\}$:

$$\omega_\mathrm{z}^2 = \frac{qV_\mathrm{r}}{md^2} \tag{2.3}$$

$$\omega_\mathrm{ct} = \frac{1}{2}\left(\omega_\mathrm{c} + \sqrt{\omega_\mathrm{c}^2 - 2\omega_\mathrm{z}^2}\right) \simeq \omega_\mathrm{c} - \frac{\omega_\mathrm{z}^2}{2\omega_\mathrm{c}} \tag{2.4}$$

$$\omega_\mathrm{m} = \frac{1}{2}\left(\omega_\mathrm{c} - \sqrt{\omega_\mathrm{c}^2 - 2\omega_\mathrm{z}^2}\right) \simeq \frac{\omega_\mathrm{z}^2}{2\omega_\mathrm{c}}\,. \tag{2.5}$$

In our apparatus, $\omega_\mathrm{z}/\omega_\mathrm{c} \approx 1/22$ (for the mass range we studied) and the trap cyclotron frequency ω_ct is the free space cyclotron frequency slightly perturbed by the presence of the electric field. The magnetron mode is a slow drift of the ion's position around the trap center at the frequency for which the magnetic force cancels the electric force on the ion. Note that ω_m is to first order independent of mass, whereas ω_z and ω_ct scale like $1/\sqrt{m}$ and $1/m$ respectively. For $m/q = 28$, typical mode frequencies in our apparatus are $\omega_\mathrm{ct}/2\pi \simeq 4.7\,\mathrm{MHz}$, $\omega_\mathrm{z}/2\pi \simeq 212\,\mathrm{kHz}$, and $\omega_\mathrm{m}/2\pi \simeq 5\,\mathrm{kHz}$.

To obtain the mass ratio from the measured frequencies, we use the invariance theorem that can easily be verified from Eqs. 2.3, 2.4, and 2.5 (and has been demonstrated by Brown and Gabrielse to hold true even in the presence of ellipticity and misalignment of the magnetic and electric fields axes [2]):

$$\omega_c = \frac{qB_0}{m} = \sqrt{\omega_{ct}^2 + \omega_z^2 + \omega_m^2}\ . \tag{2.6}$$

We produce ions by ionizing neutral gas in our trap. From a room temperature gas-handling manifold we inject a small amount of neutral gas at the top of our apparatus, which then enters the trap through a small hole in the upper endcap. From a field emission tip at the bottom of the trap (shown in Fig. 2-2), we generate a very thin electron beam ($\sim 10\,\mu$m radius) which then ionizes atoms or molecules inside the trap. Since the electron beam is parallel and close to the trap axis, the ions are created with a small magnetron radius ($\leq 100\,\mu$m).

2.1.1 SQUID Detector

The only signal we detect from a trapped ion is the image current induced between the endcaps by its axial motion ($\leq 10^{-14}$ A). Our detector consists of a dc SQUID coupled to a hand-wound niobium superconducting resonant transformer (referred to as the coil) connected across the endcaps of the Penning trap [3]. The resonance frequency of our detector f_{coil} is fixed around 212 kHz and the $Q \sim 45\,000$, i. e., the detector's full width at half maximum is $\gamma_{coil}/2\pi \sim 4.7$ Hz. We generally adjust the ring voltage to make the axial frequency of the ion ω_z resonant (or nearly resonant) with the detector's frequency ω_{coil}. This detector is also the only source of damping of the ion's motion in our system. The real part of its impedance damps the ion's axial motion with a time constant of (energy damping time on-resonance)

$$\tau^\circ = \frac{m}{QL\omega_{coil}} \left(\frac{2z_{(0)}}{qC_1}\right)^2 \frac{1}{N_{ion}}\ , \tag{2.7}$$

where $C_1 = 0.8$ is a geometrical factor, $L \approx 9$ mH is the inductance of the hand-wound detector coil, and N_{ion} is the number of (identical) ions in the trap (that is how we know when we have more than one ion). At $m/q \approx 30$, $\tau^\circ \approx 1$ s and so the axial motion is brought to thermodynamic equilibrium with the detector at 4 K in a few seconds. When ω_z is detuned from resonance, the damping time is increased to

$$\tau = \tau^\circ(1 + (\delta^*)^2) \qquad \text{where} \qquad \delta^* \equiv \frac{\omega_z - \omega_{coil}}{\gamma_{coil}/2}\ , \tag{2.8}$$

and the imaginary part of the detector's impedance shifts the axial frequency of the ion by an amount

$$\Delta\omega_z = \frac{1}{2\tau^\circ}\,\frac{\delta^*}{1+(\delta^*)^2}\ . \tag{2.9}$$

Over a bandwidth of about 50 Hz, our detection noise is dominated by the 4 K Johnson noise present in the resonant transformer. That means that if the axial frequency of the ion is anywhere inside that window, the signal-to-noise ratio remains constant (since both the ion's signal and the noise are multiplied by the same Lorentzian profile). That large bandwidth has been very important in our work with two different ions simultaneously confined in the trap since it has allowed us to detect both ions directly even though they were 15-30 Hz off-resonance (when both ω_z's were placed symmetrically on each side of the detector's resonant frequency). The dc SQUID that Michael Bradley installed in the apparatus greatly contributed to this large bandwidth by lowering the flat technical noise floor, and so did the threefold increase of the coupling between the SQUID and the detector coil that James Thompson and I achieved in 1999.

2.1.2 Mode Coupling and π-Pulses

To be able to measure the cyclotron frequency using only our axial mode detector, we use a resonant rf quadrupole electric field which couples the cyclotron and axial modes [4]. This field is applied with the split guard ring electrodes. The coupling causes the two modes to cyclically and phase coherently exchange their classical actions (amplitude squared × frequency). In analogy to the Rabi problem, a π-pulse can be created by applying the coupling just long enough to cause the coupled modes to exactly exchange their actions. The same rf quadrupole field is also used to cool the cyclotron mode by coupling it continuously to the damped axial mode. By using a different rf frequency, the same technique can be used to measure and cool the magnetron mode [5, 4].

2.1.3 The PNP technique

The basic sequence we use to make a cyclotron frequency measurement is called the PNP (for Pulse aNd Phase) [6]. This phase sensitive measurement technique is unique to our experiment. A PNP measurement starts by cooling the trap cyclotron mode via coupling to the damped axial mode as described in the previous section. The trap cyclotron motion is then driven to a reproducible amplitude and phase at $t = 0$, and then allowed to accumulate phase for some time $T_{\rm evol}$, after which a π-pulse is applied. The phase of the axial signal immediately after the π-pulse is then measured with rms uncertainty of order 10 degrees. Because of the phase coherent nature of the coupling, this determines the cyclotron phase with the same uncertainty (up to a constant phase offset). The trap cyclotron frequency is obtained by measuring the accumulated phase versus evolution time $T_{\rm evol}$. Since we can typically measure the phase within 10 degrees, a cyclotron phase evolution time of about 1 minute leads to a determination of the cyclotron frequency with a precision of about 10^{-10}.

The details of the measurement sequence will be presented in Sect. 4.1.

The PNP method has the advantage of leaving the ion's motion completely unperturbed (undetected and undamped) during the cyclotron phase evolution [4]. It is also particularly suited for measuring mass doublets – pairs of species such as CD_4^+ and Ne^+ that have the same total atomic number. Good mass doublets typically have relative mass difference of less than 10^{-3}, making these comparisons insensitive to many systematic instrumental effects.

2.2 Automation

In this section I shall briefly describe the new computer data acquisition system that we have developed over the past 3-4 years to control the experiment. If the size of each section in my thesis were proportional to the amount of time I spent on each aspect of the experiment, this one would be at least 30 pages! Many months of my graduate student life have been spent wiring LabVIEW diagrams and debugging the new system, but all of it has paid off tremendously. All the work described in this thesis would simply have not been possible without it.

In 1999 it became apparent to us that the data acquisition computer system needed to be replaced. It had been last updated by Vasant Natarajan in the early 90s and was based on LabVIEW 2 running on a Macintosh IIci. The first issue was speed. For example, each time we wanted to look at the ion's axial signal, we had to wait over 30 s for the computer to FFT and graph an 8 s ringdown ! In anticipation of the two-ion work to come, we knew that we would eventually need the computer to process the ion's signal, and based on the result, quickly send signals back to the trap to influence the ion's motion. However, an even more critical problem of the old system was that it was not upgradable. All the time-critical aspects of the system were controlled by low level C code that would not work on a more modern computer (and neither would the data acquisition cards). Finally we foresaw the development of many new experimental techniques which would require new software development. Any minor modification to the LabVIEW code on that computer was excruciating. We needed speed and above all flexibility. We needed to start from scratch. I made that my priority and after about 6 months (in March 2000), the new system was in control of the experiment. It has certainly fulfilled the requirement for flexibility, as we never stopped expanding it.

In its current version, the system is running in LabVIEW 6.1 on a dual 800 MHz processor G4 Power Macintosh. On the outside, its most striking feature is a 22" Apple Cinema Display that has given us more room to fit the multitude of front panel controls and indicators (over 400) we need to adjust and look at. Figure 2-3 shows a snapshot of the front panel of the master "virtual instrument". On the inside, the most critical part of the system is a fast digital card (PCI-DIO-32HS from National Instruments) that has the ability to

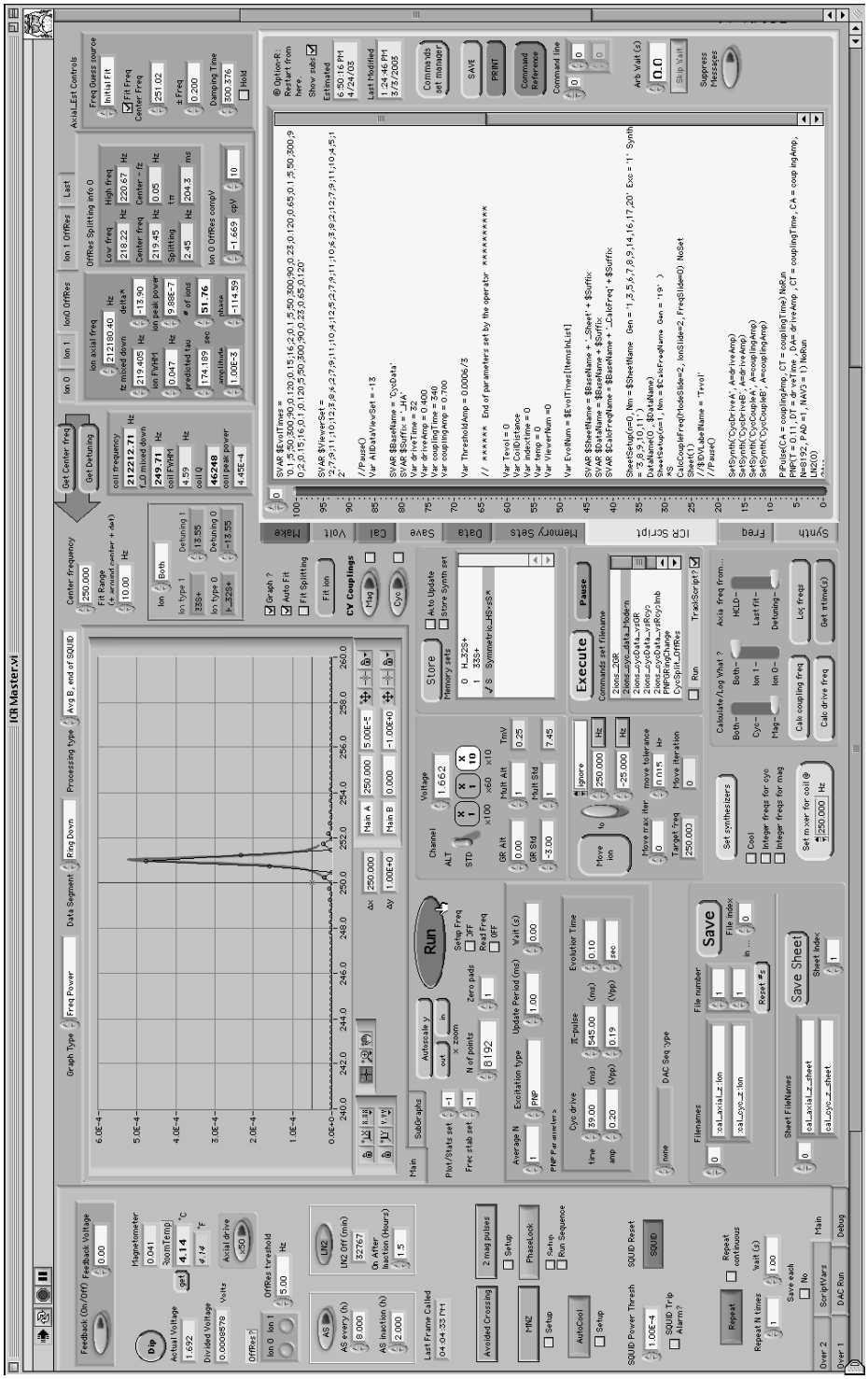

Figure 2-3: The front panel of the master virtual instrument of the new computer control system. The whole system has over 500 subvis and 400 controls and indicators

update 32 digital bits at every cycle of an external clock based on a pre-programmed time sequence. In other words, once we launch a sequence of pulses, the computer's operating system is not in charge of keeping time, which is good. Since we don't need to specify absolute times in the sequence to better than the ms level, we update the sequence with a 1 kHz clock (derived from the 10 MHz signal to which all our frequency synthesizers are locked). However, we need shot-to-shot reproducibility of about 1 µs) and that is what the fast digital card does for us. Our sequences can sometimes be very long however (15 min or more) which means that almost a million updates have to be written to memory before we start the sequence (even though the status of the bits stays the same for all these updates except about 10). But memory is cheap and we can be wasteful... (and that represents less than 4 MB).

A few new characteristics of the new system worth noting are:

- full automation of the ion making process;
- control of a small voltage added to the guard ring electrode and hence of the first order anharmonicity of the trap;
- online analysis that make the parameters (phase, frequency and amplitude) of the ion's signals available for plotting and logging as they come (fast feedback to catch something wrong);
- automatic logging of the frequencies of potentially several ions so that at the push of a button we can account for coil drifts or run a PNP off-resonance;
- a feedback system to lock the axial frequency to an external frequency reference (PhaseLock)
- ...

But the most radical addition to our system, which has realized our wildest dreams of flexibility, is the ICR Script Language. What we have done is built essentially a command line interface to ICR Master, visible on the right of Fig. 2-3. Almost anything that an operator can do by pushing buttons on the front panel can now be called by entering a text command in the "script". Many commands have parameters, (for example "AxialPulse(A=5)" excites the axial motion of the ion with a pulse of 5 Vpp), we have control statements (if-then-else, repeat) and variables. It's a mini programming language for running our experiment. A set of commands can be saved as a text file and recalled anytime (it can even be called from another script). When we have an idea for a new experiment, we can simply write the script for it and let the computer churn data out overnight! With this system, we have been able to take a lot more data, with a lot more reproducibility, than we could have ever imagined. And that has been crucial for building up confidence in our results.

Unfortunately, the advent of this new computer system did not mean that we could start a data set and take a week off while the best mass measurements in the world were happening. I think the level of automation of a system simply sets the level of complexity of the problems you can tackle with it. This new control system has allowed us to perform simultaneous measurements on two ions, which is a more complicated sequence of events than the alternating measurement technique used before. For the measurements presented in this thesis, a "fully-automated" data set could last for 5-20 hours, but we tried to usually have somebody in the lab to quickly catch potential problems.

In order to "digest" the vast amount of data that could be generated by our new system, we also had to automate a lot of the data analysis. We used Igor Pro, as we always had in the lab, but we developed a whole collection of "ICR functions" that has allowed us to efficiently perform complicated analysis of large amounts of data. Nevertheless, we were usually able to generate data faster than we could analyse them — a very new regime for our experiment. It was important though to have a preliminary feel for what the data looked like as a guide as to what to do next.

2.3 Electronic Refrigeration

As we will see in Sect. 5.6.1, the main source of random fluctuations in our data, after magnetic field noise, is the thermal variations in the cyclotron radius. Physically cooling our detector below 4 K is a sensible option, but would require some engineering. It would also be limited by the fact that the SQUID won't work below 1 K. The classical amplitude squeezing technique demonstrated by our group [7, 8] showed promise to address this problem, but in the Spring of 2000, we tried yet another approach: electronic refrigeration. The idea is to cool the effective temperature of the detector, i. e., the current/voltage fluctuations near the resonant frequency, and hence the ion's axial motion below the 4 K ambient temperature of the detector coil and trap environment. As we will see below, this technique has the added benefit of improving our signal-to-noise ratio.

The essence of electronic cooling [9] is to measure the thermal noise in our detection coil, phase shift the signal and then feed it back into the detection circuit. The reason why we could do this is that our dc SQUID has technical noise much lower than 4 K and can measure precisely the current in the coil in a time shorter than its thermalization time ($Q_0/\omega \sim$ 30 ms). This feedback also decreases the apparent quality factor Q of the coil. The technique was relatively simple to implement; the most difficult part was building the electronics for doing this without adding more noise into the system. In practice, we applied the feedback signal to the lower endcap electrode and relied on the trap capacitance to couple it back to the detector. Figure 2-4 shows the thermal noise of the coil at different gain settings of the feedback loop. By looking at the area under each peak, we find that the thermal energy in the coil is reduced below 4 K by the factor Q/Q_0, as expected from the detailed solution of

the circuit (assuming a parallel LRC coupling coil where the resistor $R = Q_0\omega_0 L$ has the usual Johnson noise current). Note that by choosing a different phase shift in the feedback loop, we can also make the Q higher (and increase the effective temperature).

Using electronic refrigeration, we could easily reduce the noise currents to an effective temperature as low as 0.5 K. With our dc SQUID, the ratio of the peak power to the noise floor level is about 200 and so the minimum temperature we could achieve is about 0.3 K. Since the only coupling between the ion and the rest of the world is the detector, the ion's motion should come into equilibrium with the colder detector, thereby reducing the problem of cyclotron radius fluctuations. Since this work was done before we developed the two-ion technique, we could not directly measure the effect of cyclotron amplitude fluctuations on the cyclotron frequency because of magnetic field fluctuations. We therefore tried to used parametric amplification to directly show that the ion's thermal motion was reduced, but despite several months of attempts, we could never observe any cooling of the ion's motion. (If anything, it looked like it was heated up a little.) Still, this technique provided us with an improved ability to estimate the ion's parameters (as described below) and we decided to move on.

Since then, the group of Gabrielse measuring the electron g-factor at Harvard has published a demonstration of electronic cooling of their electron's axial amplitude [10]. One thing that made it easier for them is that they could directly detect a reduction in the axial thermal amplitude as a narrowing of the cyclotron resonance. They also had a good idea to make their feedback affect only the ion (and not the detector): they applied feedback to the guard ring as well as to the endcap, but with a relative phase (and amplitude) adjusted so that there was no direct feedback through the trap capacitance. This leaves the Q of the detector unchanged but cools the ion's motion. Initially, we had tried to feedback only on the ion by feeding back on a sideband created by modulating the ring voltage, but did not have much success. The g-factor's group approach should be easy to implement in our experiment. Now that we can make simultaneous measurements of the cyclotron frequencies of two ions (Chap. 4), it should also be easy for us to directly detect the reduced amplitude fluctuations as a reduction in cyclotron frequency noise (see Sect. 5.6.1).

Another effect of the feedback during electronic refrigeration is to reduce the transformer voltage across the trap which is responsible for damping the ion's axial motion. This reduces the bandwidth of our signal, increasing our signal-to-noise ratio (the Johnson noise is a constant current/$\sqrt{\text{Hz}}$), and translates directly into a better ability to estimate the parameters of the axial oscillation of the ion. Using feedback, we were therefore able to measure the phase of the cyclotron motion of a single ion in the trap with an uncertainty as low as 5 degrees – more than a factor of 2 improvement. Our ability to determine the amplitude of the ion signal was also improved, again by more than a factor of 2, and we could measure the frequency of the axial motion with 4 times better precision. The better phase noise allows us to obtain the same precision on a cyclotron measurement in a shorter

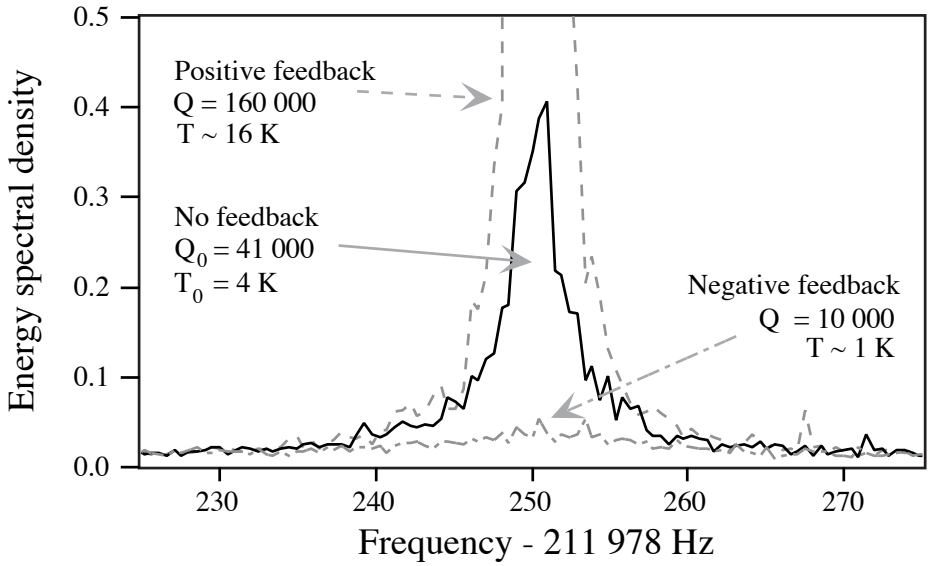

Figure 2-4: Thermal profile of the detector coil as a function of the quality factor Q adjusted with the gain of the feedback. The thermal energy in the coil (area under the peak) is proportional to Q/Q_0, where Q_0 is the Q of the detector coil without feedback. This shows that the negative feedback does indeed reduce the thermal fluctuations in the coil.

time. We can also use the improved signal-to-noise to reduce the cyclotron amplitude we use, which in turn reduces the frequency shifts due to relativity and field imperfections. Finally, this technique gives us the ability to arbitrarily select the damping time of the ion by changing the gain of the feedback. This opens the door for us to very high precision at small mass-to-charge ratio, (e.g. ^{6,7}Li, ^{3}He, ^{3}H) where we used to suffer from excessively short ion damping times.

Note that, to keep our system simpler, we did not use electronic refrigeration in all the two-ion measurements reported in this thesis, but we see no reason why it could not be done.

2.4 Amplitude Calibration

Knowing the absolute amplitude of the ion's motion in the trap (in μm) is an essential part of estimating the perturbations of its normal mode frequencies due to imperfections in the trapping fields and relativity. Until the Summer 2000, there was a factor of two uncertainty in our calibration which came from the disagreement between various methods for determining it (see Sect. 2.3). If we wanted to improve the precision of our measurements, we needed to resolve this problem and obtain a precise calibration of our ion's amplitudes.

The improvement in signal-to-noise using electronic refrigeration that we described in the previous section offered exactly what we needed to address this question. One very simple way to calibrate the cyclotron radius of an ion in the trap is to measure the relativistic shift

of its cyclotron frequency. By letting $m \to \gamma m$ in the expression for the cyclotron frequency (Eq. (2.1)) and expanding γ to lowest order in v/c, we obtain

$$\frac{\Delta\omega_c}{\omega_c} = -\frac{\omega_c^2}{2c^2}\,\rho_c^2\,, \tag{2.10}$$

where ρ_c is the cyclotron radius and c is the speed of light. Since $\omega_c \propto 1/m$, this shift is largest for light ions. Unfortunately, the damping time of the ion decreases with m (see Eq. (2.7)), and so does our signal-to-noise. But by using electronic feedback to reduce the Q of the detector as shown in Sect. 2.3, we could keep the damping time fixed, thereby allowing a precise measurement of ω_c at small mass.

We define the cyclotron amplitude calibration $\rho_c^{\rm cal}$ by expressing the cyclotron radius of an ion after being driven for a time δt as

$$\rho_c(\delta t) \equiv \rho_c^{\rm cal}\, A_d\, \delta t\,, \tag{2.11}$$

where A_d is the nominal voltage on the frequency synthesizer used to generate the cyclotron drive (expressed in volts peak-peak or Vpp). In July 2002, we took two nights of data measuring the cyclotron frequency of a single Ne^{++} ion ($m/q = 10$) for various cyclotron amplitudes (between 50 and 250 μm). We then repeated the same measurement with Ne^{+++} ($m/q = 6.7$). In order to extract the calibration from these measurements, we had to account for the fact that B_2 also shifts ω_c quadratically with ρ_c (see Sect. A.2), but it was a small correction (4 and 2 % respectively for Ne^{++} and Ne^{+++}). The effect of C_4 was 10 times smaller than that of B_2. Using for the first time the automation capabilities of the new computer control system (Sect. 2.2), we measured B_2 by looking at the shift of the axial frequency as a function of cyclotron radius. The uncertainties in our measurements of B_2 were 18 % and 9 % using Ne^{++} and Ne^{+++} respectively. The two independent cyclotron calibrations we obtained are $\rho_c^{\rm cal} = 4.248\,(68)$ μm/(Vpp ms) (1.6 %) using Ne^{++} and $\rho_c^{\rm cal} = 6.356\,(116)$ μm/(Vpp ms) (1.8 %) for Ne^{+++}. Even though these seem discrepant, they are not since $\rho_c^{\rm cal}$ depends on the cyclotron frequency. Indeed, because the transfer function $T(\omega_c)$ relating the voltage appearing on the trap electrode to A_d is not flat, $\rho_c^{\rm cal}$ has some dependence on ω_c. To probe the transfer function $T(\omega_c)$, we can compare the Rabi frequencies Ω associated with the axial-cyclotron coupling for different ions. As shown in [4], if an electric field of the form $\epsilon_p(x\hat{z} + z\hat{x})\sin(\omega_\pi t)$ is applied near the center of the trap, the axial splitting is given by

$$\Omega = \frac{e\epsilon_p}{2m\sqrt{\omega_z\omega_{ct}}}\,. \tag{2.12}$$

From an "Avoided Crossing" (described in all ICR theses and in [4]), we obtain a value of Ω (with uncertainty less than 0.5 %) from which we can deduce ϵ_p. The relative transfer function at two different frequencies is then given by ratio of the measured ϵ_p at these two

Table 2.1: Measured parameters for the Ne amplitude calibrations

	Ne^{++}	Ne^{+++}
f_{ct}	13101 769.1 Hz	19 654 625.9 Hz
f_z	212 234.0 Hz	212238.2 Hz
f_π	12 889 535.1 Hz	19 442 387.7 Hz
$\frac{\epsilon_p}{drive}$ (at f_π)	25.26 (14) V/m^2 per Vpp (0.5 %)	39.51 (11) V/m^2 per Vpp (0.3 %)
$\frac{\epsilon_p}{drive}$ (at f_{ct})	25.66 (62) V/m^2 per Vpp (2.4 %)	39.51 (61) V/m^2 per Vpp (1.5 %)
$\frac{B_2}{B_0}(\rho_c^{cal})^2$	$0.93(17) \times 10^{-13}$ per (Vpp ms)^2 (18 %)	$2.78(25) \times 10^{-13}$ per (Vpp ms)^2 (9 %)
ρ_c^{cal}	4.248 (68) μm/(Vpp ms) (1.6 %)	6.356 (116) μm/(Vpp ms) (1.8 %)
$\rho_c^{cal}(Ne^{++})$		4.127 (132) μm/(Vpp ms) (3.2 %)

frequencies. Using this procedure, we found the ratio of the transfer function for our two calibrations to be $T(Ne^{+++})/T(Ne^{++}) = 1.540\,(44)$ where the error (2.8 %) mainly comes from the small correction we had to make because $\omega_c \neq \omega_\pi$. Rescaling the $\rho_c^{cal}(Ne^{+++})$ to the frequency of Ne^{++}, we find $\rho_c^{cal} = 4.127\,(132)$ (3.2 %) which differs from $\rho_c^{cal}(Ne^{++}) = 4.248\,(68)\,\mu m/(Vpp\ ms)$ by only -2.9 %. Because we have more information about the transfer function around Ne^{++}, we chose to use rccal(Ne^{++}) as the final value and consider that we confirmed it at the 3 % level. Table 2.1 summarizes the numbers included in the calibration. The final result is then

$$\rho_c^{cal} = 4.25\,(13)\,\mu m/(Vpp\ ms) \quad (3\,\%) \tag{2.13}$$

$$\text{with} \quad \frac{\epsilon_p}{drive} = 25.66\,(62)\,\frac{V}{m^2\,V_{pp}} \ \ (2.4\,\%) \quad \text{at} \quad f_{ct} = 13\,101\,769.1\,Hz\,.$$

2.4.1 Other amplitude calibrations

We now address the important question: How does this new calibration compare with our previous routes for determining ρ_c^{cal}?

Shimming B_2

Experimentally, we can change B_2 by varying the current in one of the shim coil included in our Oxford magnet. Just before and shortly after our mass measurements of the alkali in 1998-99, we minimized B_2 using a C^+ ion (see details in [11]). In the process, we obtained a measured dependence of the axial frequency on the current in the Z2 shim coil (-4.62 Hz/(Vpp^2 A) that we can compare with the quoted strength of the shim coil from Oxford Instrument (0.153 G/cm^2) to obtain $\rho_c^{cal} = 2.31(7)\mu m/(Vpp\ ms)$ for C^+, i. e., at f_{ct}= 10.914 MHz. If we use the measured transfer function ratio (0.82) to scale this to Ne^{++}, we

find the following value, which is 55 % smaller than the calibration reported here.

$$\rho_{\rm c}^{\rm cal}({\rm Ne}^{++}) = 1.89\,\mu{\rm m}/({\rm Vpp\ ms}) \qquad (-55\,\%) \tag{2.14}$$

Relativistic shift using C^+

On 2/17/99, we performed essentially the same experiment as described here (only one night) and measured a relative shift in the cyclotron frequency of 7.11×10^{-13} 1/(Vpp ms)^2. Combined with the B_2 measurement of 2/16/99, this gives $\rho_{\rm c}^{\rm cal} = 5.7\mu$m/(Vpp ms) for C^+, i. e., at $f_{\rm ct}$= 10.914 MHz. If we use the measured transfer function ratio (0.82) to scale this to Ne++, we find the following value, which agrees to 10 % with the calibration reported here.

$$\rho_{\rm c}^{\rm cal}({\rm Ne}^{++}) = 4.67\,\mu{\rm m}/({\rm Vpp\ ms}) \qquad (+10\,\%) \tag{2.15}$$

Numerical calculations of the trap electrostatics

Trey Porto, a previous post-doc in our group has performed impressive semi-analytical calculations of the trap electrostatics (and image charge shift [12]). One can express the cyclotron radius of an ion after being driven for a time δt in terms of the geometric coefficients that he has calculated as follows:

$$\frac{\rho_{\rm c}(\delta t)}{d} = \pi \left(\frac{C_{\rm d}^{11}}{3C_{\rm d}^{21}}\right)\left(\frac{\delta t}{t_\pi}\right)\left(\frac{V_{\rm cyc}}{V_\pi}\right)\sqrt{\frac{\omega_{\rm z}}{\omega_{\rm ct}}}\,, \tag{2.16}$$

where V_x stands for a voltage *at the electrode* and $t_\pi = 1/(2\Omega)$ is the π-pulse time. Using the calculated values $C_{\rm d}^{21} = 0.0070$ and $C_{\rm d}^{11} = 0.0100$, the measured parameters for Ne^{++} ($\Omega = 0.955$ Hz ($t_\pi = 524$ ms) for $V_\pi = 0.5$ Vpp) and $d = 0.549$ cm, $f_{\rm z} = 212237.9$ Hz, and $f_{\rm ct} = 13101768.6$ Hz, we find the following value, which agrees to 6.5 % with the calibration reported here.

$$\rho_{\rm c}^{\rm cal}({\rm Ne}^{++}) = 3.97\,\mu{\rm m}/({\rm Vpp\ ms}) \qquad (-6.5\,\%) \tag{2.17}$$

Estimate of the detector coil temperature

We can use the amplitude calibration reported here to estimate what the temperature of our detector coil is. By comparing the ratio of the power in an ion signal at a known amplitude to the power in the thermal noise of the coil we obtained 3.8 K. This is further confirmation that our calibration is correct.

2.4.2 Conclusion

We are confident that we now know the absolute amplitude of the motion of an ion in the trap to 3 %, a tremendous improvement compared to the previous factor of 2 uncertainty. Our measurements of the relativistic shift of Ne^{++} and Ne^{+++} rely on a very simple principle and are practically insensitive to B_2 and C_4. The fact that both calibrations, done independently at two different m/q, agree to 3 % is a strong check that our method is correct. Finally, the calibration we obtained is in agreement with almost all previous measurements of ρ_c^{cal} [11] and also with the value extracted from numerical calculations of the trap electrostatics. Only the value derived from the B_2 shimming procedure disagrees by a factor of 2, but we now feel that all the evidences point to a flaw in that value. It is conceivable that the shim coil strength quoted by Oxford instrument is off, or modified by the presence of our apparatus in the center of the magnet.

Once we know ρ_c^{cal}, we can apply a cyclotron drive pulse to an ion in the trap and know what its cyclotron radius is in μm. To calibrate the axial and magnetron modes amplitudes, we rely on the fact that after a π-pulse

$$z = \begin{cases} \sqrt{\frac{\omega_{ct}}{\omega_z}}\,\rho_c & \text{after a cyclotron } \pi\text{-pulse,} \\ \sqrt{\frac{\omega_{ct}}{\omega_z}}\,\rho_m & \text{after a magnetron } \pi\text{-pulse,} \end{cases} \tag{2.18}$$

as shown in [4] (the π-pulse conserves classical action). By comparing the measured amplitude of the axial signal after an axial excitation pulse and after a cyclotron π-pulse we obtain the axial calibration z^{cal}. To find the magnetron calibration ρ_m^{cal} we simply need to find the magnetron drive (nominal pulse amplitude and duration) that produces the same axial amplitude after a magnetron π-pulse than a given cyclotron drive after a cyclotron π-pulse.

2.5 Characterizing the Trapping Fields

For very high precision cyclotron frequency measurements in a Penning trap, it is important that one knows as much as possible about the electric and magnetic fields confining the ions. Anharmonicities and inhomogeneities lead to frequency shifts that need to be compensated or corrected for if one wants to reach high accuracy. For the two-ion technique that will be described in the next chapters, the problem is even more serious since we are no longer measuring the mode frequencies at the center of the trap, but in a large magnetron radius of $300 - 600\,\mu m$. We therefore had to spend a significant amount of time and energy precisely characterizing our trapping fields. The basic idea is to precisely map the frequency of various modes as a function of its radial position. We also use the fact that we can change C_4 by adjusting the voltage on the guard ring electrode V_{gr}. The fact that different mode frequencies are affected differently by different mode amplitudes allow us to single out the

independent contributions from various coefficients in the expansion of our fields.

The idea of measuring f versus position is not new and had been attempted at some level by previous members of the group, but it was very painful to realize experimentally. Two key technical developments opened the door to unprecedented quantitative knowledge of the anharmonicities and inhomogeneities in our trap. First, James Thompson built a nice piece of electronics that allows us to add a computer-controlled voltage to the guard ring electrode (without adding extra noise), exactly as we have always been able to do with the ring electrode. Then the new computer system described in Sect. 2.2 allowed us to automate the measurement process. We can now start a 12 hour data set in the evening and when we come back in the morning, the computer has performed about 2100 measurements of, say, the axial frequency as a function of the magnetron radius and the guard ring voltage. Moreover, we can sit down at the data analysis computer and in less than 15 minutes have the result of the analysis. That is a completely different world than where this experiment was only a few years ago. The amplitude calibration described in Sect. 2.4 is also very useful to interpret the results.

We performed three types of experiments to measure our field imperfections. We list them below, along with the trap parameters (as defined in Appendix A) that we can extract from each:

- f_z vs ρ_m $\Rightarrow D_4$, $\widetilde{V}_{gr}^{\circ}$, and C_6,
- f_z vs ρ_c $\Rightarrow D_4$, B_2, and B_4,
- f_m vs ρ_m $\Rightarrow D_4$, $\widetilde{V}_{gr}^{\circ}$, and C_6.

To interpret the "f_z vs ρ_m" data sets, we plot the measured frequency shift versus ρ_m for each value of $\widetilde{V}_{gr}$ separately as shown in Fig. 2-5 ($\widetilde{V}_{gr}$ is defined by Eq. (5.19)). To each curve, we fit a polynomial of the form $\Delta f_z = a_4\rho_m^2 + a_6\rho_m^4$. We use Eq. (A.12) (in Appendix A) to relate a_4 and a_6 to the field expansion coefficients C_4 and C_6. The coefficient a_4 depends linearly on $\widetilde{V}_{gr}$; the slope is related to D_4 and the value of $\widetilde{V}_{gr}$ for which $a_4 = 0$ gives us $\widetilde{V}_{gr}^{\circ}$. We never identified any measurable effect of C_8 on our data. We also studied the dependence of the extracted parameters on the amplitude of the axial pulse used to measure the axial frequency and the answers behaved as expected within the error bars. Generally, we use the smallest possible axial amplitude that gives a reasonable signal-to-noise ($z \simeq 200\,\mu m$). Finally we even looked for a dependence of the measured values on changes in room temperature and found that it was $0 \pm 0.5\,\%$ and $0 \pm 0.06\,mV$ per °C.

To analyse the "f_z vs ρ_c" data sets, we go though exactly the same procedure. The only difference is that the shift from the magnetic field inhomogeneities (Eq. (A.22)) is no longer negligible (we also account for the relativistic shift). We need to input the values of V_{gr}° and C_6 measured from an "f_z vs ρ_m" data set to extract B_2 and B_4.

The third type of data sets, "f_m vs ρ_m", is very different from the other two. To measure the magnetron frequency, we use the PNP technique applied to the magnetron mode. We

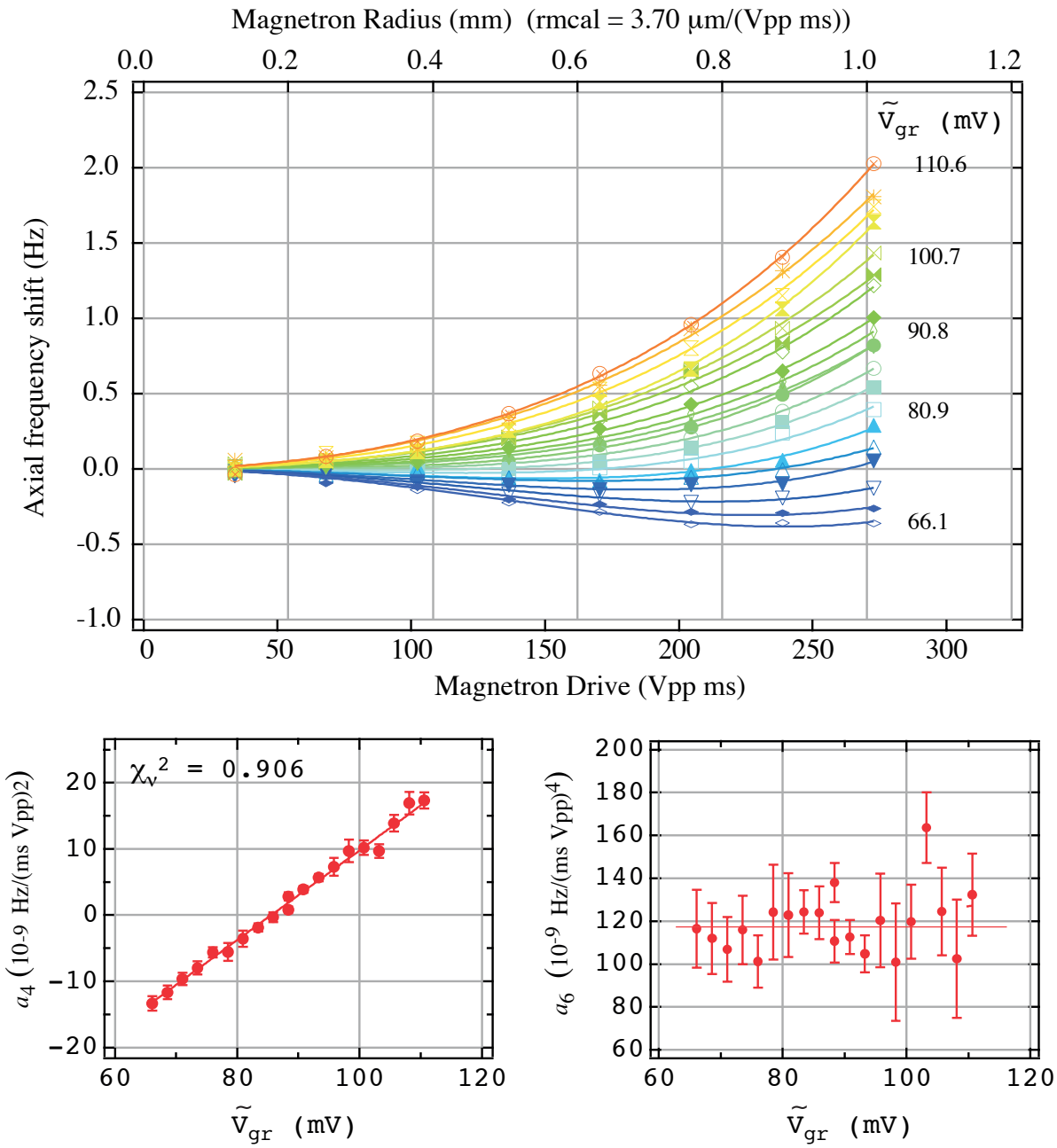

Figure 2-5: Typical "f_z vs ρ_m" data set obtained by measuring the axial frequency vs ρ_m vs $\widetilde{V}_{gr}$ with small axial pulses ($z \leq 200\,\mu m$). Each curve of Δf_z vs ρ_m is fit with a polynomial of the form $\Delta f_z = a_4\rho_m^2 + a_6\rho_m^4$.

obtain the frequency shift from the measured phase difference, and fit these curves vs ρ_m again with the quadratic and 4th order terms. Fig. 2-6 shows a typical data set. These data sets are not sensitive to magnetic field inhomogeneities and lead to the same parameters as those measured by an "f_z vs ρ_m" data set. But because we need the axial mode to be harmonic to extract the phase, we cannot explore as large a volume of the trap with this technique and so the precision of the results is less. This problem could be eliminated by jumping the guard ring voltage to a harmonic setting just before the π-pulse, as described in Sect. 4.1.6. However it is a "cleaner" measurement since it is done at zero axial amplitude. The observed agreement between the values of D_4, $\widetilde{V}^{\circ}_{gr}$, and C_6 obtained from the two (very different) techniques is a powerful check of our results.

Between July and December 2002, we took over 20 data sets to characterize our trapping fields, interleaved with two-ion measurements using $^{13}C_2H_2{}^+/^{14}N_2{}^+$and $^{14}N_2{}^+/CO^+$. The standard deviation of the measured values of D_4, $\widetilde{V}^{\circ}_{gr}$, and C_6 are 5 %, 1.0 mV and 10 % respectively. The fact that these parameters do not change in time is giving us further confidence in our measurement technique. We also made new ions several times during that period and so it appears that our making procedure does not affect the trap environment.

When we switched to measuring the $H^{32}S^+/^{33}S^+$ ratio, we took several other data sets to characterize the trap environment at a different ring voltage (18.5 V instead of 15.6 V), and repeated the procedure for the $H^{28}Si^+/^{29}Si^+$ measurement. Finally, at the end of January, we took a few data sets to measure anharmonicities at $m/q = 16$ ($V_r \simeq 9$ V) using CD_2. Averaging all the data sets at each mass, we found the values listed in Table 2.2. To our big surprise, the values of D_4, $\widetilde{V}^{\circ}_{gr}$, C_6, and B_2 showed a linear variation with mass (or V_r)! In the case of $\widetilde{V}^{\circ}_{gr}$ and C_6, this would be expected if we had frozen charge patches on our electrodes that do not scale with trapping voltages, but it is completely unphysical that D_4, a purely geometric quantity, and B_2 depend on V_r. This dependence on mass however could be eliminated by changing the amplitude calibration ρ_c^{cal} at each mass as explained below.

In Sect. 2.4, we have seen how we calibrated the amplitude of motion of an ion in the trap to 3 % by measuring the relativistic shift of the cyclotron frequencies of Ne^{++} and Ne^{+++}. The procedure to adjust this calibration when changing the mass (or f_c) of the ion in the trap to account for the effect of the transfer function (by comparing the values of ϵ_p measured from Avoided Crossings) was also described there . This procedure is what we had used to determine ρ_c^{cal} at mass 28, 29 and 33. But our two-ion technique provides us yet another way to determine the amplitude calibration. By measuring the beat frequency between the two strongly coupled magnetron mode, we obtain a measure of the distance between the ions ρ_s (in μm) which is independent of ρ_c^{cal}. When the center-of-mass is cooled, $\rho_s/2$ should be the same as the rms magnetron radius of each ion, which we can determine independently by measuring $\partial f_z/\partial V_{gr}$. When comparing the measured rms magnetron radii (assuming D_4 from Table 2.2) to the measured $\rho_s/2$, we found that we

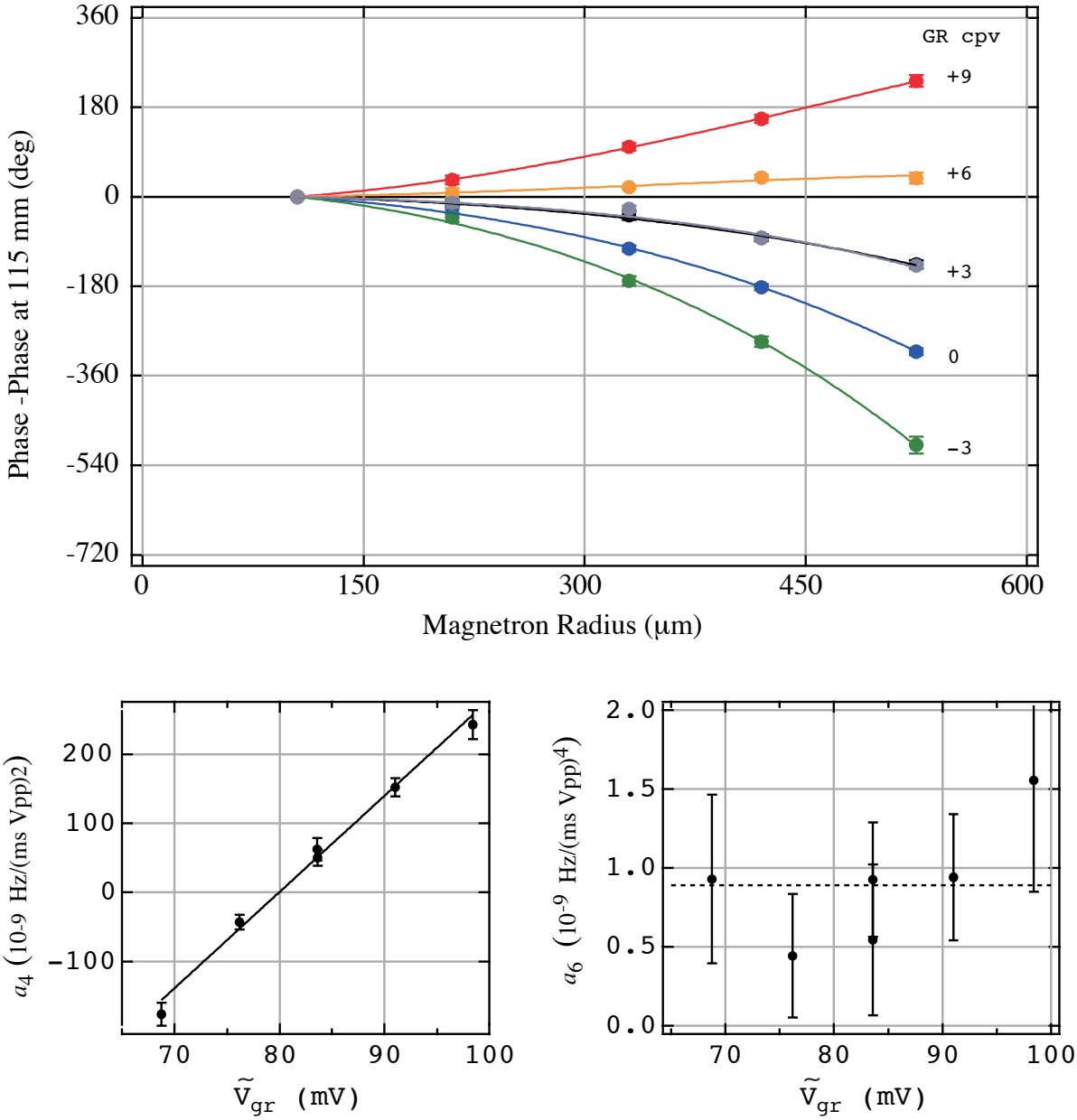

Figure 2-6: Typical "f_m vs ρ_m" data obtained by running a series of magnetron PNPs vs ρ_m vs $\widetilde{V}_{gr}$. Each curve of Δf_z vs ρ_m is fit with a polynomial of the form $\Delta f_z = a_4\rho_m^2 + a_6\rho_m^4$.

Table 2.2: Measured values of the field imperfections, using ρ_c^{cal} from the Ne calibration and Avoided Crossings data.

Mass (u)	D_4	C_6 (10^{-3})	$\widetilde{V}_{gr}^{\circ}$ (mV)	B_2/B_0 (10^{-9}/mm^2)	B_4/B_0 (10^{-9}/mm^4)
16	-0.0321(19)	0.188(25)	66.8(11)	2.08(25)	0.24(11)
28	-0.0695(42)	0.80(11)	82.3(11)	5.31(38)	0.9(73)
29	-0.0707(43)	0.80(10)	84.0(11)	6.8(14)	3.1(97)
33	-0.0836(51)	1.13(15)	89.9(11)	4.5(15)	1.6(18)

had to slightly rescale our calibration ρ_c^{cal} by various amounts at different masses to make them agree. This rescaling of ρ_c^{cal} also affected the field imperfection coefficients and the new "rescaled values" are shown in Table 2.3. The fact that D_4 and B_2 no longer depend linearly on mass is a very good indication that that was the right thing to do. However, the reason why our previous procedure to "transport" the calibration from mass to mass using Avoided Crossings failed is a complete mystery to us (especially because it worked so well between Ne^{++} and Ne^{+++}... and even $^{33}S^{+}$).

Since the measured values of D_4, C_6, B_2, and B_4 no longer depended on mass, we then decided to average them all together to extract our best estimates of these parameters to use in the final analysis of all our two-ion data. These values are given in Table 2.4, along with the final value of ρ_c^{cal} we used at each mass. The only trap parameter still exhibiting a linear dependence on mass is $\widetilde{V}_{gr}^{\circ}$ (it is independent of ρ_c^{cal}). This is not a source of concern as we mentioned above since it probably arises from charge patches. The fact that the measured values fall so nicely on a straight line (slope = 1.346 (88) mV/u; $\chi^2_\nu = 0.16$) is a further indication that our measurements are really what we think they are.

Yet, because of this rescaling, we increase the uncertainty on ρ_c^{cal} from 3 % to 7 % (about 1/2 of the largest rescaling). That $\sigma\rho_c^{cal} = 7\,\%$ uncertainty is the value we used in our analysis of all the two-ion data presented in this thesis. We also were very conservative in taking the uncertainty on our measurement of ρ_s, $\sigma\rho_s$ to be 5 %. Even though we found the measured values of ρ_s to be reproducible at the 1 % level, we wanted to allow for the possiblity of a systematic error in this measurement.

2.6 Detector Frequency vs Atmospheric Pressure

The resonant frequency of our detector f_{coil} varies from day to day over a few Hz. Experimentally, that is slightly inconvenient since it means that to keep the axial frequency of an ion in the trap on resonance, we need to continually adjust the ring voltage and the frequencies of our coupling pulses ($f_{\pi c}$, $f_{\pi m}$). About a year ago, we plotted for the first time f_{coil} and the atmospheric pressure vs time together on the same graph and the result

Table 2.3: Values of the field imperfections adjusted for the rescaling of ρ_c^{cal} to make the rms magnetron radius equal to $\rho_s/2$.

Mass (u)	Rescaling factor	D_4	C_6 (10^{-3})	$\widetilde{V}_{gr}^{\circ}$ (mV)	B_2/B_0 (10^{-9}/mm^2)	B_4/B_0 (10^{-9}/mm^4)
16	1.58	-0.0800(48)	1.17(15)	66.8(11)	5.19(63)	1.48(70)
28	1.1246	-0.0879(53)	1.28(17)	82.3(11)	6.72(49)	1.4(12)
29	1.088	-0.0836(51)	1.12(15)	84.0(11)	8.0(17)	0.4(14)
33	0.9668	-0.0782(47)	0.99(13)	89.9(11)	4.2(14)	1.4(16)

Table 2.4: Final values for the parameters characterizing our trap used in the analysis of all the two-ion data.

Mass (u)	ρ_c^{cal} μm/(Vpp ms)	D_4	C_6 (10^{-3})	$\widetilde{V}_{gr}^{\circ}$ (mV)	B_2/B_0 (10^{-9}/mm^2)	B_4/B_0 (10^{-9}/mm^4)
16	4.32(30)	-0.0821(42)	1.12(12)	66.8(11)	6.10(55)	1.19(52)
28	21.9(15)	-0.0821(42)	1.12(12)	82.3(11)	6.10(55)	1.19(52)
29	22.1(15)	-0.0821(42)	1.12(12)	84.0(11)	6.10(55)	1.19(52)
33	21.0(15)	-0.0821(42)	1.12(12)	89.9(11)	6.10(55)	1.19(52)

is shown in Fig. 2-7. The correlation is almost perfect, except for a few discrete steps in the frequency that are related to liquid helium and nitrogen fills of the experimental dewar. The source of our atmospheric pressure data is the value recorded every hour at the Station 44013 of the National Data Buoy Center (25 miles east of Boston) available online (http://www.ndbc.noaa.gov/station_page.phtml?$station=44013). The dependence of the detector's frequency f_{coil} on the atmospheric pressure P_{atm} is found to be

$$\frac{\partial f_{coil}}{\partial P_{atm}} \simeq 0.1629\,(3)\ \text{Hz/mb}\ . \tag{2.19}$$

From a quick "back-of-the-envelope" calculation of the expected variations in the resonance frequency of our detector coil from changes in its physical dimensions (using the Young's modulus and thermal expansion coefficient of niobium), we predicted an order of magnitude smaller dependence. Thus the physical explanation of this dependence is not perfectly clear, but could be related to physical movements of the apparatus (or cabling) changing the capacitance in our detector's circuitry.

Our discovery of this dependence has allowed us to predict what the frequency will do in the following days by looking at a weather map. In our two-ion technique the drifts of the detector's frequency is not relevant compared to the detuning of the ions during our measurements ($> 15\,Hz$), but it affects the cooling between each PNPs. A drift of f_{coil} by 2.5 Hz would lengthen the damping time of the ion by a factor 2. So during long data sets, we made sure that the ion was cooled at an axial frequency within 2 Hz of f_{coil}.

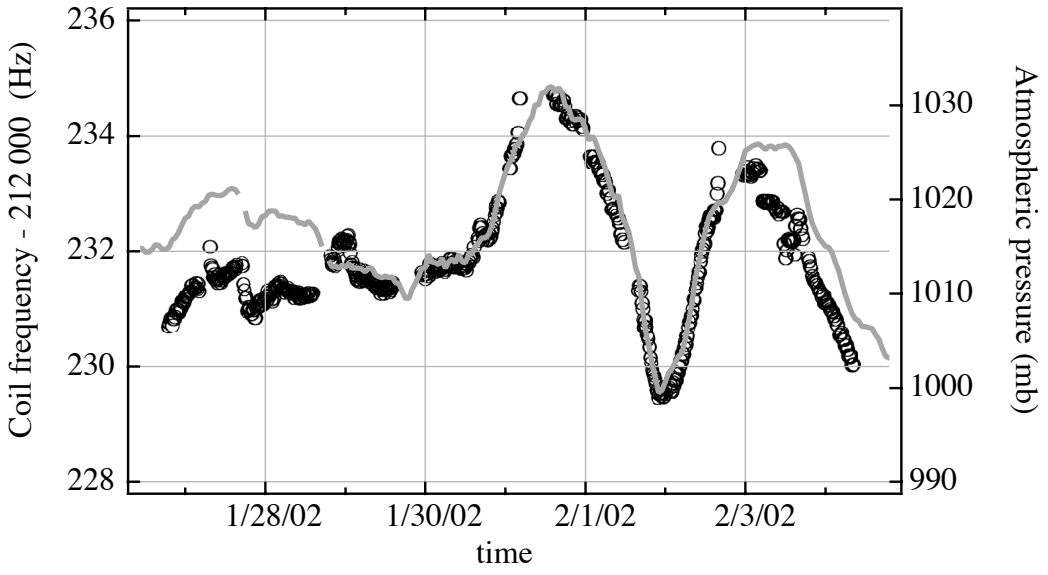

Figure 2-7: Our detector's resonant frequency $f_{\rm coil}$ as a function of time (over about a week). This shows the very clear dependence of $f_{\rm coil}$ (circles) on the atmospheric pressure, also shown as the solid line. The dependence is found to be 0.1629(3) Hz/mb. The barometric pressure was recorded at the Station 44013 of the National Data Buoy Center (25 miles east of Boston).

Chapter 3

Two Ions in One Trap

There are two different approaches to measuring the mass of an object. The first one is to hang the object on a spring and measure the resulting displacement. If the displacement reading is then calibrated by hanging an object of a known mass on the same spring, the unknown mass can be determined — if nothing else has changed. If one seeks high precision, one quickly realizes that the assumption that nothing else has changed is true only to a certain extent. To work around this problem, one can compare the two objects on a balance, thereby directly comparing the two masses to one another. That principle has been used for ages to obtain precision when comparing macroscopic masses. But for the masses of atoms and molecules, where precision is even more desirable, all the mass spectrometry techniques used today are analogous to the spring method above. The reason why it has been nevertheless possible to achieve high precision is that the spring is typically replaced by a magnetic field, which can be extremely stable in time. Still, just like in the case of the spring, fluctuations in the magnetic field has limited the best mass comparisons in the world. The topic of this thesis is a new technique that we have developed, which effectively put the two ions to be compared on a balance. It opens the door to much higher precision.

I must acknowledge that I did not come up with the idea of simultaneously trapping two ions. Eric Cornell, David Pritchard and Deborah Kuchnir laid down the basis of this method about 10 years ago [13, 1], and various members of our group have expanded on their ideas [14, 15]. What James Thompson and I did was to make it a reality, demonstrate that it leads to a much improved accuracy, and determine a few important mass ratios using it.

James and I have worked very closely all along and contributed as a team to almost every aspect of the development of the two-ion technique. We have had to make a very arbitrary division of the topics we would discuss in our respective theses. To write things up more efficiently, we decided that he would describe in details the dynamics of the two ions in the trap, and all the tools we developed to experimentally measure and control the motion of the ions. Our discovery of the novel cyclotron frequency shift arising from polarization forces, and our measurement of the dipole moment of CO^+ will also be covered

in his thesis. To make my thesis somewhat self-contained, I will present in this chapter a very brief summary of these topics. The following three chapters will describe "my" part of the division: the simultaneous measurement technique (Chap. 4), the various sources of errors associated with it (Chap. 5), and finally the two mass ratios we have measured for a new test of special relativity (Chap. 6). But before diving into the details, I give below an overview of the technique and some motivations for our work.

A quick comment about publications. We have not yet submitted any papers presenting results from our two-ion technique. (The publications resulting from a few conferences attended last summer [16] discussed some of the new tools we have developed but did not present any results.) The reason is essentially that we performed the final analysis of our data only recently because we were too busy taking more data. Once we understood the source of the jumps in the ${}^{14}N_2{}^+/CO^+$ data, things started working so well that we collected data as fast and as long as we could. The move of the experiment to Florida and the desire to graduate in June 2003 was setting a strict deadline for us. Now that we have stopped taking data, we are writing up our results in at least three publications:

1. A demonstration of the two-ion technique (using the data from the ${}^{13}C_2H_2{}^+/{}^{14}N_2{}^+$), describing our new tools to measure and control the motion of the ions, the tremendous gain in precision we have, and our control of systematic errors at the 10^{-11} level.

2. A description of the novel effect of polarization forces on precise cyclotron frequency measurements, with our non-perturbing observation of the quantum state of a single molecule over many days and a measurement of the dipole moment of CO^+.

3. A report of the other two mass ratios we have measured involving sulfur and silicon isotopes for a new test of special relativity.

We are also considering writing a fourth, longer paper describing in more details the two-ion technique.

3.1 Motivation and Overview

Before this work, high-precision mass measurements were done by *alternately* creating individual ions of the two species being compared and measuring their cyclotron frequencies separately. The precision of this technique is limited almost entirely by temporal fluctuations of the magnetic field. The relative magnetic field fluctuations for our apparatus are typically 3×10^{-10} during the several minutes required to trap a new single ion. We were also restricted to take precision cyclotron frequency measurements only during the period between about 01:00 and 05:30 at night during which Boston's electric subway is not running[†]. Figure 3-1 shows the random fluctuations of about 4 mG (1 mG = 10^{-7} T) that the

[†]Saturday night was the best night to take data because the subway starts one hour later on Sunday morning.

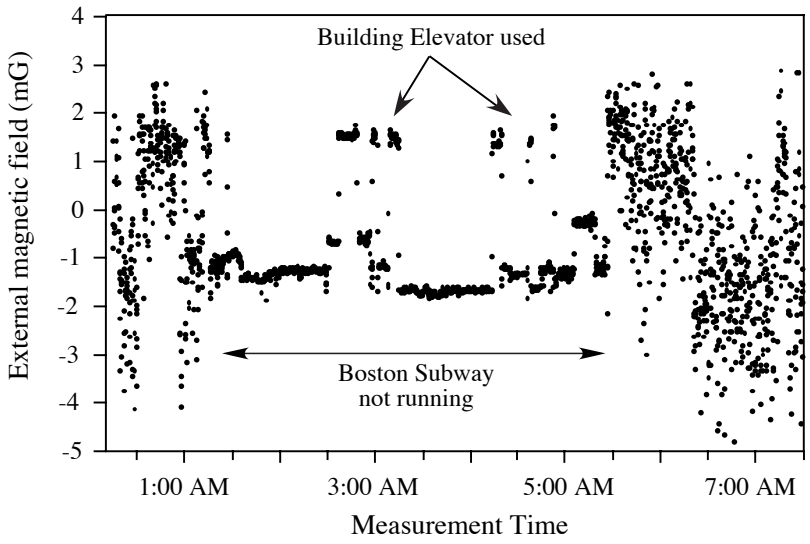

Figure 3-1: The magnetic field in our laboratory, as recorded by a magnetometer.

subway creates in our lab during the day. Given that our 8.5 T magnet has a shielding factor of about 8, the cyclotron frequency of an ion is shifted by about 1.5×10^{-9} for each mG change in the external magnetic field. Thus during the day, ω_c is randomly fluctuating by about 6×10^{-9}. The sudden jumps during the night visible in Fig. 3-1 are caused by the elevator of the building. We had to shut it down (after negotiating with the night-shift janitors!) during our precise cyclotron frequency measurements.

To avoid the effect of magnetic field fluctuations, we decided to make *simultaneous* measurements of the cyclotron frequencies of the two ions being compared. Simultaneously comparing the cyclotron frequencies of two different ions in the same trap offers the best protection against magnetic field fluctuations and field gradients, but introduces a new complication: ion-ion perturbations. To keep the Coulomb interaction between the two ions under control, we need to keep them about 1 mm apart from each other. In order to achieve this we park the two ions on a common magnetron orbit with a radius of 500 µm. In the next Section, we will explain why the two ions stay on opposite sides of the trap on this orbit, always 1 mm away from each other, and briefly how we get them there. This solves the ion-ion interaction problem, but it means that we are no longer measuring the cyclotron frequencies of the ions near the center of the trap. Being about 500 µm away from the trap center makes our measurements a lot more susceptible to electric field anharmonicities and magnetic field inhomogeneities. As we will see in Chapter 5, our solution has been to characterize our trapping fields to an unprecedented level (see Sect. 2.5) and optimize the trap so that the various contributions to the cyclotron frequency shifts all cancel out for a given measurement. Another general problem is that all the sources of errors we dismissed before as "below our uncertainty of 10^{-10}" have to be accounted for and brought under

control. Fortunately the majority of them are vastly reduced because of the simultaneous nature of the measurement and also because we used pairs of ions with very similar masses ($\Delta m/m \leq 6 \times 10^{-4}$). For example the requirement on voltage stability is greatly relaxed: to reach a final precision of 10^{-11} with the alternating single ion technique, the voltage has to be stable to 1×10^{-8} (!), whereas this requirement is only 1.5×10^{-5} in our simultaneous technique because both ions experience the same electric field.

It is worth mentioning here that there are other approaches one could take to tackle the problem of magnetic field fluctuations. We have spent some time thinking about a double-trap system in which we could make simultaneous measurements on a pair of ions located in two traps one above the other. To cancel the systematic difference in magnetic field between the two trap centers ($\sim$2.5 cm away in the current version), we would periodically exchange the position of the two ions. VanDyck at the University of Washington has taken the "engineering" approach by redesigning his magnet/cryostat and has demonstrated a very impressive temporal stability for his magnetic field of less than 2×10^{-11} per hour [17]. His main limitation now is voltage stability, since he does not perform simultaneous measurements. For their comparison of the antiproton and proton masses, Gabrielse et al. have simultaneously trapped $\bar{p}$ and H^+- by alternately storing one of them in a large cyclotron orbit ($\rho_c > 1.6$ mm) [18]. That has allowed them to repeatedly make measurements on these species which are very difficult to load. However, because they performed alternating measurements too, they were still subject to magnetic field fluctuations.

3.2 Magnetron Mode Dynamics

In order to keep systematic errors small and for many other reasons that will become apparent in the next few sections, we simultaneously trap two different ions with very similar masses – typically with $\Delta m/m \leq 10^{-3}$. In [13], Cornell et al. have described the dynamics of such a pair of ions in our Penning trap. I will briefly summarize the main results here to make the thesis more complete and establish the notation that I will use in the next chapters (which is slightly different from the one of [13]). The reader is also referred to James Thompson's thesis for a more complete discussion of this topic and insightful interpretations of the results.

In contrast to Cornell et al. we refer to our two ions as 'ion 0' and 'ion 1' (instead of 1 and 2). The fundamental reason is that in developing the new computer control system for the experiment and expanding it for working with two ions simultaneously, that was a much more convenient convention; boolean correspond to 0's and 1's, not 2's. The downside of our convention is that we have lost the very nice possibility of giving the suffix 0 to the average properties of the two ions; we use the traditional (but more awkward) over bar instead (like $\bar{m}$). We use the suffix '2' to refer to differences between properties of the two ions — we always subtract 0 from 1, e. g., $\omega_{c2} \equiv \omega_{c1} - \omega_{c0}$. In doing so, we have favored

compactness at the cost of some clarity (ω_{c10} would have been less confusing for example). By convention, we always define ion 0 as the heavier ion such that

$$\begin{array}{ll} m_0 = \bar{m}(1+\eta) & \\ m_1 = \bar{m}(1-\eta) & \end{array} \quad \Rightarrow \quad \begin{array}{l} m_0 > m_1 \ , \quad f_{z1} > f_{z0} \ , \\ f_{ct1} > f_{ct0} \quad \text{and} \quad f_{m0} > f_{m1} \ . \end{array} \tag{3.1}$$

This definition makes $\eta = \Delta m/(2\,\bar{m})$. We define the ion-ion Coulomb interaction expressed as an angular frequency (in CGS)

$$\Omega_E^2 \equiv \frac{e^2}{\bar{m}\rho_s^3} \ , \tag{3.2}$$

where ρ_s is the radial distance between the ions, $\bar{m}$ is the average mass of the two ions and e is the charge of the electron. To characterize the strength of the ion-ion coupling, in frequency units, we write the effective axial and radial "Rabi frequencies"

$$\Omega_\rho = \frac{2\Omega_E^2}{\bar{\omega}_c} \qquad \text{and} \qquad \Omega_z = \frac{\Omega_E^2}{2\,\bar{\omega}_z} \ . \tag{3.3}$$

At $m = 28$ and $\rho_s = 800\,\mu\text{m}$, $\Omega_\rho/2\pi \simeq 0.10\,\text{Hz}$ and $\Omega_z/2\pi \simeq 0.58\,\text{Hz}$. Because the magnetron frequency is to first order independent of mass (see Eq. 2.5), Ω_ρ is much larger than the difference between the magnetron frequencies of the two ions for all the pairs we used. That means that the two individual magnetron modes are no longer independent, and the dynamics is better described in terms of two collective magnetron normal modes that we call the 'center-of-mass' mode (COM) and the 'difference' mode. If $\vec{\rho}_0$ and $\vec{\rho}_1$ are the vectors in the radial plane ($z = 0$) from the center of the trap to the position of ion 0 and 1 respectively, then the new mode amplitudes are $\vec{\rho}_{com} \equiv (\vec{\rho}_1 + \vec{\rho}_0)/2$ (center-of-mass vector) and $\vec{\rho}_s \equiv \vec{\rho}_1 - \vec{\rho}_0$ (separation vector), as shown in Fig. 3-2 (a). The COM mode corresponds to the center-of-mass of the ions orbiting at the average magnetron frequency ($\sim 5\,\text{kHz}$) about the center of the trap. The difference mode corresponds to an $E \times B$ drift of the ions about the center-of-mass due to the Coulomb interaction between them. The frequency of the difference mode is $\Omega_\rho/2\pi \approx 0.10\,\text{Hz}$ higher than that of the COM mode. From conservation of energy and canonical angular momentum, one can show that the amplitudes of both modes, ρ_s and ρ_{com}, are approximate constants of the motion [13].

This coupling of the magnetron modes is actually very useful from our point of view, and that is why we work with pairs of similar masses. Since ρ_s is constant, the possible systematic errors associated with the Coulomb interaction between the ions are at least constant in time. Also the slow rotation of the ions about the center of mass (with a period $T_{swap} = 2\pi/\Omega_\rho \simeq 10\,\text{s}$) insures that, on that time scale, the two ions will average out the spacial inhomogeneities of the magnetic field. If $\rho_{com} = 0$, i. e., the center-of-mass is at the center of the trap, the ions go around the trap center on almost the same magnetron orbit (on opposite sides), and experience nearly the same fields at all times. That is the ideal configuration for a precise comparison of the ions' cyclotron frequencies. We have developed

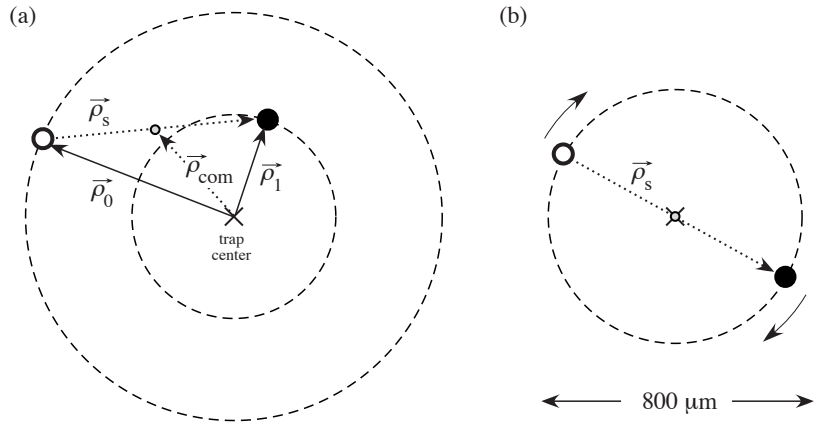

Figure 3-2: Two-ion magnetron modes dynamics. The magnetic field is pointing out of the plane of the figure. The center of the trap is indicated by a cross and the center-of-mass of the ions is the small gray dot. Because of the Coulomb interaction between the ions, the dynamics is better described in terms of two collective magnetron normal modes. The center-of-mass ($\vec{\rho}_{\rm com}$) orbits about the trap center at the average magnetron frequency ($\sim 5\,$kHz), and the two ions rotate around the center of mass about 10 mHz faster (for $|\vec{\rho}_{\rm s}| \simeq 800\,\mu$m). Note that the distance between the ions $|\vec{\rho}_{\rm s}|$ is constant in time. (a) If $|\vec{\rho}_{\rm com}| \approx |\vec{\rho}_{\rm s}|/2$, each ion moves in and out of the center of the trap every 10 s. (b) The ideal configuration for making precise cyclotron frequency comparisons: $|\vec{\rho}_{\rm com}| \approx 0$, i. e., the ions go around the trap center on almost the same magnetron orbit.

tools (briefly described in the next section) to "park" the ions in this ideal configuration. The biggest benefit of this configuration is to make each ion's mode frequencies constant in time. This is very important since we rely on the stability of the axial frequency to detect each ion's signal, and perform π-pulses to swap the action between the axial and radial modes (see [4]).

Because of the finite mass difference between the ions, their magnetron modes are not 100 % mixed and the COM normal mode of motion described above is not exactly the true center-of-mass. Practically, this means that even when the ions are parked in the ideal configuration, their rms magnetron radius will always be slightly different:

$$\begin{aligned} \rho_{\rm m0} &= \frac{\rho_{\rm s}}{2}(1+\delta_{\rm mag}) \\ \rho_{\rm m1} &= \frac{\rho_{\rm s}}{2}(1-\delta_{\rm mag}) \end{aligned} \qquad \text{where} \qquad \delta_{\rm mag} = \frac{\eta\,\bar{\omega_{\rm m}}^2}{2\Omega_{\rm E}^2}\,, \tag{3.4}$$

where η was defined in Eq. (3.1). The systematic difference in magnetron radii is the source of the sensitivity of the cyclotron frequency difference $\omega_{\rm ct2}$ to trap field imperfections (see Sect. 5.2). This expressions describe the dynamics of the ions in a perfect Penning trap. The presence of electric field anharmonicities and magnetic field inhomogeneities will slightly change $\delta_{\rm mag}$ and $T_{\rm swap}$ for example, but generally by no more than 10 %.

Finally, it is important to mention that because of their strong mass dependence, the

axial and cyclotron modes of the two ions remain uncoupled. The differences between the two axial and cyclotron frequencies are $> 30\,\mathrm{Hz}$ and $> 1000\,\mathrm{Hz}$ respectively for the pairs we worked with (see Table 4.1). These are clearly larger than the axial and radial Rabi frequencies defined above: $\Omega_z/2\pi \approx 0.58\,\mathrm{Hz}$ and $\Omega_\rho/2\pi \approx 0.10\,\mathrm{Hz}$, so the frequencies of these modes are perturbed by ion-ion interactions, but the motions remain independent.

3.3 Two-Ion Loading Techniques

To introduce a pair of ions in the trap, we simply produce the two ions one after the other using our standard single-ion making procedure: we inject small amount of neutral gas in the trapping volume and ionize a few atoms with an electron beam (4-20 nA at $\sim$ keV). However, since ρ_s is fixed by the separation distance between the ions when their magnetron modes couple, we must avoid making them too close to each other. Since our ions are created near the center of the trap ($\rho_m \lesssim 100\,\mu\mathrm{m}$), we create the first ion, clean it up, cool it to the center of the trap, and then drive it out in a large magnetron orbit ($\rho_m \sim 1\,\mathrm{mm}$) before making the second one in the center. We have developed a variety of techniques to take the ions from this configuration where $\rho_{com} = \rho_s/2$ to the ideal configuration ($\rho_{com} = 0$) in which we want to take precise data. Our initial approaches involved applying discrete excitation pulses to drive the COM to the center of the trap. However we discovered along the way a more subtle but more robust way to redistribute the angular momentum between the center-of-mass and the difference modes in which we essentially modulate the axial amplitude of one ion to create a resonant coupling between the magnetron normal modes. That technique has allowed us to place the two ions in the ideal configuration shown in Fig. 3-2 to make precise comparisons of their cyclotron frequencies.

3.4 Diagnostic Tools

By simultaneously trapping two different ions in our Penning trap, we introduce two new possible sources of systematic errors on our measurement of the cyclotron frequency ratio: (1) the Coulomb interaction between the ions and (2) the imperfection of the trapping fields away from the center of the trap. In contrast to our previous technique where we alternately trapped single ions, we expect that these systematic errors will now completely dominate our final uncertainty. Since we are doing a high-precision experiment, we cannot simply rely on our model of the dynamics of the two ions in our trap and start making measurements. A crucial aspect of the development of this technique has been to invent new tools to experimentally confirm the model above (in our imperfect trap) and measure the separation distance between the ions. The big challenge in doing this is that we have very limited access to the ions. Recall that we can only measure the tiny image current induced in our detector when the ions are bouncing up and down in the trap and apply

various rf and dc fields on our trap electrodes. The fact that we somehow manage to extract precise information on the trajectory of each individual ion in our trap is remarkable to me.

A key observation that lies at the heart of all our diagnostic tools is that in an anharmonic trap, the axial frequency depends on the magnetron radius (as shown in Fig. 2-5). A tremendous technical advance in our experiment was to gain automated control of the voltage applied to the guard ring electrode, which gives us the ability to easily vary the level of anharmonicity of our trapping electric field (C_4). This has allowed us to map very carefully our field imperfections (with a single ion in the trap) as described in Sect. 2.5. Once we know the various coefficients describing our electric and magnetic fields (C_4, C_6, B_2, ...), we can simply look at how much the axial frequency of one ion varies when we change the guard ring voltage and extract the rms magnetron radius for that ion at that time; it is clear from Fig. 2-5 that if the axial frequency changes a lot, then the ion is far from the center of the trap. This gives us a tool to measure ρ_{m} for each member of a pair of ions in our trap *independently* and verify that their magnetron radii are the same to a few percent.

If $\rho_{\mathrm{com}} \neq 0$, we expect that the magnetron radius of each ion (and therefore ω_{z} if the trap is made anharmonic) will be slowly modulated over a time scale of $T_{\mathrm{swap}} \approx 10\,\mathrm{s}$. We have developed a computer-based feedback system to lock the axial frequency of an ion in the trap to an external frequency reference (referred to as the 'PhaseLock' system). Figure 3-3 shows the observed signal when continuously monitoring the axial frequency of one member of a pair of ions. The "beat frequency" between the strongly coupled magnetron modes is clearly visible and matches well our expectations from Eq. (3.3). Not only has this confirmed our model of the dynamics of two trapped ions, but it has also provided us with a sensitive probe of the ion-ion separation. Indeed, it is clear from Eqs. (3.3) and (3.2) that $T_{\mathrm{swap}} \propto \rho_{\mathrm{s}}^3$. Using this technique, we have observed that ρ_{s} is indeed constant in time at the few percent level, even over several days ! When comparing independent measurements of ρ_{s} (say looking at one ion, then the other one) we find that the standard deviation of the measured values is less than 1%. We have to apply a small correction to the measured T_{swap} because of anharmonicities and the fact that we are performing this measurement with a finite $z \approx 250\,\mu\mathrm{m}$, but this correction is typically smaller than 5 % and we certainly know it to better than 50 %. To be conservative, we give an uncertainty of 5 % to all our measurements of ρ_{s}.

The techniques described above allow us to measure the position of the ions in the trap, but for studying systematic errors, we also need the ability to change ρ_{s}. In order to bring the ions closer together we can slowly reduce the magnetron radius of each ion by applying a series of very brief coupling pulses between the magnetron mode of each ion and its axial mode. We need to cool the axial mode between each coupling pulse to avoid driving the ions into a very large axial motion. By applying magnetron excitation pulses we can only drive the COM mode. But that introduces angular momentum into the system which we

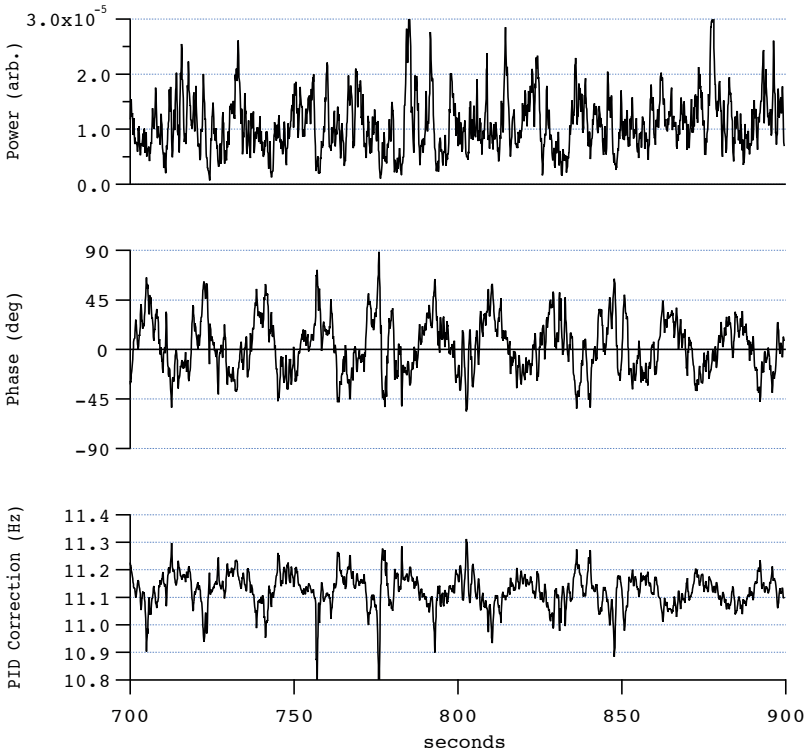

Figure 3-3: Observed signal from our "PhaseLock" system. The bottom graph shows the instantaneous axial frequency of the $^{13}C_2H_2{}^+$ in the presence of one $^{14}N_2{}^+$ when $\rho_{\mathrm{com}} \neq 0$ and $\rho_{\mathrm{s}} \approx 900\,\mu\mathrm{m}$. The top and middle graphs show the power and phase of the detected signal, the latter being used as the error signal of our LabVIEW-based PID feedback loop.

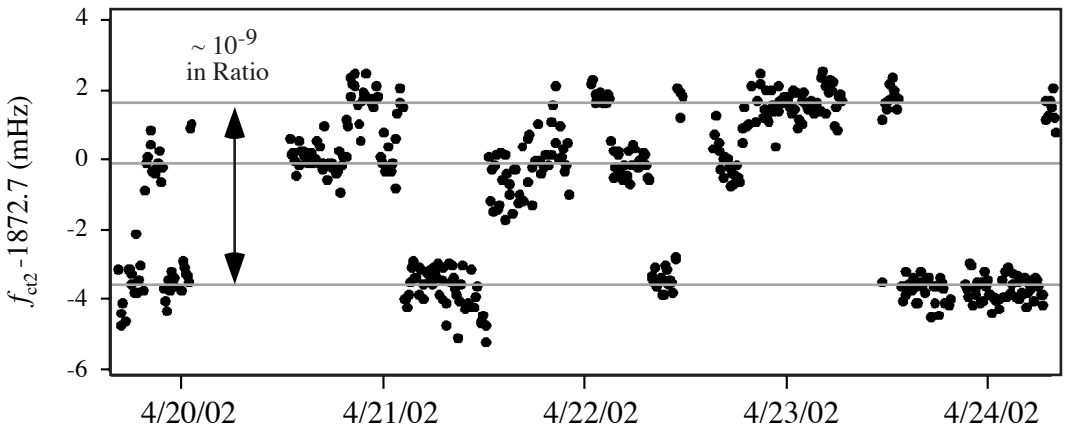

Figure 3-4: The measured (trap) cyclotron frequency difference ω_{ct2} vs time for ${}^{14}N_2{}^+/CO^+$. The data exhibit abrupt and very large jumps between a few discrete values. Note that these jumps occurred on average every 8 hours, which made them very painful to study (this data set spans over 100 hours of data !). After over one year of investigation, we found that these correspond to black-body induced quantum jumps between the first few rotational states of the CO^+ molecule.

can then transfer into the difference mode (thereby pushing the ions further apart) using the technique I briefly mentioned in Sect. 3.3.

3.5 N_2^+ vs CO^+ Mystery

In 1989, Cornell et al. reported the first mass ratio measurement with a precision below 10^{-9}. For their demonstration, they had measured $M[CO^+]/M[{}^{14}N_2{}^+]$ by alternately loading each ion in the trap [6]. In 1992, they used the same pair of ions to illustrate their proposal for the two-ion technique, although they could not make simultaneous cyclotron frequency measurements at the time [13]. The reason why ${}^{14}N_2{}^+$and CO^+ions were used is that they are very easy to load in the trap using N_2 and CO gas (no fragments produced), and 28 is a convenient m/q for our setup. Very naturally, that was then the pair James Thompson and I started working with when we began implementing the simultaneous two-ion technique in 2000. When we succeeded in directly measuring the difference frequency between CO^+ and ${}^{14}N_2{}^+$, we observed abrupt and very large ($\sim 1 \times 10^{-9}$) jumps between a few discrete values, as shown in Fig. 3-4. These jumps occurred on average every 8 hours, which made them very painful to study.

For more than a year, we designed new experiments to track down the source of these jumps and never succeeded in finding anything that correlated with them. It was a very frustrating time, but it forced us to think a lot about our system and develop tools to experimentally probe every aspect of the behavior of the ions in the trap that we could think of. I think the results I will present in the next few chapters would have never been so

complete had we not made that "unfortunate" choice at the beginning. For the longest time, we did not know what to wish for: finding that we had been making a silly experimental mistake all along (flip a switch and everything would be fine), or realizing that we had overlooked some physics principle related to the dynamics of two ions in a Penning trap that would prevent this technique from ever working (in which case we were ready to move on to the double-trap approach). In the end, the explanation turned out to be the best of all possibilities: some scientifically interesting phenomenon that could be avoided with a careful choice of molecules.

Correcting the measured phases for the ambient magnetic field noise using an external magnetometer showed that it was the cyclotron frequency of CO^+ that was jumping in time. The explanation hinges on the fact that CO^+ has a very large dipole moment ($\sim 1\ e\ a_0$) that gives it a large dc polarizability α. Because it moves very quickly in a large magnetic field, the molecule sees in its own reference frame an effective electric field $\vec{E} = \vec{v} \times \vec{B}$ that "pulls" the center-of-charge of the molecule away from the center-of-mass, thereby shifting the cyclotron frequency. In other words the polarization energy $-\alpha E^2/2 = -\alpha B^2 v^2/2$ leads to an effective mass increase proportional to the dc polarizability of the molecule. Hence the cyclotron frequency depends on the quantum state of the molecule. The observed jumps can then be explained as 4 K black-body photons inducing quantum jumps of the CO^+ molecule between its lowest rotational states. To our big surprise, the predicted shift and rate of transition from this model matches our observations quite well. We even hope to be able to extract the first experimental measurement (to our knowledge) of the dipole moment of CO^+ (or any charged molecule) from our data. We will shortly submit the details of our observations on this effect for publication. The reader is also encouraged to read James Thompson' thesis for all the details about this effect.

As soon as we found this explanation, we loaded $^{13}C_2H_2{}^+$ instead of CO^+(still comparing to $^{14}N_2{}^+$) and sure enough the jumps went away. The $^{32}SH^+$ and $^{28}SiH^+$ molecules used in the measurements discussed in Chapt. 6 do have dipole moments but they are much smaller and their molecular structure is such that they always stay in the ground rotational state in our trap. We do however have to apply a small correction to our measured ratios because of this effect. Even the $^{13}C_2H_2{}^+$ molecule has a bent structure which could lead to a systematic shift of our measured frequency ratio, but because it is not a diatomic molecule the molecular structure calculation is much harder to carry out.

Because we wanted to perform mass comparisons below 10^{-11}, we selected molecules to minimize this polarization force shift. But another approach might be to use it to measure dipole moments of ions, or to do molecular spectroscopy of single molecules (detecting the rotational state by this shift ?!). It is a challenging way to do spectroscopy, but in some cases where it is difficult to obtain large samples (we need only one molecule!), it might be worthwhile.

Chapter 4

Simultaneous Measurements on Two Ions

Once we have a pair of ions in the trap, parked in the ideal configuration depicted in Fig. 3-2, we can make a simultaneous measurement of the cyclotron frequencies of both ions. We use the same "pulse and phase" (PNP) technique used to measure a single ion's cyclotron frequency except that we now apply it to both ions simultaneously. Since the single-ion case has been discussed in great details in all the previous theses from the MIT ICR group, the next section will not repeat all the details of the measurement technique, but give a general outline, emphasizing only the aspects that are new.

4.1 Simultaneous Measurement Sequence

In contrast to the magnetron modes of the two ions which are strongly coupled by the Coulomb interaction (see Sect. 3.2), the two axial and cyclotron modes remain nearly independent. Since ω_z and ω_c depend on mass, the axial and cyclotron frequencies of the ions are well separated as can be seen from Table 4.1. This is a key feature in all the pairs we chose to work with since it allows us to address each ion's cyclotron mode separately.

Table 4.1: Typical mode frequencies for the pairs of ions which we worked with. The subscript 2 refers to the difference frequency ($f_{ct2} = f_{ct1}$ - f_{ct0}), and the overbar indicates the average quantity for the pair ($\bar{f}_{ct} = (f_{ct0} + f_{ct1})/2$).

ion 0 vs ion 1	$\bar{m}$ (u)	η (10^{-4})	f_{z2} (Hz)	$\bar{f}_{ct}$ (Hz)	f_{ct2} (Hz)
$^{13}C_2H_2^+/^{14}N_2^+$	28.013 705 295	2.89	61.4	4 670 686	2 706
$^{14}N_2^+/CO^+$	28.007 662 853	2.00	42.6	4 670 685	1 873
$H^{32}S^+/^{33}S^+$	32.975 128 527	1.28	27.2	3 966 353	1 016
$H^{28}Si^+/^{29}Si^+$	28.980 074 562	1.42	30.3	4 514 608	1 288

The basic sequence for a cyclotron frequency measurement is called a PNP (for Pulse aNd Phase). It consists of four steps (the typical time for each step is indicated in parentheses):

1. **Cyclotron Drive** (30 ms) The cyclotron mode of each ion is driven to a radius of about 70 μm using a dipole electric field generated by the split guard ring electrodes.

2. **Evolution Time** (0.1 s - 10 min) The cyclotron motions of both ions are allowed to evolve for a time T_{evol}. During that time, the ions accumulate phase completely "in the dark", i. e., not coupled to any detector.

3. **π-Pulse** (300 ms) The cyclotron motion of each ion is phase coherently converted into axial motion by applying an rf quadrupole electric field for just the right amount of time for a complete transfer (π-pulse — see Sect. 2.1.2).

4. **Axial Ringdown** (8 s) The axial motion of the ions induce a signal in our detector that we record. From this signal, we extract the phase (and frequency) of each ion's axial motion. This phase is related to the phase of the cyclotron motion at the start of the π-pulse by only a constant phase offset (independent of T_{evol}).

A cyclotron frequency ratio measurement consists of a series of PNPs with different evolution times T_{evol}. The slope of the measured axial phase vs T_{evol} gives the cyclotron frequency of each ion. Since we use two ions with very similar masses, their mass ratio is mostly determined by the cyclotron frequency difference between the two ions, which we can obtain from the axial phase difference vs T_{evol}. Note that because of magnetic field fluctuations, we loose track of the total phase accumulated by an individual ion in a few minutes, but since we are interested only in the relative phase, we can let T_{evol} be as large as 30 minutes. There are many technical details one has to worry about to make this technique work. The main ones are presented in the following sections.

4.1.1 Phase Coherence

If we are to compare the phases from one PNP to the next, we need to maintain phase coherence, i. e., two identical PNPs should result in the same measured phase (within the detection noise). There are many arbitrary phases in the system like the relative phase of the two initial cyclotron drives or the phase shifts from the electronics between the frequency synthesizers and the trap electrodes. The key to this technique is to make sure that all those arbitrary phases are constant from one PNP to the next and do not vary when we change T_{evol}. That is done by rounding all the frequencies on the synthesizers to integers and triggering the start of every PNP with a 1 Hz signal derived from the 10 MHz clock which we use as reference for all frequency synthesizers. (One of my first electronics project in the lab was to modify the "Clock Box" to output a 2 Hz signal so that one could round the synthesizers frequencies to 0.5 Hz if more frequency resolution was needed). For all the

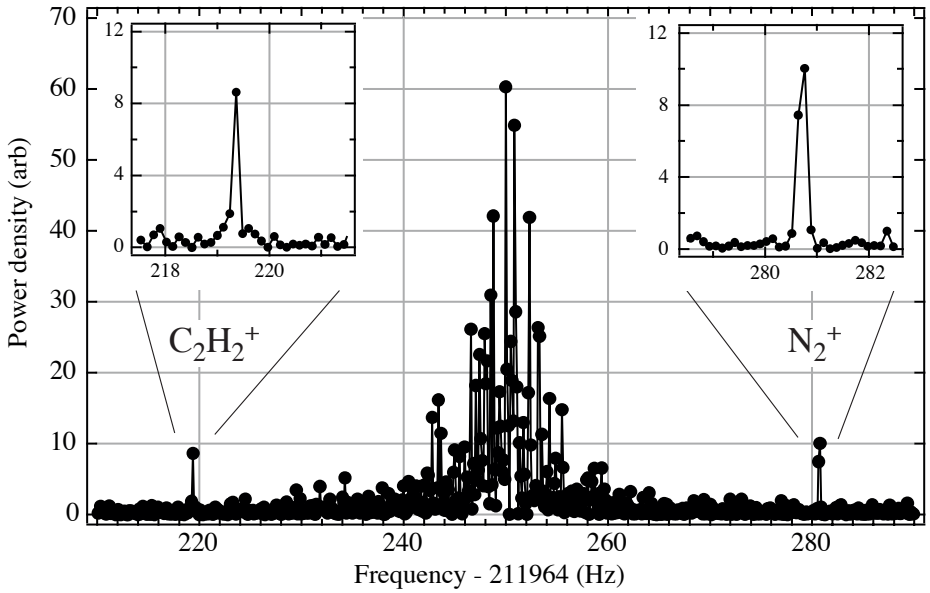

Figure 4-1: Detected signal from a $^{13}C_2H_2^+/^{14}N_2^+$ pair of ions. This graph shows the power spectrum of the induced currents in our detector from the axial motion of the ions after a PNP (recorded for 8 s). The amplitude of axial oscillations is about 330 µm for both ions. The Lorentzian thermal noise profile (4 K) of the detector coil is clearly visible in the middle. Due to the mass difference between the ions, their axial frequencies are clearly well separated ($f_{z2} \simeq 61.4$ Hz in this case). We adjust the trapping voltage so that the ions' signals are symmetrically located on each side of the resonant frequency of our detector (250 Hz).

measurements presented here, we did not directly measure what is referred to in other theses as "HP Phase", namely the relative phase of the cyclotron drive, cyclotron coupling and mixer synthesizers. It was superfluous because we did not change any of the synthesizers frequencies for the entire duration of a measurement (5–15 hours). Doing so destroys the phase coherence but had to be done when making alternating measurements since we did not have as many synthesizers. In any case, that "HP Phase" determines the offset in fitting the phase vs T_{evol}, but is never required since we are interested only in the slope. The phase coherence requirement is crucial for this technique and prevents us from changing anything during data taking that would change the relative phases of the frequency synthesizers (for example changing any frequency).

4.1.2 Signal Processing

Figure 4-1 shows the power spectrum of the induced currents in our detector from the axial motion of the ions after a PNP (recorded for 8 s), i. e., a typical "axial ringdown". In his thesis, Vasant Natarajan presented a detailed discussion of the digital Laplace transform procedure we use to extract the phase for the axial signal of one ion [14]. In all our si-

multaneous measurements on two-ions, the same procedure was used on each ion's signal independently (they are well separated in frequency) and simply subtracted the resulting phases to obtain the phase difference. Another possibility would have been to directly extract the phase difference from the data (as was done in the early demonstration of simultaneous trapping of two ions [13, 1]) . This could be done by filtering our recorded signal (amplitude of the current in our detector due to the ion's axial motion vs time) to select only the frequency components near the two ions signals and squaring the filtered data. Squaring the data generates a signals at the sum and difference frequencies. We can then process only the frequency component at the difference frequency with our standard algorithm to extract the difference phase. The real benefit of this signal processing technique is that it would allow one to precisely determine the phase (and frequency) difference between the ions, even if both axial frequencies were "chirping" together (as the axial motion damps for example). For all the data we took, ions were far from resonance with our detector and therefore not significantly damping during the 8 s we recorded their signals ($\tau \approx 150$ s). We saw no improvement in the standard deviation of the phase differences directly extracted from the data compared to the independent processing approach, so we used the latter for simplicity. (But by looking directly at the component at the difference and sum frequencies, we can observe the magnetron beat frequency in the resolved sidebands limit – see [19])

4.1.3 Phase Unwrapping

Since all the measured phases are between 0 and 360 degrees, we need to manually add to them an integer multiple of 360° corresponding to the total number of full cyclotron cycles. If the uncertainty on our initial guess of the frequency is 1 Hz, we can in principle wait 1 s before we loose track of a full cycle. In practice, we are very conservative and we typically take many PNPs with T_{evol} between 0.1 and 1 s. By fitting a straight line to the phase resulting from those short PNPs vs T_{evol}, we extract a better estimate of the cyclotron frequency, which can then be used to figure out the number of cycles we need to add to the PNP with $T_{\text{evol}} = 2$ s. We then include the "unwrapped" phase at $T_{\text{evol}} = 2$ s in our fit and extract an even better estimate of the cyclotron frequency. By repeating this process we can bootstrap our way up to longer and longer T_{evol}, or more and more precise measurement of the cyclotron frequency. Since the standard deviation of the phases measured at a fixed T_{evol} is never bigger than 60°, we can increment T_{evol} by a factor of 3 or 4 each time and be confident that we never loose a cycle. The list of evolution times we use typically looks like: (0.1; 0.15; 0.2; 0.65; 1; 2; 7; 20; 50; 160; 400) s. The longest evolution time is selected to optimize resolution (see Sect. 5.6.2). When actually taking the data, we like to take about twice as many points with the longest and the shortest evolution times since those are the points that contribute the most to the slope. We also somewhat randomize the list of T_{evol} to avoid any potential systematic effect from, say, always taking the 160 s PNP after the 50 s one (even though we cannot think of any reason why this should have any systematic

effect on the phase).

In Sect. 4.3 we will see that in order to extract the mass ratio of the two ions being compared, we not only need to know the trap cyclotron frequency difference, but also the individual cyclotron frequencies of each ion (although not so precisely). The individual frequencies are obtained simply by phase unwrapping separately the phases of ion 0 and ion 1. However, the individual cyclotron frequencies are affected by magnetic field fluctuations and so unwrapping is impossible beyond the evolution time for which a typical magnetic field jump affects the phase by 360°. We typically used 7 s as the longest evolution time for measuring each ion's cyclotron frequency; 30° noise in the phase then corresponds to a precision of 2.6×10^{-9}, which is more than adequate.

Here are a few technical details about the analysis of simultaneous cyclotron frequency data. The first thing we do is to separate the data according to the evolution time that was used for each point. We then have a series of phase difference vs time for each $T_{\rm evol}$ as shown in Fig. 4-2. We consider each PNP with the longest $T_{\rm evol}$ (400 s in the example above) to be one measurement of the cyclotron frequency difference. We refer to those as the "long-time points". Each of these measurements was taken at a time $t_{\rm long}$, which in our analysis was taken to be the time of the start of the long PNP. Since we believe that most of the shot to shot variations in the phase difference (for a given $T_{\rm evol}$) are due to measurement noise, we smooth the phases for all the $T_{\rm evol}$ except the longest before performing the fitting procedure described above. We more heavily smooth the points at short $T_{\rm evol}$ since we have never seen any drift of the phase vs time in these data. For example for the list of $T_{\rm evol}$ given above, we would typically smooth the phases by averaging the nearest 5 points (which corresponds to about 2 hours) for all $T_{\rm evol}$ except 50 and 160 s, which we would smooth over 3 points. (We don't smooth the long-time points at all). Then, to account for the fact that all PNPs are not taken simultaneously, we perform a linear interpolation between the two nearest points to determine our best estimate of the phase for each time $T_{\rm evol}$ at each $t_{\rm long}$. Figure 4-3 shows the measured phases, the smoothed phases and the interpolated phases for a series of phases after $T_{\rm evol}$=150 s. Using the interpolated phases, we can then extract a cyclotron frequency difference for each long time point, with the fitting procedure ("phase unwrapping") described above. The result is a series of measurements of the cyclotron frequency difference vs time as shown in Fig. 4-4.

4.1.4 Cooling

For simultaneously measuring the cyclotron frequencies of two ions, we execute the entire PNP sequence described above with the trapping voltage adjusted such that the two axial frequencies are symmetrically located on each side of the resonant frequency of our detector (see Fig. 4-1). We refer to this as the symmetric configuration or voltage. In this configuration the damping time of the ions axial motion is very long, i. e., the axial motion damps very little during the 8 s "ringdown" that we record. For example, the damping time of an

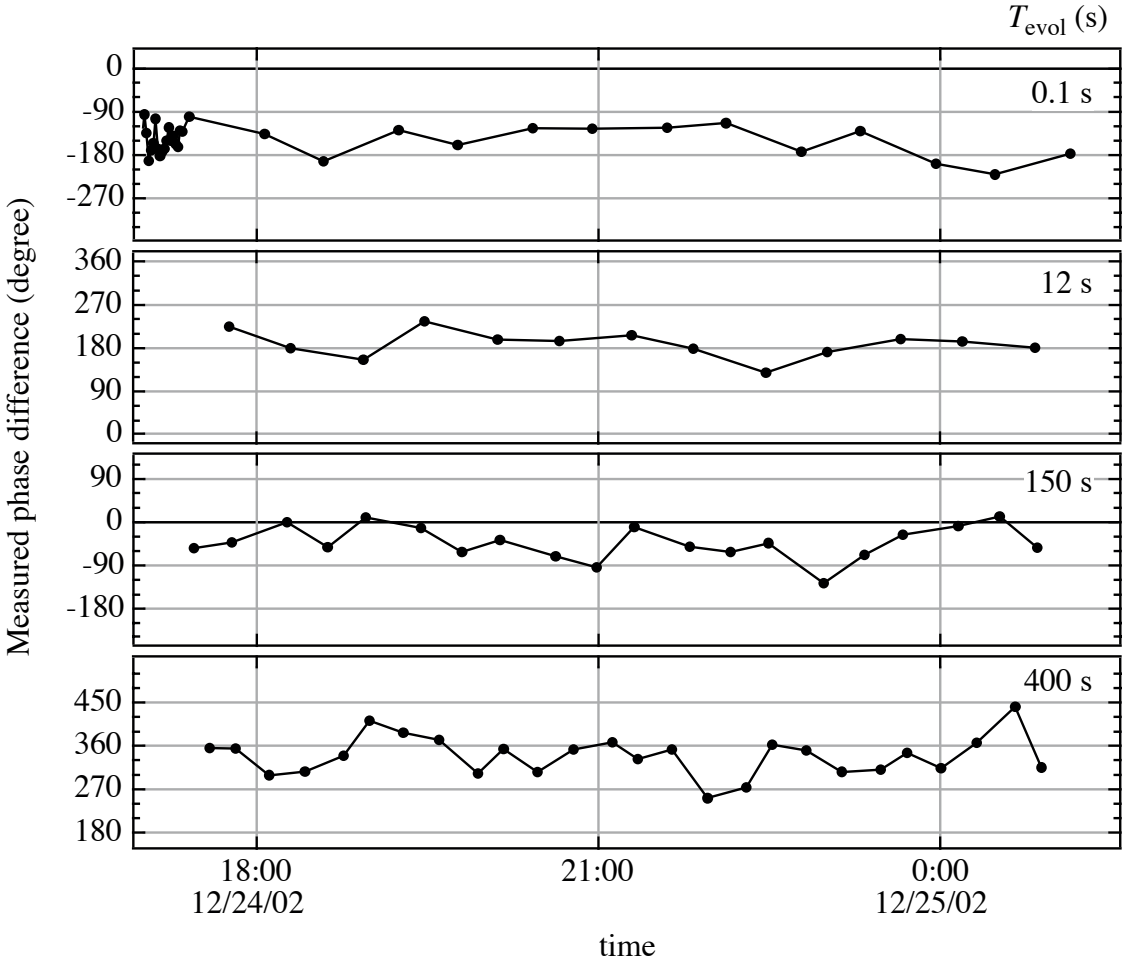

Figure 4-2: The raw data from a data set: the cyclotron phase differences (modulo 360°) accumulated after various T_{evol} as a function of time.

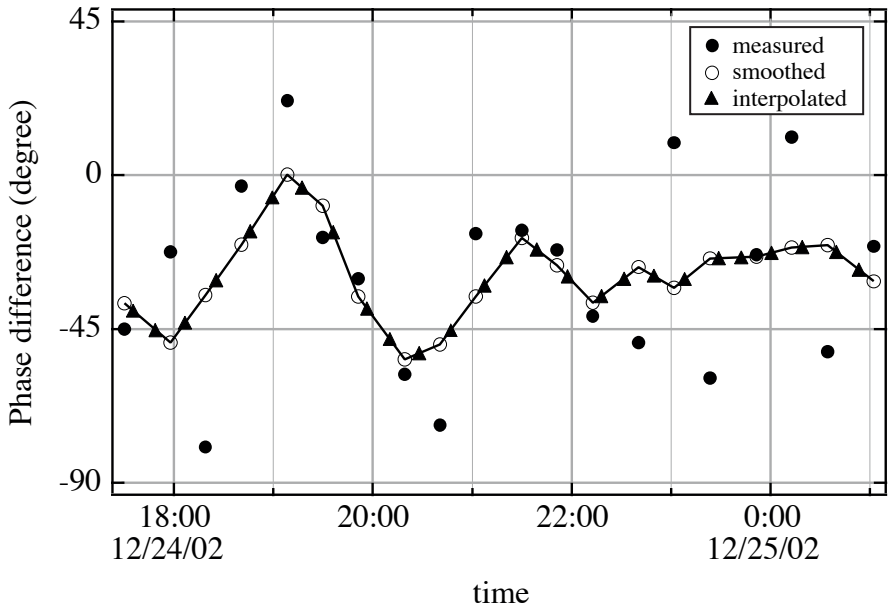

Figure 4-3: Typical sequence of measured cyclotron phase differences at a fixed $T_{\rm evol}$ (150 s here). Since this is not the longest $T_{\rm evol}$ for that data set, we first smooth the data ($\circ$), and then interpolate the smoothed phases to extract a value of the phase at that $T_{\rm evol}$ for each $t_{\rm long}$. The interpolated phases ($\blacktriangle$) are used for phase unwrapping.

$N_2{}^+$ ion 30 Hz away from the detector is about 150/,s (from Eq. 2.8). That helps us to precisely determine the axial frequency and phase of each ion since the signals don't chirp due to axial amplitude dependent frequency shifts. However between each PNP, we need to cool the axial and cyclotron modes of both ions to always start with the same initial conditions.

To efficiently cool the axial motion of each ion we change the ring voltage to alternately move each ion's $f_{\rm z}$ into resonance with the detector which damps its axial motion in a few seconds (on-resonance damping time $\tau \approx 1$ s).

If the axial motions remain cold during the evolution time of the PNP and the π-pulses are perfect, the cyclotron motions are already cooled at the end. But in practice we need to do extra cooling of the cyclotron modes before restarting another PNP. We do so by performing another π-pulse in the symmetric configuration to transfer any left over cyclotron motion into the axial mode. We can then cool again by alternately moving each ion into resonance. However, remember that the π-pulse swaps the axial and cyclotron motions and therefore, if either axial mode were not perfectly cooled before this extra π-pulse, the remaining motion would now be in the cyclotron mode. It is therefore preferable to perform yet another π-pulse and then cool the axial motions before starting the next PNP. Note that in the case where the dominant limitation is an imperfect cooling of the axial motion between the π-pulses, the coldest cyclotron modes are achieved after an even

number of extra cooling π-pulses. We typically used two cooling π-pulses (so the sequence after the PNP is: cool, π-pulse, cool, π-pulse, cool) and we found that this was reducing the cyclotron amplitude fluctuations to the thermal limit (see Sect. 5.6.1), but we may have been too conservative.

All this cooling between PNPs takes a significant amount of time. For the data presented in this thesis the entire cooling sequence took about 55 s, which represented on average about 35 % of the data taking time. Reducing the cooling time by a factor of two would largely eliminate it as a source of concern. One could do the cooling differently by for example modulating the ring to create sidebands of the ions on resonance with the detector and cooling them both simultaneously, but it's not obvious that a significant gain in speed could be obtained. With an extra frequency synthesizer available, one could also turn on the axial-cyclotron coupling continuously for each ion on-resonance, cooling the cyclotron and axial modes simultaneously. Since the phase coherence of that synthesizer is not important, its frequency could be changed back and forth for the two ions.

4.1.5 Frequency Synthesizers

In order to perform the simultaneous measurement outlined above, we need to be able to apply four distinct frequencies to the trap: the trap cyclotron frequencies of both ions (f_{ct0} and f_{ct1}) and the corresponding cyclotron coupling frequencies ($f_{\pi 0} = f_{\mathrm{ct0}} - f_{\mathrm{z0}}$ and $f_{\pi 1} = f_{\mathrm{ct1}} - f_{\mathrm{z1}}$). The simplest approach is to have four frequency synthesizers set to those four frequencies and combine both drives and both couplings together. One alternative would have been to set one synthesizer to the average f_{ct} and use another one to amplitude modulate its signal at the difference frequency $f_{\mathrm{ct1}} - f_{\mathrm{ct0}}$ (and do the same for the coupling frequencies)[†]. One advantage of that configuration is that none of the individual synthesizers frequencies is resonant with either ion in the trap. That might be preferable if one is concerned about leakage from the synthesizers into the trap. However we never had any indication of such a problem and so we did not bother with the extra complexity of this setup. If leakage were really a problem, one would ideally turn on the amplitude modulation only when the signals are applied to the trap. We did exactly that for the coupling frequencies as one of the many things we tested for in our search of the mysterious jumps in the CO^+ vs $N_2{}^+$ data. In order to keep everything phase coherent we set the synthesizer providing the modulation to "burst mode" (and we triggered it with the Cyc Pulse bit of the sequence).

4.1.6 Changing V_{gr} During the Evolution Time

When we started taking precision measurement data on $^{13}C_2H_2{}^+/^{14}N_2{}^+$, we observed (low statistics) that if the guard ring voltage V_{gr} was very far from $V_{\mathrm{gr}}^{\mathrm{optz}}$ during the Ringdown

[†]All our synthesizers have the ability to amplitude modulate their output based on the signal on an external input.

(see Sect. 5.2), the dynamics of the ions tended to be more unstable, i. e., the center-of-mass mode would "heat up" more quickly (in a few hours, sometimes very abruptly). We now have a better idea of why that might be: large anharmonicities could induce a relative change in the magnetron frequencies of both ions when the axial amplitudes are large (during the Ringdown), which could then result in a small phase advance (or lag) between the two individual magnetron motions. Angular momentum could thereby slowly diffuse into the center-of-mass mode [19]. From this model, the ideal $V_{\rm gr}$ to minimize this problem is not $V_{\rm gr}^{\rm optz}$, but the $V_{\rm gr}$ that makes $f_{\rm m}$ insensitive to the axial amplitude. Also, the range of acceptable deviations from the ideal $V_{\rm gr}$ should be a function of the distance between the ions $\rho_{\rm s}$, consistent with our observations ($\sim$3 mV at $\rho_{\rm s}$=1000 μm, but we never observed this problem for $\rho_{\rm s} \lesssim 800\,\mu$m).

To be able to take data at $V_{\rm gr}^{\rm optct}$ at large $\rho_{\rm s}$, we expanded our computer control system to be able to use two different guard ring voltage for the Evolution Time and the Ringdown. We typically set $V_{\rm gr}$ to the value we want during the Ringdown all the time, except between 15 ms after the cyclotron drive pulse of the PNP and 250 ms before the π-pulse. We don't know what is the RC time constant to change $V_{\rm gr}$ at the trap, but extensive testing has convinced us that it is at least reproducible from shot-to-shot. We add 2 s to all the evolution times in our list of PNPs to give plenty of time for the voltage to settle even for our shortest $T_{\rm evol}$. Since we measure only the slope of the phase vs $T_{\rm evol}$ this does not matter — as long as the magnetic field fluctuations do not affect the measured phase after 2 s, which we have verified.

4.2 Simultaneous Measurement Results

The result of running series of simultaneous two-ion PNPs with the technique described above is shown in Fig. 4-4. Each point corresponds to a series of PNP measurements that include one measurement with the longest evolution time. For each of these measurements, we converted the resulting phase difference between the two ions into a frequency difference using the other PNPs with smaller $T_{\rm evol}$ (see Sect. 4.1.3). Each data set typically consists of 5-15 hours of simultaneous PNPs leading to about 15-45 measurements of the cyclotron frequency difference.

The most striking feature of these data is the flatness of the cyclotron frequency difference in time. In other words, our measurement of the difference frequency is now completely independent of magnetic field.

Another impressive characteristic of Fig. 4-4 is that data can now be taken continuously. There are three main reasons why we can take so much more data now than we used to. First and foremost, we no longer need to wait until the electrical Boston subway is shut down for the night before we can take useful cyclotron frequency data. In Fig. 4-4, the gray bands indicate the 4-hour "quiet magnetic field windows" which were the only measurement

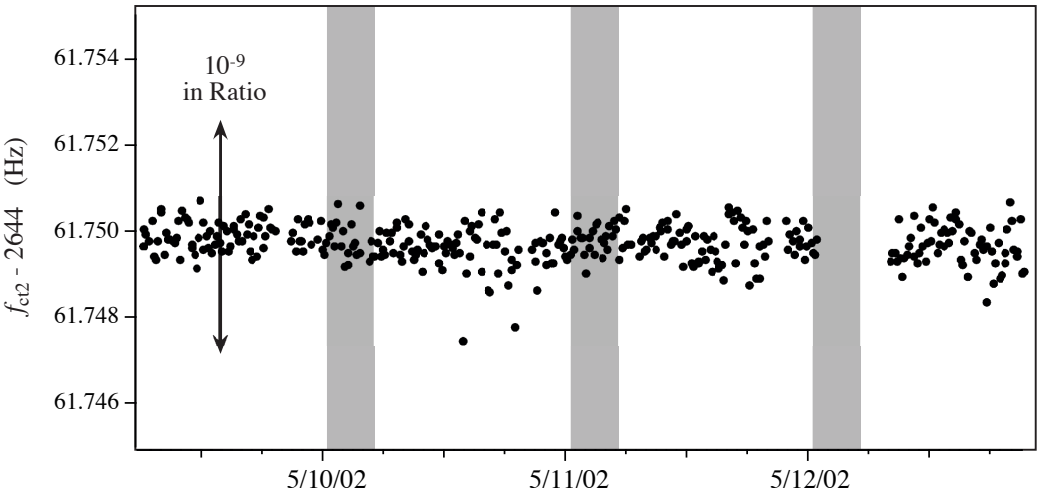

Figure 4-4: The trap cyclotron frequency difference f_{ct2} as a function of time for $^{13}C_2H_2{}^+/^{14}N_2{}^+$. The longest evolution time here was 200 s. Each point is the result of a linear fit of cyclotron phase difference vs T_{evol} using the phase unwrapping procedure. This is a exceptionally long data set (4 days!) that shows the stability of the measured frequency difference with time. The gray bands are the time windows during which the Boston subway is shut down and so measurements can be done using the single-ion alternating technique.

times available previously. By taking data 24 hours a day, we have gained a factor of 6 in run time. The second aspect which makes it possible to benefit from all this extra time is automation of the data taking process. The two-ion technique would never have been possible without the new computer control system (see Sect. 2.2), but it also streamlined the data taking process and made it more time efficient (it used to take 30 s to FFT and graph the ion's signal each time we looked at it!) Finally, we don't have to make new ions all the time. Once we have loaded a pair in the trap, we can perform measurements on it for many weeks. Together with the automation, this means that we can now take data without any operator in the laboratory. There are new aspects of the two ion data taking which require human intervention but those are required only every 5-10 hours and we have even taken some data sets for 20 hours straight without interruption. During our most intense data taking period, between 11/13 and 12/01/2002, these intervention were kept to about 30 minutes and we actually managed to take useful data about 75% of the time!

4.3 Deriving the Cyclotron Frequency Ratio

The previous section described how we make simultaneous measurements of the cyclotron frequencies of two ions in a Penning trap. Now we need to address the question of how to combine these frequencies to extract the mass ratio of the two ions, and how the precision of the final answer is affected by our uncertainty in each of these input parameters.

From every data set, we obtain a series of measurements of the difference between the cyclotron frequencies of the two ions in our trap as shown in Fig. 4-4. We then quote the mean[‡] as the final value of f_{ct2} for that data set, and use the standard deviation of the mean as the error σf_{ct2}. As described in Sect. 4.1.3, we also extract from the data f_{ct0} and f_{ct1} vs time, and we average these the same way. Finally, ω_{z0} and ω_{z1} are computed from the average of all the ringdowns. Thus for each data set we obtain the following pieces of information (in order of precision):

1. The difference between the two ions trap cyclotron frequencies ω_{ct2} (from unwrapping the phase difference ϕ_2 vs T_{evol}),
2. The trap cyclotron frequencies of each individual ion ω_{ct0} and ω_{ct1} (from unwrapping the individual phases ϕ_0 and ϕ_1 vs T_{evol}),
3. The axial frequencies of each individual ion ω_{z0} and ω_{z1} (from the recorded axial signals),

and an uncertainty associated with each of these frequencies from the standard deviation of the mean. The best way to combine these to obtain the free space cyclotron frequency ratio was described in [13]. We begin by defining the ratio

$$R \equiv \frac{m_1}{m_0} = \frac{1-\eta}{1+\eta} = \frac{\omega_{c0}}{\omega_{c1}} \,. \tag{4.1}$$

Because we *always* choose ion 0 to be the heaviest one (lowest axial and cyclotron frequencies), the above definition implies that $R < 1$. Note that the frequencies in the above definition are free space cyclotron frequencies. To relate these frequencies to the trap cyclotron frequencies that we measure, we write down for each ion the invariance theorem demonstrated by Brown and Gabrielse [2]:

$$\omega_{c0}^2 = \omega_{ct0}^2 + \omega_{z0}^2 + \omega_{m0}^2 \,, \tag{4.2a}$$

$$\omega_{c1}^2 = \omega_{ct1}^2 + \omega_{z1}^2 + \omega_{m1}^2 \,. \tag{4.2b}$$

The equations 4.2 apply to a harmonic trap with a pure quadratic potential but have been shown to remain valid for a non-cylindrical electrostatic field and in the presence of a misalignment between the electric and magnetic fields axes. Since we use two ions with very similar masses, we make the approximation

$$\omega_{m0} \approx \omega_{m1} \,. \tag{4.3}$$

[‡]We typically compute the unweighted average but we have tried using the weighted and the answer did not change.

We also define

$$\omega_{\mathrm{ct2}} \equiv \omega_{\mathrm{ct1}} - \omega_{\mathrm{ct0}} \ , \tag{4.4}$$

and, since the ions share the same electrostatic environment, the definition of R leads to

$$\omega_{\mathrm{z0}}^2 = R\omega_{\mathrm{z1}}^2 \ . \tag{4.5}$$

We can then subtract Eq. (4.2b) from Eq. 4.2a and use Eqs. (4.3), (4.4), and (4.5) to eliminate the frequencies of ion 0. The result is a quadratic equation for R:

$$R^2 - \left(\frac{\omega_{\mathrm{z1}}}{\omega_{\mathrm{c1}}}\right)^2 R - \left(1 - \left(\frac{\omega_{\mathrm{z1}}}{\omega_{\mathrm{c1}}}\right)^2 + \frac{\omega_{\mathrm{ct2}}(\omega_{\mathrm{ct2}} - 2\omega_{\mathrm{ct1}})}{\omega_{\mathrm{c1}}^2}\right) = 0 \ , \tag{4.6}$$

which we then solve to obtain

$$R_1 = \frac{1}{2}\left(\frac{\omega_{\mathrm{z1}}}{\omega_{\mathrm{c1}}}\right)^2 + \sqrt{\left(1 - \frac{1}{2}\left(\frac{\omega_{\mathrm{z1}}}{\omega_{\mathrm{c1}}}\right)^2\right)^2 + \frac{\omega_{\mathrm{ct2}}(\omega_{\mathrm{ct2}} - 2\omega_{\mathrm{ct1}})}{\omega_{\mathrm{c1}}^2}} \ . \tag{4.7}$$

In order to calculate R using the measured frequencies of ion 0 instead, we can make the substitutions $R \to 1/R$, $1 \to 0$, and $\omega_{\mathrm{ct2}} \to -\omega_{\mathrm{ct2}}$ in the above expression to find

$$R_0 = \left(\frac{1}{2}\left(\frac{\omega_{\mathrm{z0}}}{\omega_{\mathrm{c0}}}\right)^2 + \sqrt{\left(1 - \frac{1}{2}\left(\frac{\omega_{\mathrm{z0}}}{\omega_{\mathrm{c0}}}\right)^2\right)^2 + \frac{\omega_{\mathrm{ct2}}(\omega_{\mathrm{ct2}} + 2\omega_{\mathrm{ct0}})}{\omega_{\mathrm{c0}}^2}}\right)^{-1} \ . \tag{4.8}$$

Note the presence of the free space cyclotron frequencies ω_{c1} and ω_{c0} in (4.7) and (4.8) respectively. To calculate these, we use Eq. (4.2) with the added approximation that $\omega_{\mathrm{mi}} \approx \omega_{\mathrm{zi}}^2/2\omega_{\mathrm{cti}}$. Therefore, to obtain a value of the ratio R, it is sufficient to measure only ω_{ct2}, ω_{ct0} and ω_{z0} (or ω_{ct1} and ω_{z1}). Since we measure all five frequencies in each data set, we normally calculate both R_0 and R_1 from (4.8) and (4.7) and take the average as our final measure of R. Figure 5-11 (on page 88) shows the difference between R_0 and R_1 for the $^{13}C_2H_2{}^+$ vs $N_2{}^+$ data. The fact that they always agree ($\chi_\nu^2 = 1.15$) gives us further confidence in our data. (In particular it lessens the chance that we have missed a 2π in ω_{ct0} or ω_{ct1} since they are "phase unwrapped" independently.)

We now need to discuss the important question of errors. In order to derive the effect of our uncertainty in ω_{ct2} and $\omega_{\mathrm{ct0,1}}$ on R, we can expand the square root in (4.7) and keep only the leading order term containing ω_{ct2}:

$$R_1 \approx 1 + \frac{\omega_{\mathrm{ct2}}(\omega_{\mathrm{ct2}} - 2\omega_{\mathrm{ct1}})}{2\omega_{\mathrm{ct1}}^2} \approx 1 - \frac{\omega_{\mathrm{ct2}}}{\omega_{\mathrm{c1}}} \ , \tag{4.9}$$

where we have used $\omega_{\rm ct1} \approx \omega_{\rm c1}$ (good to $\sim$0.1 %). From this expression (and $\partial\omega_{\rm c1}/\partial\omega_{\rm ct1} = \omega_{\rm ct1}/\omega_{\rm c1}$), we find

$$\left.\frac{\Delta R}{R}\right|_{\omega_{\rm ct2}} \simeq -\frac{\omega_{\rm ct1}}{\omega_{\rm c1}}\,\frac{\Delta\omega_{\rm ct2}}{\omega_{\rm ct1}} \approx -\frac{\Delta\omega_{\rm ct2}}{\omega_{\rm ct1}} \qquad \text{and} \tag{4.10}$$

$$\left.\frac{\Delta R}{R}\right|_{\omega_{\rm ct1}} \simeq 2\eta\,\frac{\Delta\omega_{\rm ct1}}{\omega_{\rm ct1}}\,, \tag{4.11}$$

where 2η is the fractional mass difference between the ions. To obtain the effect of the uncertainty in $\omega_{\rm z1}$ on R, we need to include one more term in the square root expansion:

$$R_1 \approx 1 - \frac{\omega_{\rm ct2}}{\omega_{\rm c1}}\left(1 + \frac{1}{2}\left(\frac{\omega_{\rm z1}}{\omega_{\rm c1}}\right)^2\right)\,. \tag{4.12}$$

Using $\partial\omega_{\rm c1}/\partial\omega_{\rm z1} = \omega_{\rm z1}/\omega_{\rm c1}$ and keeping again only the leading order term, we find

$$\left.\frac{\Delta R}{R}\right|_{\omega_{\rm z1}} \simeq 2\eta\left(\frac{\omega_{\rm z1}}{\omega_{\rm c1}}\right)^2\frac{\Delta\omega_{\rm z1}}{\omega_{\rm z1}}\,. \tag{4.13}$$

Numerically, one can compare the above expressions for $\Delta R/R$ with the actual derivatives of (4.7) and find that they are valid to better than 0.5%. For $^{13}C_2H_2{}^+$ vs $N_2{}^+$, $2\eta \simeq 5.8\times10^{-4}$ and $\omega_{\rm z1}/\omega_{\rm c1} \simeq 1/21.2$. Thus if we want the mass ratio with a relative precision of 10^{-11}, we only need to measure $\omega_{\rm ct1}$ to 1.7×10^{-8} (or 78 mHz) and $\omega_{\rm z1}$ to 7.8×10^{-6} (or 1.6 Hz). The only quantity we need to measure very precisely is $\omega_{\rm ct2}$ (to $\sim 50\,\mu$Hz).

4.3.1 Approximations

In our derivation of the ratio (Eq. (4.7) above), we ignored the mass dependence of $\omega_{\rm m}$ (see Eq. (4.3)) and the effect of a misalignment between the electric and magnetic field axes. The effect of these approximations will now be estimated. We have also completely ignored the various frequency shifts due to ion-ion interactions, electric field anharmonicities, and magnetic field inhomogeneities, but that will be the topic of the next chapter.

From [2], the complete expressions for $\omega_{\rm z}$ and $\omega_{\rm m}$ in a Penning trap, allowing for tilt between the electric and magnetic field axes and also for non-cylindrical distortion of the electrostatic field are

$$\omega_{\rm z}^2 \simeq \left(\frac{eV_{\rm r}}{md^2}\right)^2\left(1 - \frac{3}{2}\sin^2\theta_{\rm m}\left(1 + \frac{\epsilon}{3}\cos 2\varphi_{\rm m}\right)\right) \qquad \text{and} \tag{4.14}$$

$$\omega_{\rm m} \simeq \frac{\omega_{\rm z}^2}{2\omega_{\rm c}}\sqrt{1-\epsilon^2}\left(1 - \frac{3}{2}\sin^2\theta_{\rm m}\left(1 + \frac{\epsilon}{3}\cos 2\varphi_{\rm m}\right)\right)^{-3/2}\,, \tag{4.15}$$

where $\theta_{\rm m}$ and $\varphi_{\rm m}$ describe the angle between the magnetic and electric fields axes (in spher-

ical coordinates) and ϵ accounts for a non-cylindrically symmetric trap (ϵ is the fractional difference between the principal axes). In contrast to what is described in [13], I find that the relation between the axial frequencies of the two ions Eq. (4.5) is not affected by Eq. (4.14) and is therefore exact[§]. In [2], Brown and Gabrielse showed that the invariance theorem (Eq. (4.2)) holds true to all orders even in the presence of the above imperfections. In other words, the trap cyclotron frequency also depends on ϵ, $\theta_{\rm m}$, and $\varphi_{\rm m}$ such that the free space cyclotron frequency is independent of these effects. Therefore, using the measured frequencies ("perturbed" by ellipticity and tilt) in Eq. (4.7) does not introduce any error in the ratio. However in practice we don't plug in a measured value of $\omega_{\rm m}$ but use $\omega_{\rm zi}^2/2\omega_{\rm cti}$ instead. The question is then: how big of an effect does that have on R? To simplify the answer, let us set $\epsilon = 0$ because it's effect is smaller than that of $\theta_{\rm m}$ and expand Eq. (4.15) for small $\theta_{\rm m}$. Let us also include the first mass-dependent term of $\omega_{\rm m}$ in the expansion for the ideal trap

$$\omega_{\rm m} = \frac{1}{2}\left(\omega_{\rm c} - \sqrt{\omega_{\rm c}^2 - 2\omega_{\rm z}^2}\right) \approx \frac{\omega_{\rm z}^2}{2\omega_{\rm c}}\left(1 + \frac{\omega_{\rm z}^2}{2\omega_{\rm c}^2} + \frac{\omega_{\rm z}^4}{2\omega_{\rm c}^4} + \ldots\right) . \tag{4.16}$$

The complete expression for $\omega_{\rm m}$ we need to consider is then

$$\omega_{\rm m} \simeq \frac{\omega_{\rm z}^2}{2\omega_{\rm c}}\left(1 + \frac{\omega_{\rm z}^2}{2\omega_{\rm c}^2}\right)\left(1 + \frac{9}{4}\sin^2\theta_{\rm m}\right) . \tag{4.17}$$

If we don't use the approximation $\omega_{\rm m0} \approx \omega_{\rm m1}$, then Eq. (4.6) becomes

$$R^2 - \left(\frac{\omega_{\rm z1}}{\omega_{\rm c1}}\right)^2 R - \left(1 - \left(\frac{\omega_{\rm z1}}{\omega_{\rm c1}}\right)^2 + \frac{\omega_{\rm ct2}(\omega_{\rm ct2} - 2\omega_{\rm ct1})}{\omega_{\rm c1}} + \frac{\omega_{\rm m1}^2 - \omega_{\rm m0}^2}{\omega_{\rm c1}^2}\right) . \tag{4.18}$$

If we treat the added term ($\propto \omega_{\rm mi}$) as a small perturbation and do not consider it's dependence on R, we find that it shifts the ratio by

$$\frac{\Delta R}{R} \approx \frac{\omega_{\rm m1}^2 - \omega_{\rm m0}^2}{2\omega_{\rm c1}^2} \approx \frac{-\eta}{4}\left(\frac{\omega_{\rm z1}}{\omega_{\rm ct1}}\right)^6\left(1 + \frac{9}{2}\sin^2\theta_{\rm m}\right) . \tag{4.19}$$

For our $^{13}C_2H_2{}^+$ vs $N_2{}^+$ data and $\theta_{\rm m} = 0.5°$, this gives a shift of -6×10^{-13} (and -2×10^{-16} for the term dependent on $\theta_{\rm m}$).

The other way in which $\omega_{\rm m}$ could have an effect on R is due to our approximation of the single-ion free-space cyclotron frequencies by

$$\omega_{\rm ci} = \sqrt{\omega_{\rm cti}^2 + \omega_{\rm zi}^2 + \left(\frac{\omega_{\rm zi}}{2\omega_{\rm cti}}\right)^2} . \tag{4.20}$$

The effect on the ratio due to this approximation (as opposed to using the measured $\omega_{\rm mi}$)

[§]To break the relation (4.5), one needs mass-dependent trap imperfections, which are pretty hard to imagine.

is

$$\frac{\Delta R}{R} = \frac{\partial R}{\partial \omega_{\mathrm{ci}}}\Delta\omega_{\mathrm{ci}} \simeq 2\eta\frac{\Delta\omega_{\mathrm{ci}}}{\omega_{\mathrm{ci}}} = 2\eta\left(\frac{\omega_{\mathrm{mi}}}{\omega_{\mathrm{ci}}}\right)^2\frac{\Delta\omega_{\mathrm{mi}}}{\omega_{\mathrm{mi}}}\,, \tag{4.21}$$

where we have used Eq. (4.13). Using again Eq. (4.17), we find two possible shifts of the ratio: one from the mass dependence of ω_{m}

$$\frac{\Delta R}{R} = \frac{\eta}{2}\left(\frac{\omega_{\mathrm{zi}}}{\omega_{\mathrm{ci}}}\right)^6 \qquad \sim 1\times10^{-12} \text{ for } {}^{13}\mathrm{C_2H_2}^+/\mathrm{N_2}^+\,, \tag{4.22a}$$

and the other from the misalignment of the electric and magnetic field

$$\frac{\Delta R}{R} = \frac{9\eta}{4}\left(\frac{\omega_{\mathrm{zi}}}{\omega_{\mathrm{ci}}}\right)^4\sin^2\theta_{\mathrm{m}} \qquad \sim 2\times10^{-13} \text{ for } \theta_{\mathrm{m}}{=}\ 0.5^\circ\,. \tag{4.22b}$$

Half of the shift from Eq. (4.22a) is cancelled by Eq. (4.19) so that we can safely conclude that ignoring the mass dependence of ω_{m} introduces an error in our expression for the ratio (Eq. (4.7)) of less than 1×10^{-12}. The effect of trap ellipticity and trap tilt is completely negligible as it is less than 2×10^{-13}. Of course in future work, these corrections could be added with no significant increase in complexity and do not represent a limitation of the two-ion technique.

4.4 Obtaining Neutral Mass Difference

In the previous section, we described how we convert the measurable frequencies into a free space cyclotron frequency ratio, which is simply the inverse mass ratio of the two ions we compared. But generally, the metrology community (CODATA group) compiles input data as mass differences between neutral atoms. To go from one to the other, we simply need to account for the mass and binding energy of the missing electron(s), and the molecular binding energies if molecules are involved. Since these are small corrections and they are known relatively well, we can generally do this without loss of precision. We will describe here the procedure for the case of ${}^{13}\mathrm{C_2H_2}^+$ vs $\mathrm{N_2}^+$ as an example. We write the measured ratio

$$R = \frac{M[\mathrm{N_2}^+]}{M[{}^{13}\mathrm{C_2H_2}^+]} = \frac{2M[\mathrm{N}] - M[\mathrm{e}] + \Delta E[\mathrm{N_2}^+]}{2M[{}^{13}\mathrm{C}] + 2M[\mathrm{H}] - M[\mathrm{e}] + \Delta E[{}^{13}\mathrm{C_2H_2}^+]}\,, \tag{4.23}$$

where $\Delta E[\mathrm{X}^+]$ is the amount of energy needed to form the ion X^+ from the individual atoms spaced an infinite distance apart. From (4.23) we obtain

$$2M[^{13}\mathrm{C}] + 2M[\mathrm{H}] - 2M[\mathrm{N}] = \\ \left(2M[^{13}\mathrm{C}] + 2M[\mathrm{H}] - M[\mathrm{e}]\right)(1-R) + \Delta E[{\mathrm{N}_2}^+] - R\Delta E[{}^{13}\mathrm{C}_2{\mathrm{H}_2}^+] \,. \quad (4.24)$$

Note that the masses of ^{13}C, H and the electron appearing on the right-hand side of the equation are multiplied by $(1-R)$ and so do not need to be known very precisely. We can use the masses from the 1995 atomic mass evaluation [20] with an error of typically 10^{-8}-10^{-9}.

The energy of formation $\Delta E[{}^{13}\mathrm{C}_2{\mathrm{H}_2}^+]$ (for example) is obtained by considering the reaction

$$ {}^{13}\mathrm{C}_2{\mathrm{H}_2}^+ \longrightarrow 2\,{}^{13}\mathrm{C}_{(\mathrm{g})} + 2\,\mathrm{H}_{(\mathrm{g})} - e^- + \Delta E \,. \quad (4.25)$$

ΔE is then obtained from the heats of formation at 0 K as follows

$$\Delta E[{}^{13}\mathrm{C}_2{\mathrm{H}_2}^+] = \Delta_\mathrm{f}H^0[{}^{13}\mathrm{C}_2{\mathrm{H}_2}^+] - 2\,\Delta_\mathrm{f}H^0[\mathrm{C}] - 2\Delta_\mathrm{f}H^0[\mathrm{H}] \quad (4.26a)$$

$$= \Delta_\mathrm{f}H^0[{}^{13}\mathrm{C}_2\mathrm{H}_2] + IE[{}^{13}\mathrm{C}_2{\mathrm{H}_2}^+] - 2\,\Delta_\mathrm{f}H^0[\mathrm{C}] - 2\,\Delta_\mathrm{f}H^0[\mathrm{H}] \quad (4.26b)$$

The heat of formation $\Delta_\mathrm{f}H^0$is defined as the increment in enthalpy associated with the formation of a given compound from its elements, with each substance in its thermodynamic standard state at the given temperature. The standard state is the most stable state at room temperature, e. g., $\mathrm{N}_{2(\mathrm{g})}$, $\mathrm{H}_{2(\mathrm{g})}$, or $\mathrm{C}_{(\mathrm{gr})}$. Note that we are using here the "ion convention" in which the heat of formation of the electron cancels out in calculating of the heat of formation of the ion (the same convention used by the NIST compilation). Whenever the heat of formation at 0 K of the ion $\Delta_\mathrm{f}H^0_{(+)\mathrm{ion,0K}}$ is found in the literature, we use it directly in Eq. (4.26a). Otherwise, the heat of formation of the ion is obtained by adding the heat of formation of the precursor neutral molecule to the adiabatic ionization energy (IE), and Eq. (4.26b) is used. The isotopic shifts are only a few tenths of a kJ/mol, or a few 10^{-12} u, and thus have a negligible effect on the ratio ($< 10^{-13}$).

All the heats of formation and ionization energies we needed to convert our ratios to neutral mass differences have been obtained from [21] and the NIST Chemistry WebBook [22], and are shown in Table 4.3. The neutral mass differences resulting from our mass ratio measurements are given in Table 7.2.

Table 4.2: Heats of formation and ionization energies (from [21] and [22]) used to calculate the energy of formation of the ions we trapped (Table 4.3). The number in parentheses indicates the uncertainty on the last digits.

Species	$\Delta_f H^0$ (kJ/mol)	Species	$\Delta_f H^0$ (kJ/mol)	Species	IE (eV)
$H_{(g)}$	216.035 (6)	$S_{(g)}$	274.73 (25)	C_2H_2	11.400 (2)
$C_{(g)}$	711.19 (46)	$SH_{(g)}$	136.5 (50)	N_2	15.581 (8)
$N_{(g)}$	470.82 (10)	$Si_{(g)}$	446. (8)	CO	14.0140(3)
$O_{(g)}$	246.79 (10)	$SiH_{(g)}$	374.9 (84)	S	10.360 (1)
$C_2H_{2(g)}$	235.76 (79)	$S^+{}_{(g)}$	1274.31 (40)	SH	10.422 (1)
$N_{2(g)}$	0. (0)	$SH^+{}_{(g)}$	1143.0 (40)	Si	8.1517(1)
$CO_{(g)}$	−113.81 (17)	$Si^+{}_{(g)}$	1232.2 (40)	SiH	7.90 (7)
$N_2{}^+{}_{(g)}$	1503.303 (40)	$SiH^+{}_{(g)}$	1140. (11)		

Table 4.3: Energies of formation ΔE of the ions we trapped (calculated from the values in Table 4.2), which we used to obtain neutral mass differences from our measurements. The conversion factor we used to convert kJ/mol into u is $1.112\,650\,06(12) \times 10^{-11}$. The number in parentheses indicated the uncertainty on the last two digits.

ion	ΔE (10^{-12} u)	$\Delta E/m$ (10^{-12})
$^{13}C_2H_2{}^+$	−5 772. (14)	−206.14 (49)
$^{14}N_2{}^+$	6 249.3 (23)	223.191 (81)
CO^+	3 119.4 (56)	111.41 (20)
$^{33}S^+$	11 121.8 (52)	337.03 (16)
$^{32}SH^+$	7 257. (45)	219.9 (14)
$^{29}Si^+$	8 748. (100)	301.6 (34)
$^{28}SiH^+$	5 321. (154)	183.5 (53)

Chapter 5

Sources of Error in the Two-Ion Technique

We now turn to the very important topic of errors in our measurements. In Sect. 4.2, we have seen the tremendous gain in precision that the two ion technique has allowed. By simultaneously measuring the cyclotron frequencies of the two ions, we have virtually eliminated the magnetic field fluctuations as a limitation in our mass comparisons (see Sect. 5.6). However, this came at the price of a more complex system. The main source of this new complexity is the Coulomb interaction between the ions, which could potentially perturb our measurements to a higher level than before. To keep these perturbations small, we keep the ions $\sim$1 mm away from each other. Unfortunately, this then requires the ions to be away from the center of the trap, and this makes our measurements a lot more sensitive to imperfections in our trapping electric and magnetic fields. The first two sections of this chapter discuss the effect of ion-ion interactions (Sect. 5.1) and trap imperfections (Sect. 5.2) on our measurements of the mass ratio. Both of these aspects could lead to large systematic errors in our measurements but we understand them well enough to quote a final relative uncertainty of about 10^{-11} as shown in Sect. 5.3.

How we analyzed our data and the effect of the various approximations we made (but excluding the effects of ion-ion interactions and trap anharmonicities) was discussed in Chapter 4. In Sect. 5.4 we will provide the details of the various corrections we had to make to our data before extracting the final ratio. Various tests we performed to ensure that our analysis was not biased will then be described in Sect. 5.5. This chapter will conclude with a discussion of the current limitations of our two-ion technique (Sect. 5.6).

5.1 Ion-Ion Coulomb Interactions

As we have seen in Sect. 3.2, the main effect of the Coulomb interaction between the ions is to couple the nearly-degenerate individual magnetron modes, leading to two new

magnetron normal modes of motion: the center-of-mass mode and the difference mode. In contrast, the differences between the two axial and between the two cyclotron frequencies keep these modes independent. However, we expect the frequencies to be perturbed by the extra electric field from the other ion. The topic of this section is to describe the experimental observations we have made of these perturbations and the limit they impose on our measurement of the ratio R. In the next two sub-sections, I will briefly summarize various expressions for these perturbations. For a derivation or explanation of these expressions, the reader is referred to [13] and James Thompson's thesis.

5.1.1 Ion-Ion perturbation of the axial frequency

In the limit of small axial amplitudes ($\langle z_{0,1}^2 \rangle \ll \rho_s^2$), the shift to the axial frequencies is given by Eq. (2.19) and (2.20) of [13]. The common shift of both axial frequencies and the shift in the difference are given respectively by

$$\Delta\omega_{z0} \simeq \Delta\omega_{z1} \simeq \frac{-\Omega_E^2}{2\,\bar{\omega}_z} \qquad \text{and} \tag{5.1}$$

$$\Delta\omega_{z2} \equiv \Delta(\omega_{z1} - \omega_{z0}) \simeq +\frac{\Omega_E^2}{\omega_z}\,\frac{\Omega_E^2}{2\eta\,\bar{\omega}_z{}^2}\,, \tag{5.2}$$

where Ω_E is the ion-ion Coulomb interaction expressed as an angular frequency — defined by Eq. (3.2) (page 41). As shown in Figures 5-1, the differential shift is very small but the common shift is easily observable. By comparing the axial frequency of a single ion in the trap before and after we load the second member of the pair, we have a rough idea of the separation between them. Also, when we bring the two ions closer tp each other with a series of short magnetron coupling pulses (Sect. 3.4) we can monitor ρ_s by watching the ions' axial frequencies. The observed shift usually agrees with Eq. (5.1) within about 20 % . It is not surprising that the agreement is not better since to measure the axial frequency, we usually excite the axial motion to an amplitude of $z \approx 500\,\mu m$, which is no longer insignificant compared to ρ_s. When that happens, the effective distance between the ions is larger and $\Delta\omega_z$ is reduced. James Thompson has numerically calculated an expression for $\Delta\omega_z$ as a function of z. It can be approximated to a good level by a Lorentzian:

$$\Delta\omega_z = \frac{\Delta\omega_z^0}{1 + \left(\frac{2}{\Gamma_0}\,\frac{z}{\rho_s}\right)^2} \qquad \text{where} \quad \Gamma_0 = 1.089 \;\; (\text{for } z_{z0} = z_{z1} = z)\,, \tag{5.3}$$

and $\Delta\omega_z^0$ is the common axial frequency shift in the limit of small axial amplitude given by Eq. (5.1). When we perform a simultaneous PNP to measure ω_{ct2} we observe ω_{z0} and ω_{z1} at a finite z, but what we need in our expression for the ratio (Eq. (4.8)) is ω_{z1} in the limit of $z = 0$. We use 5.3 to apply that correction. Of all the corrections we make this is the largest one but it's effect on the ratio is still less than 4×10^{-12} at all ion-ion separations

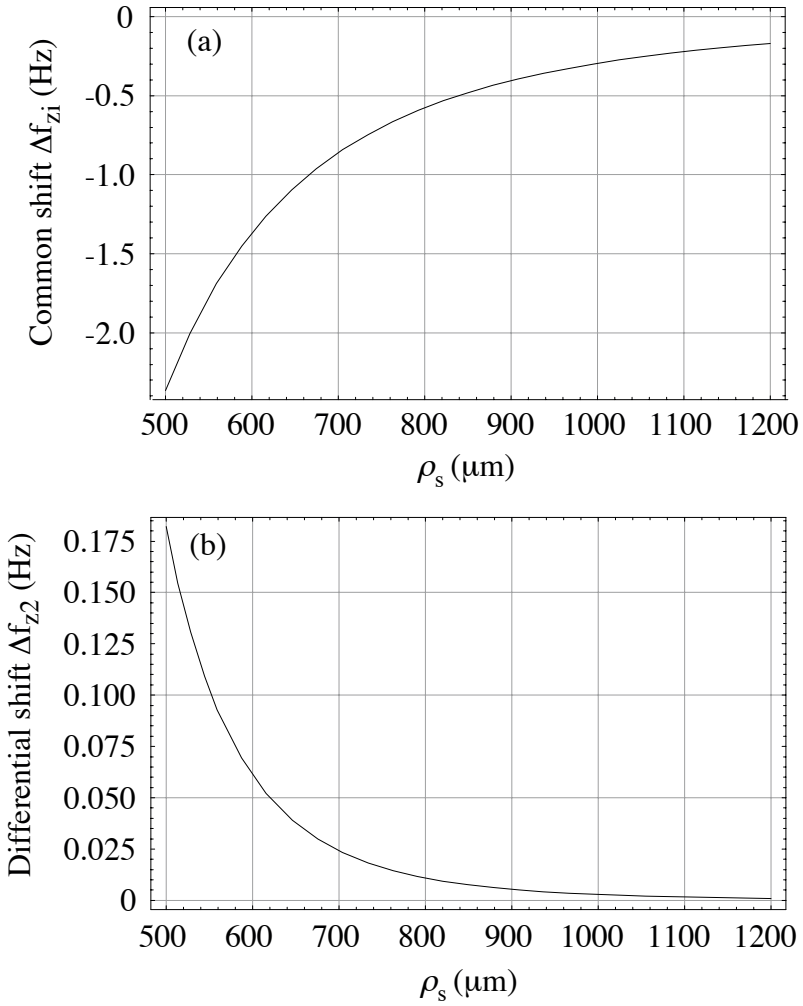

Figure 5-1: (a) Common shift of the axial frequencies Δf_{zi} and (b) differential shift Δf_{z2} due to ion-ion interactions as a function of ρ_{s} for ${}^{13}\mathrm{C}_2\mathrm{H}_2{}^{+}/{}^{14}\mathrm{N}_2{}^{+}$. Note that the differential shift is smaller than the common shift by about an order of magnitude and has the opposite sign.

(see Table 5.4).

5.1.2 Ion-Ion perturbation of the cyclotron frequency

We have considered two effects of ion-ion interactions on the cyclotron frequency. When linearizing the Coulomb force between two point charges, one gets a common shift of both trap cyclotron frequencies given by

$$\Delta\omega_{\mathrm{ct0}} = \Delta\omega_{\mathrm{ct1}} \simeq \frac{\Omega_{\mathrm{E}}^2}{2\,\bar{\omega_{\mathrm{ct}}}} \,. \tag{5.4}$$

Interestingly, for each ion independently the axial frequency shift due to ion-ion interactions (given by Eq. (5.1)) exactly cancels the shift in ω_{ct} common to both ions (Eq. (5.4)) when the free space cyclotron frequency is computed with the invariance theorem (Eq. (4.2)). The measured cyclotron frequency ratio is therefore completely independent of these. In the same approximation, the lowest order shift of the difference frequency between the ions is given by Eq. (4.11) in [13]:

$$\left.\frac{\Delta\omega_{\mathrm{c2}}}{\bar{\omega_{\mathrm{c}}}}\right|_{\mathrm{dyn}} = \frac{\Omega_{\mathrm{E}}^4}{4\eta\,\bar{\omega_{\mathrm{ct}}}^4} \,. \tag{5.5}$$

We call this the "dynamical effect" because it can be identified as the shift obtained from considering the two cyclotron modes as coupled oscillators whose frequencies repel each other. (On that basis, we conclude that the sign in [13] is wrong, and corrected it in the equation above.) This shift is very small however (1×10^{-13} for ${}^{13}C_2H_2{}^+/{}^{14}N_2{}^+$ at $\rho_{\mathrm{s}} = 800\,\mu\mathrm{m}$) and practically we don't have to worry about it.

The most important shift of the difference frequency ω_{ct2} comes from considering the ions as thin rings of uniform charge and keeping higher orders in the expansion of the Coulomb force. The shift obtained is then given by Eq. (4.14) in [13] (again we believe the expression has to be multiplied by -1, giving the expression below):

$$\left.\frac{\Delta\omega_{\mathrm{c2}}}{\bar{\omega_{\mathrm{c}}}}\right|_{\rho_{\mathrm{cimb}}} = -\left(\frac{9\,\Omega_{\mathrm{E}}^2}{16\;\bar{\omega_{\mathrm{c}}}^2}\right)\frac{\rho_{\mathrm{c1}}^2 - \rho_{\mathrm{c0}}^2}{\rho_{\mathrm{s}}^2} \,. \tag{5.6a}$$

If we define δ_{cyc} by expressing the two cyclotron radii as

$$\rho_{\mathrm{c0}} = \bar{\rho}_{\mathrm{c}}(1-\delta_{\mathrm{cyc}}) \quad \text{and} \quad \rho_{\mathrm{c1}} = \bar{\rho}_{\mathrm{c}}(1+\delta_{\mathrm{cyc}}) \,, \tag{5.6b}$$

then we obtain

$$\left.\frac{\Delta\omega_{\mathrm{c2}}}{\bar{\omega_{\mathrm{c}}}}\right|_{\rho_{\mathrm{cimb}}} = -\left(\frac{9\Omega_{\mathrm{E}}^2}{4\,\bar{\omega_{\mathrm{c}}}^2}\right)\left(\frac{\bar{\rho_{\mathrm{c}}}^2}{\rho_{\mathrm{s}}^2}\right)\delta_{\mathrm{cyc}} \propto \frac{1}{\rho_{\mathrm{s}}^5} \,. \tag{5.6c}$$

We see that there should be no perturbation of the cyclotron frequency difference ω_{ct2} if the two cyclotron radii ρ_0 and ρ_1 are equal, i. e., if $\delta_{cyc} = 0$. Experimentally, a systematic difference in the two cyclotron radii would arise from an imbalance in the initial cyclotron drives of the PNP sequence (see Sect. 4.1). We can imagine two possible sources for such an imbalance: 1) the two synthesizers used for the drives could output signals of different amplitudes even though they are nominally set to the same voltage, and 2) the small difference between the two drive frequencies combined with some frequency dependent transfer function in the electronics between the synthesizers and the trap. The first possibility can be simply tested by directly looking at the output of the two synthesizers on an oscilloscope. We can probe the transfer function in the electronics between the synthesizers by comparing the Rabi frequencies associated with the axial-cyclotron coupling for different ions (i. e., measuring the axial splitting from an Avoided Crossing). As we have seen in Sect. 2.4, the Rabi frequency is proportional to the strength of the electric field used to couple the axial and cyclotron modes. From these data, the maximum slope in the transfer function is about 0.40 MHz at 3 MHz (Fig. 3-5 in [11]). Since the difference between the cyclotron frequencies is about 2 kHz, that leads to an upper limit of $\delta_{cyc} = 0.0004$. Moreover, the cyclotron frequencies of $^{13}C_2H_2{}^+$ and $^{14}N_2{}^+$ (4.7 MHz) are very near the peak in our transfer function where the slope should be even less. However, we generally take δ_{cyc}=0.005 to be a conservative upper limit for the cyclotron radii imbalance due to these effects. The relative shift in ω_{ct2} should then be about 4×10^{-12} for $\rho_c = 70\,\mu m$ and $\rho_s = 600\,\mu m$. In the next section, we will see that purely from various simultaneous measurements on a pair of ions we obtain the limit $\delta_{cyc} \leq 0.013$. To be conservative, we use this larger value. The predicted shift in ω_{ct2} is still only 1.1×10^{-11} at $\rho_s = 600\,\mu m$, but grows very rapidly as the ions are brought closer (like ρ_s^{-5}).

5.1.3 Observed effect on ratio

Since the shift of ω_{ct2} due to ion-ion interactions scales like $1/\rho_s^5$, the obvious thing to do is look for this shift by bringing the ions closer together, hoping that we can observe a change in the ratio. Unfortunately, many things prevent us from taking data at $\rho_s \lesssim 600\,\mu m$.

First, there are small technical (but practically significant) issues. It becomes difficult to look at an ion on-resonance since its axial frequency chirps as it damps due to the varying ion-ion interaction shift (large at small ρ_s) (see Eq. (5.3)) . Also if the magnetron swapping period T_{swap} gets smaller than a few seconds ($T_{swap} = 4\,s$ at $\rho_s = 600\mu m$) , it becomes comparable to the ion's damping time and our PhaseLock system can't work. Our PhaseLock system (mentioned in Sect. 3.4 and discussed in detail in [19]) is crucial both for measuring the separation distance between the ions and cooling the center-of-mass magnetron mode. A more fundamental problem however arises from the shot to shot thermal fluctuations in the radii, which lead to a dramatic increase in cyclotron phase and frequency noise as the ions get closer (see Sect. 5.6.1).

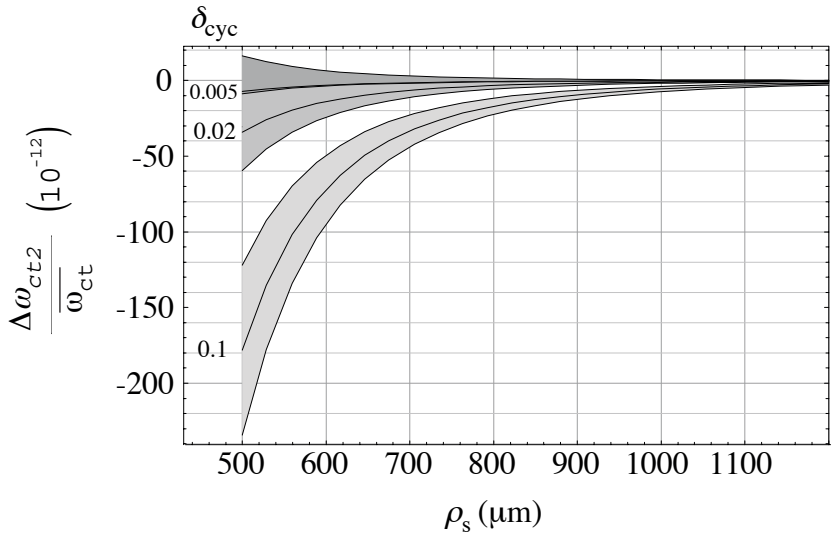

Figure 5-2: Fractional shift of the difference frequency $\omega_{\rm ct2}$ due to ion-ion interactions for various values of $\delta_{\rm cyc}$ as a function of $\rho_{\rm s}$. The gray bands represent an effective uncertainty on this shift due to a 5 % and 7 % uncertainty on $\rho_{\rm s}$ and $\rho_{\rm c}^{\rm cal}$ respectively.

In order to probe the effect of ion-ion interaction over the workable range of $\rho_{\rm s}$, we have done three experiments that will be described below.

Large Cyclotron Radii Imbalance

Since we can't make $\rho_{\rm s}$ smaller than 600 μm, another way to directly observe the effect of ion-ion interactions is to deliberately drive the ions to different cyclotron radii by adjusting the amplitudes on the cyclotron drive synthesizers to be unequal. The various curves in Fig. 5-2 show the expected $\Delta\omega_{\rm ct2}$ for different values of $\delta_{\rm cyc}$ as a function of $\rho_{\rm s}$. Experimentally, we only need to make a "differential" measurement of the difference in relative phase accumulated by the two ions during a long PNP and see how this varies as we change $\rho_{\rm c0}$ and $\rho_{\rm c1}$ independently. To make this clear, let's define the cyclotron phase (in degree) accumulated by ion 0 in a time $T_{\rm evol}$ as $\phi_0(T_{\rm evol})$ (and similarly for $\phi_1(T_{\rm evol})$). The relative phase accumulated between the ions in that time is

$$\phi_2(T_{\rm evol}) \equiv \phi_1(T_{\rm evol}) - \phi_0(T_{\rm evol}) \; . \tag{5.7}$$

Let us further define $\phi_2^+(T_{\rm evol})$ as the $\phi_2(T_{\rm evol})$ accumulated while $\rho_{\rm c0} = \bar{\rho}_{\rm c}(1+\delta_{\rm cyc})$ and $\rho_{\rm c1} = \bar{\rho}_{\rm c}(1-\delta_{\rm cyc})$. Similarly we define $\phi_2^-(T_{\rm evol})$ as the $\phi_2(T_{\rm evol})$ accumulated in the opposite situation, i. e., when $\rho_{\rm c0}$ is smaller ($\delta_{\rm cyc} < 0$). So a "Cyclotron Imbalance Data Set" consists of measuring the difference in $\phi_2^+(T_{\rm evol}) - \phi_2^-(T_{\rm evol})$. Practically, we also need to measure the short-time relative phase since it might be different for each configuration, i. e., we also want $\phi_2(T_{\rm evol}^{\rm s})$ where $T_{\rm evol}^{\rm s}$ is typically 0.1 s. Thus the measured quantity in these

experiments is the phase difference (in degree)

$$\Delta\phi_2|_{\rm imb} \equiv \phi_2^+(T_{\rm evol}^\ell) - \phi_2^+(T_{\rm evol}^{\rm s}) - \left(\phi_2^-(T_{\rm evol}^\ell) - \phi_2^-(T_{\rm evol}^{\rm s})\right) \ . \tag{5.8}$$

We convert $\Delta\phi_2|_{\rm imb}$ into a frequency shift using

$$\left.\frac{\Delta\omega_{\rm ct2}}{\bar{\omega_{\rm ct}}}\right|_{\rm imb} = \frac{\Delta\phi_2|_{\rm imb}}{360\,\bar{\omega_{\rm ct}}(T_{\rm evol}^\ell - T_{\rm evol}^{\rm s})} \ , \tag{5.9}$$

which should then correspond to twice the result given by Eq. (5.6c). We typically used $\delta_{\rm cyc} = 0.1$ since we are limited in the range of cyclotron radii we can use. If $\rho_{\rm c}$ is made too small, we lose signal-to-noise and the phase noise becomes prohibitively large. If it is made too large, the axial amplitude of each ion after the π-pulse could be large enough to briefly decouple the two magnetron motions and therefore heat up the magnetron center-of-mass mode. $T_{\rm evol}^\ell$ is typically chosen to be as large as possible to maximize precision (see Sect. 5.6.1), but such that the expected $\Delta\phi_2|_{\rm imb}$ is much less than 180° (say 60 °) to avoid phase unwrapping ambiguity. Table 5.1 and Figure 5-3 show the results of the two cyclotron imbalance data sets we took with ${}^{13}C_2H_2{}^+/{}^{14}N_2{}^+$, along with the predicted shift from Eq. (5.6c). The prediction also accounts for the small effect of trap imperfections on these measurements that can be calculated from the expressions given in Appendix A (the main contribution here is from the $C_6\rho_{\rm m}^2\rho_{\rm c}^2$ term).

The good agreement at $\rho_{\rm s} = 700\,\mu$m is reassuring in that in confirms our model for the effect of a mismatch in cyclotron orbit size on the difference cyclotron frequency (Eq. 5.6c). The disagreement at large separation ($-16.5(68) \times 10^{-12}$ or 2.4 σ) is not a major source of concern since we have made $\delta_{\rm cyc}$ about 10 times larger than the maximum it could be when we make precise measurements of $\omega_{\rm ct2}$. This means that if the measured discrepancy truly represents some effect that we did not account for, the size of this effect is less than 2×10^{-12} at $\rho_{\rm s} = 1060\,\mu$m when we take precise data; and less than 2.5×10^{-12} at $\rho_{\rm s} = 700\,\mu$m. This potential unknown effect is probably not related to ion-ion interactions since it does not seem to scale with $\rho_{\rm s}$. If anything, it could be related to trap imperfections. The conclusion is therefore that we have experimentally put an upper limit of 4×10^{-12} for any unknown effect dependent on the relative size of the two cyclotron orbits $\delta_{\rm cyc}$ in the range of $\rho_{\rm s}$ we are interested in (700–1000 μm).

Table 5.1: Results of the cyclotron imbalance data sets taken with $^{13}C_2H_2{}^+/^{14}N_2{}^+$. Both data sets were taken with $\delta_{cyc} = 0.1$. The last column gives the difference between the observed and predicted $\Delta\omega_{ct2}/\bar{\omega_{ct}}$.

Data Set	ρ_s (μm)	$\bar{\rho}_c$ (μm)	V_{gr}^t (mV)	T_{evol}^{ℓ} (s)	Observed $\frac{\Delta\omega_{ct2}}{\bar{\omega_{ct}}}$ (10^{-12})	Predicted $\frac{\Delta\omega_{ct2}}{\bar{\omega_{ct}}}$ (10^{-12})	Δ (10^{-12})
CycData_AQ	1060	66	-9.5	1000	-38.7(64)	-22.2(23)	-16.5(68)
CycData_BM	698	66	-3.5	400	-100(17)	-80(19)	-20(25)

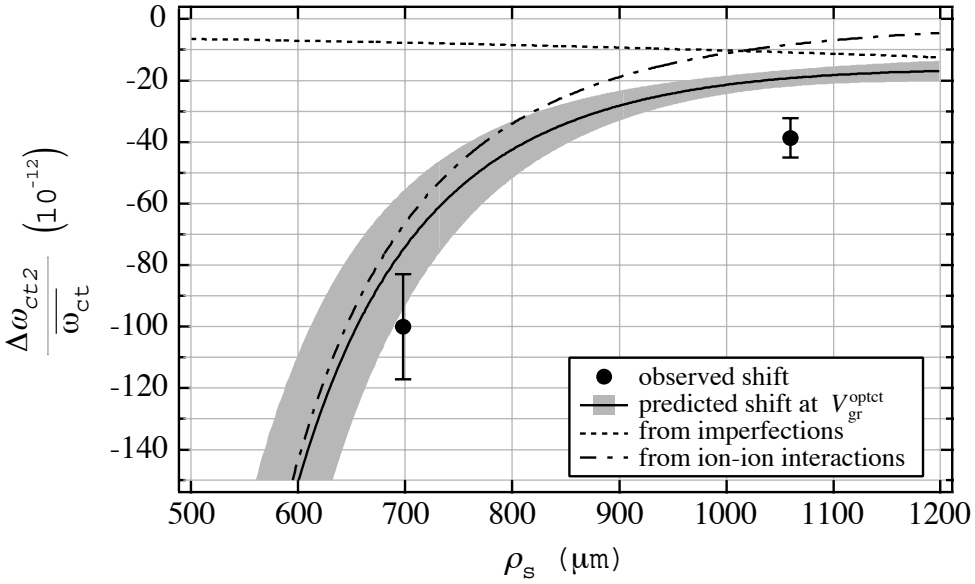

Figure 5-3: Observed and predicted shifts of ω_{ct2} in the ρ_c imbalance experiments. The imbalance was purposefully set to be as large as possible: $\delta_{cyc} = 0.1$. The dashed lines are the two contributions to the predicted shift from trap imperfections and ion-ion interactions. The solid line is the total predicted shift and the gray band around it represents our uncertainty of the prediction, which is dominated by our uncertainty in ρ_s (taken to be 5 %).

Varying $\bar{\rho}_c$

Now that we have showed that we understand the effect of a systematic cyclotron orbit mismatch δ_{cyc} on our measurement, we must try to estimate the size of δ_{cyc} in our experiment, i. e., when we make the amplitudes of the two cyclotron drives the same. As mentioned above, we previously assumed an upper limit of $\delta_{cyc} \simeq 0.01$ based on our knowledge of the transfer function and direct measurements of the amplitudes of the two signals coming out of the drive synthesizers. In this section and the next, we will describe how we measured δ_{cyc}, or at least experimentally put an upper limit on it with a pair of ions in the trap.

From Eq. (5.6c) we see that $\Delta\omega_{c2}/\,\bar{\omega}_c$ is also proportional to $\bar{\rho}_c{}^2$. To check for the presence of an imbalance in the cyclotron radii, we can therefore look for a dependence of the cyclotron frequency difference ω_{ct2} on $\bar{\rho}_c$. As in the previous section, we can take this kind of data in differential mode, i. e., by simply comparing the relative cyclotron phase accumulated after a time T_{evol} at two values of $\bar{\rho}_c$. Again we are limited in the minimum value of $\bar{\rho}_c$ we can use by signal-to-noise considerations, but here we can actually use a larger $\bar{\rho}_c$ than we used for the cyclotron imbalance data set. We avoid the large axial amplitude problem by doing a partial π-pulse, i. e., transferring only a fraction of the cyclotron motion into the axial mode for measuring the phase accumulated. This means that we need additional π-pulses to cool the cyclotron modes between each PNP. The extra amount of time required to completely cool the cyclotron motions eventually limits the size of the cyclotron motions we can use. (We obviously also need to keep $\rho_c < \rho_s/2$ to avoid the possibility of a hard collision). Typically, we alternate between setting $\rho_{c0} = \rho_{c1} = \bar{\rho}_c{}^{min}$ slightly smaller than what we normally use (by $\sim$20 %) and then setting $\rho_{c0} = \rho_{c1} = \bar{\rho}_c{}^{max} \sim \sqrt{2}\,\bar{\rho}_c{}^{min}$. For these "cyclotron average data sets", it is particularly important to also measure the relative phase difference after a short evolution time T^s_{evol} since the different π-pulse time clearly will introduce a phase offset between the ϕ_2 measured at $\bar{\rho}_c{}^{min}$ and the one measured at $\bar{\rho}_c{}^{max}$. The result of these measurements is then

$$\Delta\phi_2|_{avg} \equiv \Big(\phi_2(T^\ell_{evol}) - \phi_2(T^s_{evol})\Big)\Big|_{\bar{\rho}_c{}^{max}} - \Big(\phi_2(T^\ell_{evol}) - \phi_2(T^s_{evol})\Big)\Big|_{\bar{\rho}_c{}^{min}} . \tag{5.10}$$

When converted into a frequency shift (using Eq. (5.9)) this can then be plugged in Eq. (5.6c)

$$\frac{1}{360\,\bar{\omega}_{ct}(T^\ell_{evol} - T^s_{evol})}\,\Delta\phi_2|_{avg} = \left(\frac{9\Omega_E^2}{16\,\bar{\omega}_c{}^2}\right)\frac{4\delta_{cyc}\left((\,\bar{\rho}_c{}^{max})^2 - (\,\bar{\rho}_c{}^{min})^2\right)}{\rho_s^2}\,, \tag{5.11}$$

from which we can extract a value of δ_{cyc}. In this case, the effect of field imperfections is completely negligible. Expressing the result of these data sets as a measured δ_{cyc} allows us

Table 5.2: Results of the "cyclotron average data sets" with $^{13}C_2H_2{}^+/^{14}N_2{}^+$

Data Set	ρ_s (μm)	V_{gr}^t (mV)	$\bar{\rho}_c{}^{min}$ (μm)	$\bar{\rho}_c{}^{max}$ (μm)	$\Delta\phi_2\|_{avg}$ (10^{-12})	δ_{cyc}
CycData_AM	602	-5.4	66	94	−34(22)	−0.045(32)
CycData_AKb	602	-5.4	66	94	−52(45)	0.069(63)
CycData_BO	694	-9.4	66	94	−10(16)	−0.028(45)
CycData_BL	698	-3.5	66	94	−21(22)	−0.069(73)
CycData_AW	1066	-7.1	66	94	3(17)	−0.011(349)
Weighted Avg					−9.6(90)	−0.028(20)

to directly compare them with each other. Table 5.2 gives the results of all the data sets varying the average cyclotron radii taken with $^{13}C_2H_2{}^+/^{14}N_2{}^+$. The weighted average of all the data gives $\delta_{cyc} = -0.028(20)$, which is not as precise as the result obtained from the test described in the next section.

Swapping drive synthesizers

Another test we can do to probe for the presence of an imbalance in cyclotron radii is simply swap the role of the two synthesizers we use for the initial cyclotron drive of the two ions[†]. If there is any difference in amplitude calibration between the two synthesizers, we should obtain a different answer since this effectively flips the sign of δ_{cyc}. We cannot do this in differential mode however because it would involve changing the frequencies of the synthesizers and that would break the phase coherence across consecutive PNPs. We have to compare the ratio obtained from two separate data sets taken with identical experimental parameters (ρ_s, V_{gr}^t, ρ_c, etc.) but where the roles of the two cyclotron drive synthesizers have been reversed. Again, we extract from the observed difference a limit on δ_{cyc}[‡]. There are three data sets we can use for this test in our $^{13}C_2H_2{}^+/^{14}N_2{}^+$ data (at $\rho_s = 700\,\mu m$ and $V_{gr}^t = -9.5\,mV$). Averaging 'CycData_BJ' and '_BK' together and subtracting '_BN', we find a difference of $-6(13) \times 10^{-12}$ in the ratio, which corresponds to $\delta_{cyc} = +0.008(17)$.

Conclusion

In conclusion, we have experimentally confirmed that we understand the effect of a systematic imbalance between the two cyclotron orbit sizes (the dominant perturbation of the difference frequency due to the ion-ion Coulomb interaction) at the 4×10^{-12} level.

When we combine the estimates of δ_{cyc} from the previous two sections, we obtain $\delta_{cyc} = -0.003(13)$. In our analysis, we use $\delta_{cyc} = 0 \pm 0.013$, a conservative value given that we had

[†]Typically HP1 and HP2.

[‡]Caution: Remember that $\Delta R \propto -\Delta\omega_{ct2}$ to get the sign right.

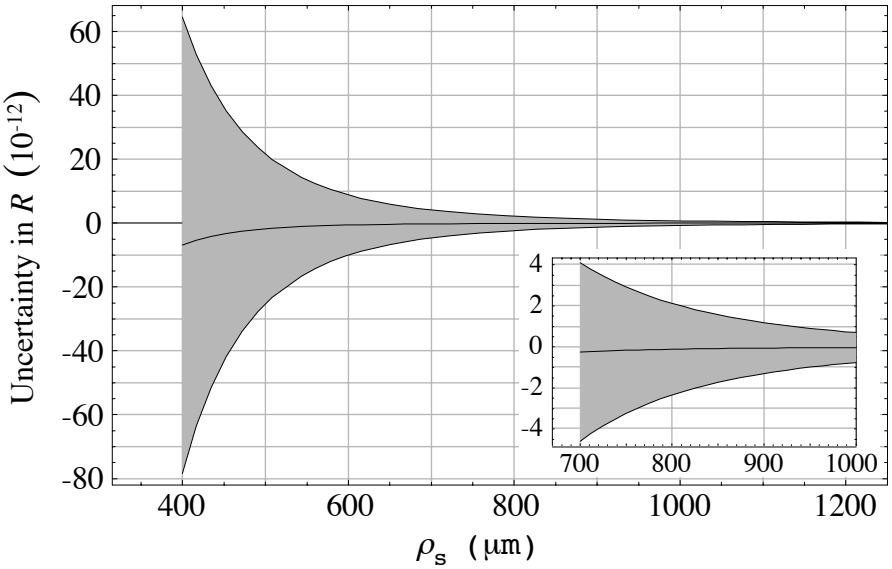

Figure 5-4: Uncertainty band on R vs ρ_s due to ion-ion interactions. δ_{cyc} is taken to be 0.000(13), as measured experimentally from the data sets where we varied the average cyclotron radii and exchanged the role of the two drive synthesizers. For very small ρ_s, ω_{ct2} is slightly shifted down because of the contribution from the dynamical effect given by Eq. (5.5) (remember Eq. (5.15)). The only source of uncertainty is $\sigma\delta_{cyc}$ since $\delta_{cyc} = 0$.

estimated previously that is should not be bigger than 0.005 by directly measuring the size of the cyclotron drive signals going to the trap and the transfer function. With $\delta_{cyc} = 0.013$, the shift from ion-ion interaction due to cyclotron radii imbalance is less than 4×10^{-12} at $\rho_s = 700\,\mu m$. Figure 5-4 shows the uncertainty band on our measurement of the ratio due to ion-ion interactions for $\delta_{cyc} = 0 \pm 0.013$.

5.2 Trap Imperfections

Even though the main concern in our two ion technique is the Coulomb interaction between the ions, we have spent a lot more time worrying about the effect of electrostatic anharmonicities and magnetic field inhomogeneities on the measured ratio. There are many reasons for this. First, there is not much we can do about the ion-ion interactions except move the ions apart, which moves them away from the center of the trap into a region where the effect of trapping field imperfections is a lot more important. Experimentally, it is also easier to work with a pair of ions when the separation between them is greater than about $700\,\mu m$ (for $m/q \approx 30$), for reasons described in Sect. 5.1.3. To address the problem of the sensitivity of our measured ratio to trapping field imperfections, we characterized our trapping fields very well (see Sect. 2.5). Based on this knowledge, we optimized C_4 to make our measurements insensitive to these imperfections as we now describe.

The individual frequencies of each ion are shifted by the field imperfections as described in Appendix A. Since the measured frequency ratio in the two-ion technique is insensitive to $\omega_{\rm m}$ (see Sect. 4.3), we are mostly concerned about $\omega_{\rm ct}$ and $\omega_{\rm z}$. The shifts of these two frequencies due to electric field anharmonicities (up to C_6) and magnetic field inhomogeneities (up to B_4) are

$$\frac{\Delta\omega_{\rm z}}{\omega_{\rm z}} = \left(-\frac{3}{2}\frac{C_4}{d^2}+\frac{1}{4}\frac{B_2}{B_0}\right){\rho_{\rm m}}^2+\left(\frac{45}{16}\frac{C_6}{d^4}-\frac{3}{8}\frac{B_4}{B_0}\right){\rho_{\rm m}}^4\,, \tag{5.12}$$

$$\frac{\Delta\omega_{\rm ct}}{\omega_{\rm ct}} = \left(3\frac{\omega_{\rm m}}{\omega_{\rm c}}\frac{C_4}{d^2}-\frac{1}{2}\frac{B_2}{B_0}\right){\rho_{\rm m}}^2+\left(-\frac{45}{8}\frac{\omega_{\rm m}}{\omega_{\rm c}}\frac{C_6}{d^4}+\frac{3}{8}\frac{B_4}{B_0}\right){\rho_{\rm m}}^4\,. \tag{5.13}$$

For simplicity, only the dependence on $\rho_{\rm m}$ is given above since $\rho_{\rm m}$ is necessarily large in the two-ion method — during $T_{\rm evol}$, $\rho_{\rm m}\approx 500\mu$m, $\rho_{\rm c}\lesssim 75\mu$m and $z\lesssim 50\mu$m so that the effect of $\rho_{\rm c}$ and z is a shift of $\omega_{\rm ct2}$ of less than 2×10^{-12} independent of $\rho_{\rm s}$. (When calculating perturbations for our measurements, we also included the effect of finite $\rho_{\rm c}$ and z.)

If the two ions had the same magnetron radii, the shift given by Eq. (5.13) for both ions would exactly cancel when we measure the difference between the two trap cyclotron frequencies $\omega_{\rm ct2}\equiv\omega_{\rm ct1}-\omega_{\rm ct0}$. But as we have seen in Sect. 3.2, because of the finite mass difference between the ions, their rms magnetron radii are different:

$$\rho_{\rm m0}=\frac{\rho_{\rm s}}{2}(1+\delta_{\rm mag})\quad\text{and}\quad\rho_{\rm m1}=\frac{\rho_{\rm s}}{2}(1-\delta_{\rm mag})\quad\text{where}\quad\delta_{\rm mag}=\frac{\eta\,{\bar\omega_{\rm m}}^2}{2\Omega_{\rm E}^2}\,. \tag{5.14}$$

Remember from Eqs. (3.1) and (3.2) that 2η is the fractional mass difference between the ions and $\Omega_{\rm E}$ is the strength of the Coulomb interaction in frequency units. For scale, $\delta_{\rm mag}\approx 1.0\,\%, 2.0\,\%$ and $3.5\,\%$ at $\rho_{\rm s}=720, 900$ and $1100\,\mu$m for ${}^{13}C_2H_2{}^+$ vs $N_2{}^+$. To calculate the effect of field imperfections on $\omega_{\rm ct2}$, we simply differentiate Eq. (5.13) and substitute $\Delta\rho_{\rm m}\to-2\rho_{\rm m}\delta_{\rm mag}$. Using Eq. (3.2) and $\rho_{\rm m}\to\rho_{\rm s}/2$ we obtain a function of $\rho_{\rm s}$ only. Finally, since we are ultimately interested in the mass ratio R, we use the definition Eq. (4.1) which implies that

$$R=1-\frac{\omega_{\rm c2}}{\omega_{\rm c1}}\approx 1-\frac{\omega_{\rm ct2}}{\bar\omega_{\rm ct}}\,, \tag{5.15}$$

to obtain (in CGS units):

$$\frac{\Delta R}{R}\simeq-\frac{\Delta\omega_{\rm ct2}}{\bar\omega_{\rm ct}}=\frac{\bar m\eta}{256\,e^2}\left(\frac{\omega_{\rm z}}{\omega_{\rm ct}}\right)^4\left(\left(48\,\frac{C_4}{d^2}\omega_{\rm z}^2-16\,B_2\,{\omega_{\rm ct}}^2\right)\rho_{\rm s}^5-\left(45\,\frac{C_6}{d^4}\omega_{\rm z}^2+6\,B_4\,{\omega_{\rm ct}}^2\right)\rho_{\rm s}^7\right)\,. \tag{5.16}$$

Note the very strong scaling with $\rho_{\rm s}$. Experimentally, we can vary C_4 by changing the

voltage applied to the guard ring electrode of our trap. Thus we express C_4 in terms of measurable and controllable parameters:

$$C_4 = \frac{D_4}{V_\mathrm{r}} \left(V_\mathrm{gr} - V_\mathrm{gr}^\circ\right) = \frac{D_4}{V_\mathrm{r}} \left(\widetilde{V}_\mathrm{gr} - \widetilde{V}_\mathrm{gr}^\circ\right) = \frac{D_4}{V_\mathrm{r}} V_\mathrm{gr}^\mathrm{t} \,, \tag{5.17}$$

where

$$D_4 \equiv \frac{\partial C_4}{\partial V_\mathrm{gr}} V_\mathrm{r} \,. \tag{5.18}$$

V_gr° is the voltage that we have to apply on the guard ring to set $C_4 = 0$ and V_gr^t is what we call the "guard ring tuning". The "guard ring difference" $\widetilde{V}_\mathrm{gr}$ is defined as

$$\widetilde{V}_\mathrm{gr} \equiv \frac{V_\mathrm{r}}{2} - V_\mathrm{gr} \,, \tag{5.19}$$

and similarly for $\widetilde{V}_\mathrm{gr}^\circ$. Note that in all the expressions above, the voltages are taken to be positive (even though they are negative in reality since we trap positive ions). The trap geometry was chosen so that C_4 should be zero when $V_\mathrm{gr} = V_\mathrm{r}/2$ or $\widetilde{V}_\mathrm{gr} = 0$. We believe the main reason why $\widetilde{V}_\mathrm{gr}^\circ$ is non-zero is that we have charge patches which create a constant C_4 independent of V_r. Thus as our detector's resonant frequency changes from day to day, so does V_r, and hence a fixed C_4 then corresponds to a different V_gr. But $\widetilde{V}_\mathrm{gr}$ stays constant and that is why it is a better parameter to keep track of.

Figure 5-5 shows the shift in the cyclotron frequency difference ω_ct2 as a function of ρ_s, calculated from Eq. (5.16) and using the numerical values in Table 2.4. Also shown are the individual contributions to the total shift from C_4 (for $V_\mathrm{gr}^\mathrm{t} = +1\,\mathrm{mV}$), C_6, B_2, and B_4. It is clear from the figure that the predicted shift is important (1.9×10^{-10} at ρ_s= $1000\,\mu\mathrm{m}$) and dominated by the effect of C_6 at large ρ_s. However, we can adjust V_gr^t so that the effect of C_4 cancels out all the other contributions at a given ρ_s. In other words, C_4 can be such that the trap cyclotron frequency of one ion at $\rho_\mathrm{m} = \rho_\mathrm{s}/2$ is, to first order, independent of ρ_m. We call the voltage V_gr^t corresponding to this situation the "optimal f_ct guard ring" $V_\mathrm{gr}^\mathrm{optct}$. Similarly, there is an "optimal f_z guard ring" $V_\mathrm{gr}^\mathrm{optz}$ for which the *axial* frequency of one ion at $\rho_\mathrm{m} = \rho_\mathrm{s}/2$ is independent of ρ_m. The expressions for $V_\mathrm{gr}^\mathrm{optct}$ and $V_\mathrm{gr}^\mathrm{optz}$ are given below:

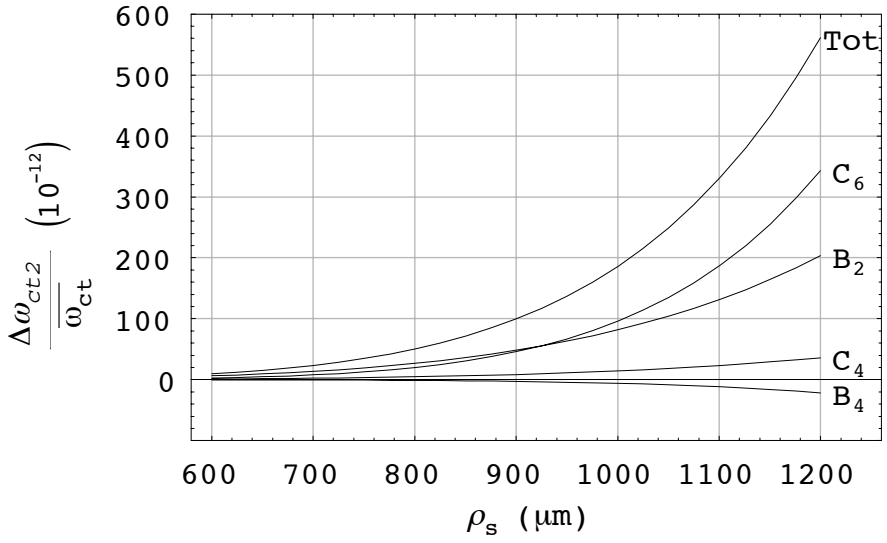

Figure 5-5: Fractional shift in the ratio R as a function of ρ_s due to field imperfections, calculated from Eq. (5.16) for the pair $^{13}C_2H_2{}^+$ vs $N_2{}^+$. The contribution from each term is also shown. The shift due to C_4 is calculated for $V_{gr}^t = +1\,\mathrm{mV}$. Clearly the perturbations are large if V_{gr}^t is kept fixed.

$$V_{gr}^{optct} = \frac{B_2\, d^2\, {\omega_{ct}}^2\, V_r}{3\, D_4\, {\omega_z}^2} + \frac{15\, C_6\, V_r}{16\, d^2\, D_4}\left(4{\rho_c}^2 + {\rho_s}^2 - 8z^2\right) - \frac{B_4\, d^2\, {\omega_{ct}}^2\, V_r}{8\, D_4\, {\omega_z}^2}\left(8{\rho_c}^2 + {\rho_s}^2 - 8z^2\right)\,, \tag{5.20}$$

$$V_{gr}^{optz} = \frac{B_2 d^2 V_r}{6\, D_4} + \frac{15 C_6 V_r}{16 d^2\, D_4}\left(8{\rho_c}^2 + {\rho_s}^2 - 4z^2\right) - \frac{B_4 d^2\, V_r}{8\, D_4}\left({\rho_s}^2 - 2z^2 + 4{\rho_c}^2\left(2\frac{\omega_{ct}^2}{\omega_z^2} + 1\right)\right). \tag{5.21}$$

Experimentally, we can measure R as a function of ρ_s, and if we always set the guard ring voltage to V_{gr}^{optct} (different for each ρ_s), the answer should always be the same. However, the uncertainties in our knowledge of D_4, $\widetilde{V}_{gr}^{\circ}$, C_6, B_2, B_4, and ρ_s limit our ability to do this perfectly and thus lead to an "uncertainty band", which grows very quickly with ρ_s. Figure 5-6 shows V_{gr}^{optct} and V_{gr}^{optz} as a function of ρ_s and their uncertainties, and in Figure 5-7 we plot the uncertainty band for our measurement of R (and each individual contribution) resulting from this imperfect knowledge of V_{gr}^{optct}. Both of these plots are for a $^{13}C_2H_2{}^+/^{14}N_2{}^+$ pair and the uncertainties in our trap parameters given in Table 2.4. Recall from Sect. 2.5 that our empirical measurements of D_4, $\widetilde{V}_{gr}^{\circ}$, C_6, B_2, B_4 all depend on our amplitude calibration ρ_c^{cal}, but we like to keep that dependence separate. That is why there is a curve labeled ρ_c^{cal} in Fig. 5-7. Note that the errors in the uncertainty band for various ρ_s are correlated. In other words, if the value of $\widetilde{V}_{gr}^{\circ}$ were to change by $+2\,\mathrm{mV}$, all our

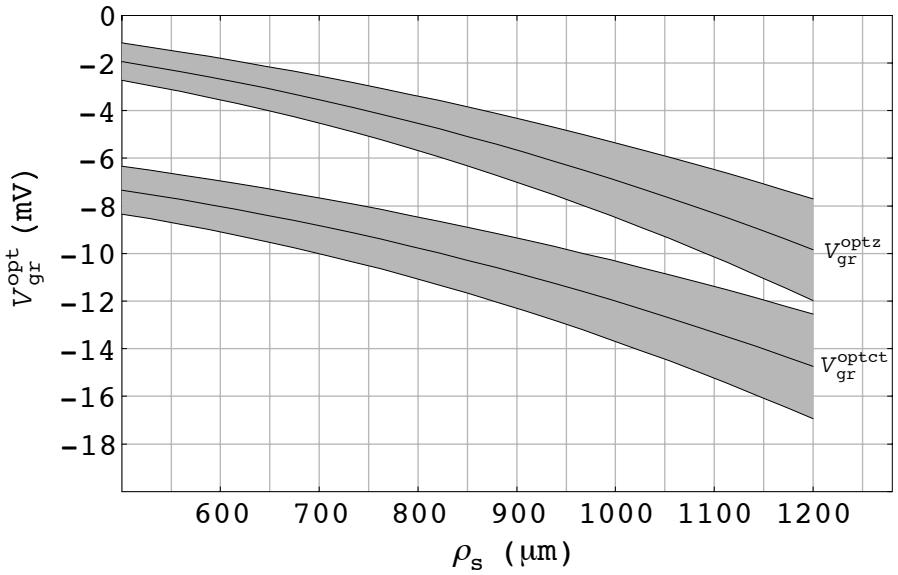

Figure 5-6: $V_{\rm gr}^{\rm optct}$ and $V_{\rm gr}^{\rm optz}$ as a function of $\rho_{\rm s}$. The plotted band are the 1σ uncertainties on these voltages with contributions from σD_4, $\sigma\widetilde{V}_{\rm gr}^{\circ}$, σC_6, σB_2, σB_4, $\sigma\rho_{\rm s}$ and $\sigma\rho_{\rm c}^{\rm cal}$.

measurements of $\omega_{\rm c2}$ vs $\rho_{\rm s}$ would move in the same direction. Therefore these uncertainties won't average out as we take more points.

In principle, measuring R at $V_{\rm gr}^{\rm optct}$ and showing that it does not vary with $\rho_{\rm s}$ is all we need to obtain an accurate measure of R. However to further confirm that we understand the effect of trap imperfections on R, we also measured it as a function of $V_{\rm gr}^{\rm t}$ at a few fixed $\rho_{\rm s}$ (see Fig. 5-8). From Eqs. (5.16) and (5.17), we can predict the slope $\partial R/\partial V_{\rm gr}^{\rm t}$ to be

$$\frac{\partial R}{\partial V_{\rm gr}^{\rm t}} = -\frac{\partial \omega_{\rm ct2}}{\partial V_{\rm gr}^{\rm t}} = \frac{3\ \bar{m}\,\eta}{16\,d^2\,{\rm e}^2}\ \frac{D_4}{V_{\rm r}}\ \frac{{\omega_{\rm z}}^6}{{\omega_{\rm ct}}^4}\ \rho_{\rm s}^5\ . \tag{5.22}$$

The solid curve in Fig. 5-9 is calculated from Eq. (5.22) (with associated uncertainty from σD_4, $\sigma\rho_{\rm s}$ and $\sigma\rho_{\rm c}^{\rm cal}$) and the points represent the measured slopes at various $\rho_{\rm s}$ extracted from the data shown in Fig. 5-8. The agreement is very good; the χ_ν^2 of the differences between measurements and theory is 1.4. This is a very powerful confirmation that our model for the dynamics of the two ions in the trap is correct (especially our expression for $\delta_{\rm mag}$), that we know the field imperfections in our trap, and that we understand their effect on the ions' frequency ratio at the level below the 10^{-11} level.

5.3 Obtaining the Final Mass Ratio

Between 10/18 and 11/30/2002, we took about 35 data sets to measure the ratio R for a ${}^{13}C_2H_2{}^+/{}^{14}N_2{}^+$ pair in the trap. Each data set consisted of typically 5-15 hours of repeated measurements of $\omega_{\rm ct2}$ in a fixed configuration ($\rho_{\rm s}$, $V_{\rm gr}^{\rm t}$, $\rho_{\rm c}$) (see Sect. 4.3). Some of these

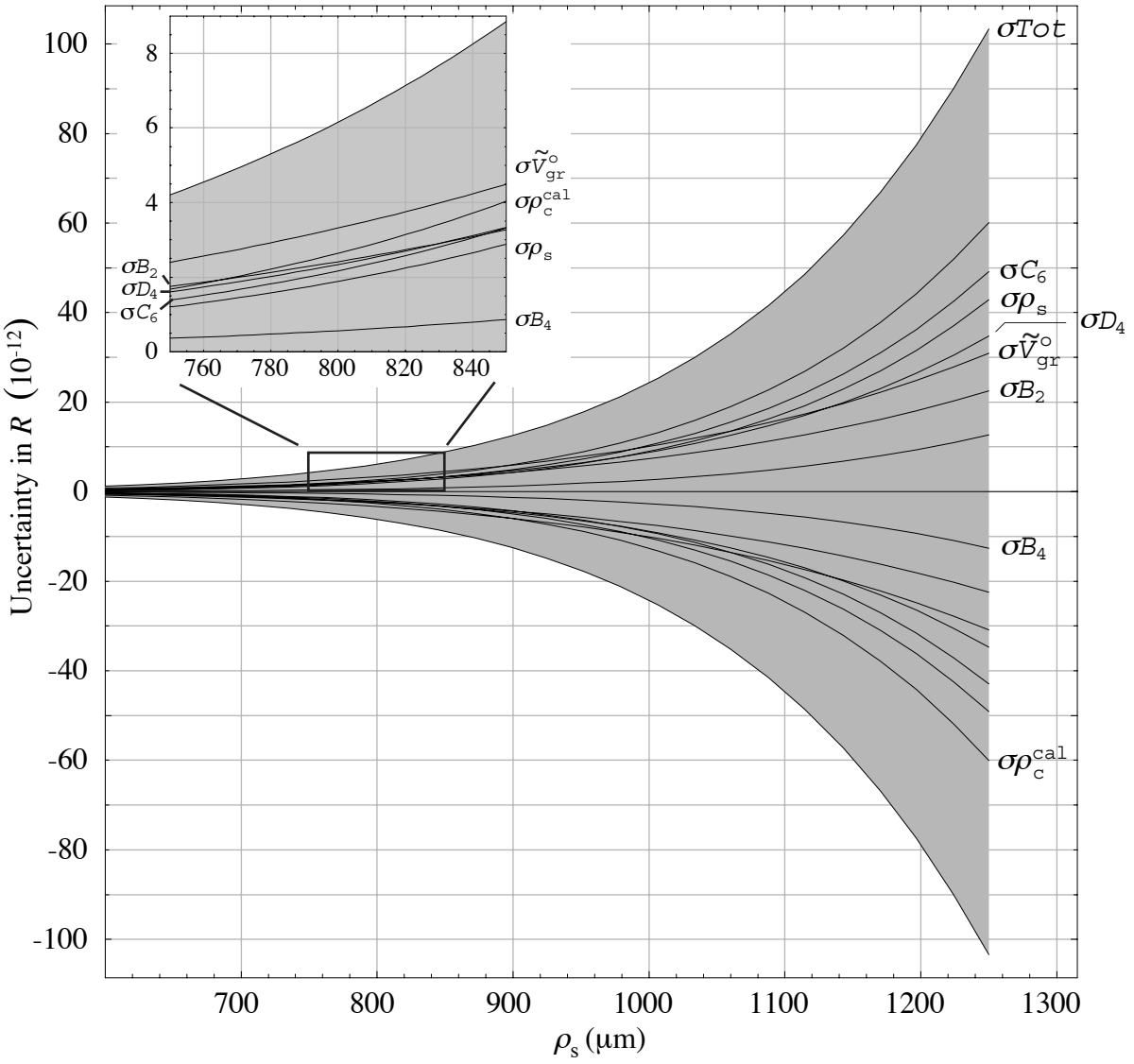

Figure 5-7: Uncertainty band on $\Delta\omega_{ct2}/\omega_{ct2}$ vs ρ_s from trap imperfections. Individual contributions from σD_4, $\sigma\widetilde{V}^{\circ}_{gr}$, σC_6, σB_2, σB_4, $\sigma\rho_s$ and $\sigma\rho_c^{cal}$ are plotted and the gray band is the total uncertainty. The plot is symmetric upon reflection about the x-axis and the label positions indicate the sign of each contributions. For instance, if ρ_c^{cal} increased, the measured ratio would be smaller.

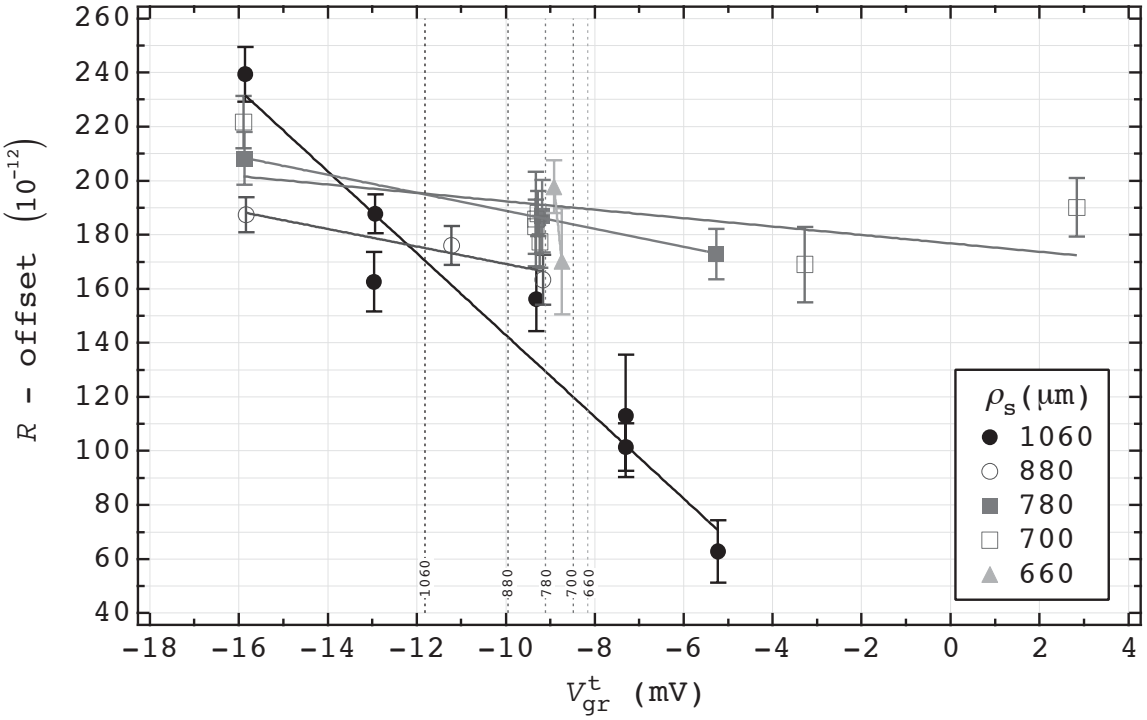

Figure 5-8: Measured ratio $R = \omega_{c0}/\omega_{c1}$ vs V_{gr}^{t} at various ρ_s with a $^{13}C_2H_2{}^+/^{14}N_2{}^+$pair (only the data from pair#2 are shown). The solid lines are linear fits to the data points taken at the same ρ_s. The vertical dashed lines show the values of V_{gr}^{optct} for each ρ_s (label is ρ_s).

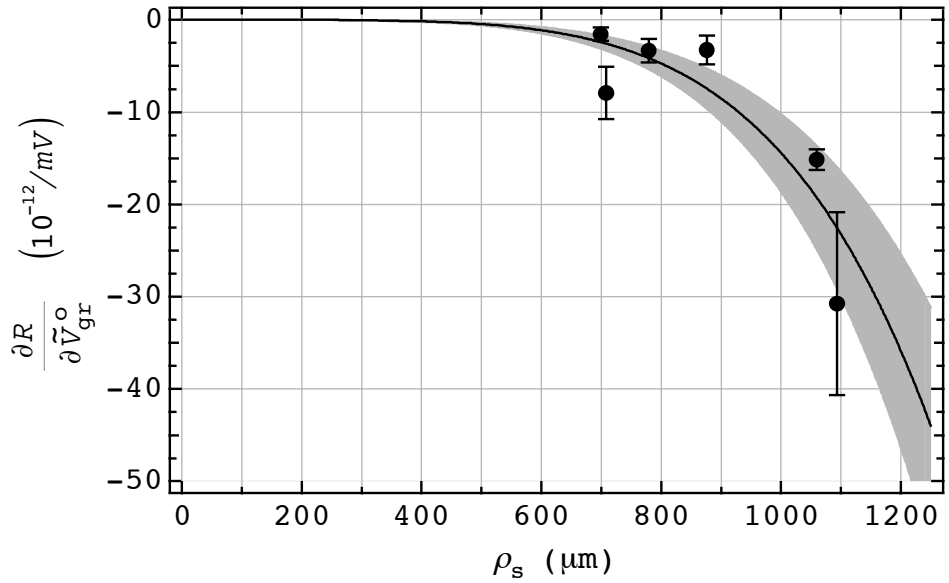

Figure 5-9: Measured slope $\partial R/\partial V_{gr}^{t}$ for various ρ_s with a $^{13}C_2H_2{}^+/^{14}N_2{}^+$pair. The solid curve is the slope expected from Eq. (5.22) and the band is the uncertainty on that prediction.

data have already been presented to demonstrate our understanding of systematic errors and used to extract experimental limits on $\delta_{\rm cyc}$. However our goal is to condense them all to a single number (and uncertainty) representing our final measurement of the mass ratio $M[^{14}{\rm N_2}^+]/M[^{13}{\rm C_2H_2}^+]$.

From each data set, we extract a value of R as described in Sect. 4.3. Because the individual ion frequencies ($\omega_{\rm cti}$ and $\omega_{\rm zi}$) are also shifted by field imperfections, ion-ion interactions and other effects, we apply some corrections to these frequencies before plugging them into Eqs. (4.7) and (4.8) (page 59). These corrections have a very small effect on R but we do it for completeness. See Sect. 5.4 for all the details.

We first divide the data sets according to the separation distance between the ions. For all the $\rho_{\rm s}$ where we have measured R vs $V_{\rm gr}^{\rm t}$ (as shown in Fig. 5-8), we extract our best value of R at $V_{\rm gr}^{\rm optct}$ from the linear fit through the data points. When we only have one point at a given $\rho_{\rm s}$, we correct the measured value using Eq. (5.22) if it was not taken at $V_{\rm gr}^{\rm optct}$ (and add 50 % of the correction in quadrature to the error bar). Figure 5-10 shows the resulting measurements of R vs $\rho_{\rm s}$. Superimposed on the data points are the two uncertainty bands from ion-ion interactions and field imperfections. Clearly, our uncertainties in $\rho_{\rm s}$, $\rho_{\rm c}^{\rm cal}$, D_4, C_6, etc. are such that it is essentially useless for measuring R to take data beyond $\rho_{\rm s} \simeq 900\,\mu$m . However, we went up to $\rho_{\rm s}$= 1150 µm to check that we did not miss something important about field imperfections (like the effect of C_8 or B_6, ...) and to test our model of the dynamics of the ions[†]. It is very reassuring to see that the data are all consistent with our expectations. If anything, it looks as if we have overestimated our uncertainties[‡]. For $\rho_{\rm s} \lesssim 600\,\mu$m many technical difficulties (mentioned at the beginning of Sect. 5.2 on page 75) quickly make taking data impractical. But down to $\rho_{\rm s} \simeq 600\,\mu$m, we see no effect at all of the ion-ion interaction, which again confirms that we have overestimated $\delta_{\rm cyc}$. It is important to note that even though we have varied $\rho_{\rm s}$ only by a factor of 2, the size of the various systematic errors have changed by at least a factor of 30 from one end to the other, and yet all our data points lie within 2×10^{-11} of each other.

To calculate our best estimate of R from these data points, we must deweight the points at a separation where the systematic errors are potentially big. We attribute to each point three error bars: $\sigma_{\rm stat}^{\rm i}$ is the statistical error from our analysis (the error bars shown in Fig. 5-10), $\sigma_{\rm imp}^{\rm i}$ is the potential systematic error at that separation from field imperfections (given by Eq. (5.16)), and $\sigma_{\rm ii}^{\rm i}$ is the potential systematic error at that separation from ion-ion interactions (given by Eqs. (5.6c) and (5.5)).

The average ratio is then the weighted average where each point is weighted by $\sigma_{\rm tot}^{\rm i}$ where $\sigma_{\rm tot}^{\rm i} = \sqrt{\sigma_{\rm stat}^2 + \sigma_{\rm imp}^2 + \sigma_{\rm ii}^2}$. However, the error returned by the weighted average is too small because it assumes that the errors on all the points are uncorrelated. This is

[†]We even went further in subsequent data sets (see Chap. 6)

[‡]The agreement is even more dramatic in the $H^{32}S^+/^{33}S^+$and $H^{28}Si^+/^{29}Si^+$data sets that will be presented in Chapter 6 (see Fig. 6-3)

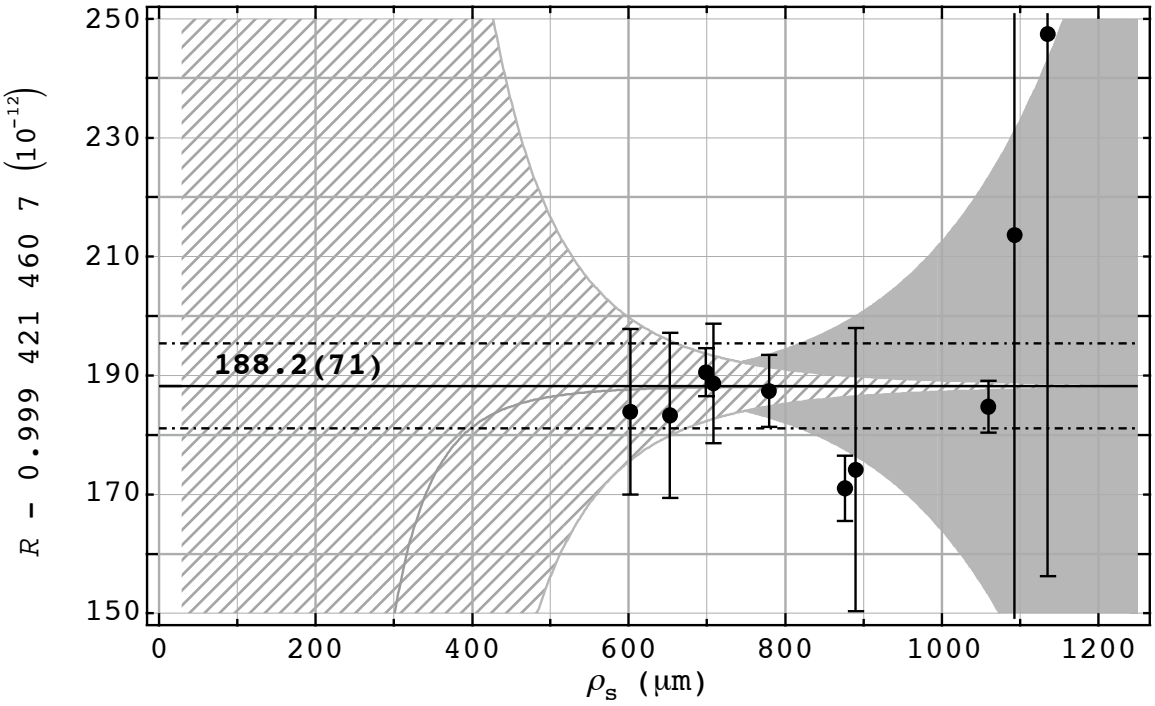

Figure 5-10: Summary of all our data for R vs ρ_s for ${}^{13}C_2H_2{}^+/{}^{14}N_2{}^+$. Each point is the result of an interpolation of the data at $V_{gr}^t = V_{gr}^{optct}$(see Fig. 5-8). Also shown are the uncertainty bands from our imperfect knowledge of the trapping field parameters (right) and the cyclotron radii imbalance (left). The final value for the measured R is represented by a solid horizontal line with the 1σ confidence interval denoted by the dashed line. The offset that was subtracted from every point is approximately the frequency difference predicted from the current mass table [20])

clearly not the case for the $\sigma^{\mathrm{i}}_{\mathrm{imp}}$ and $\sigma^{\mathrm{i}}_{\mathrm{ii}}$ (if our value of C_6 is wrong, then all the points are off in the same direction). For correlated errors, the error in the average is the average of the errors for the different points. Thus the error on the average ratio is computed as

$$\sigma R = \sqrt{(\sigma_{\mathrm{stat}})^2 + (\sigma_{\mathrm{imp}})^2 + (\sigma_{\mathrm{ii}})^2}\,, \tag{5.23}$$

where

$$\sigma^2_{\mathrm{stat}} = \left(\sum_{\mathrm{i}} \frac{1}{(\sigma^{\mathrm{i}}_{\mathrm{stat}})^2}\right)^{-1}, \tag{5.24}$$

$$\sigma_{\mathrm{imp}} = \sum_{\mathrm{i}} \frac{\sigma^{\mathrm{i}}_{\mathrm{imp}}}{(\sigma^{\mathrm{i}}_{\mathrm{stat}})^2} \Bigg/ \sum_{\mathrm{i}} \frac{1}{(\sigma^{\mathrm{i}}_{\mathrm{stat}})^2} \qquad \text{and} \qquad \sigma_{\mathrm{ii}} = \sum_{\mathrm{i}} \frac{\sigma^{\mathrm{i}}_{\mathrm{ii}}}{(\sigma^{\mathrm{i}}_{\mathrm{stat}})^2} \Bigg/ \sum_{\mathrm{i}} \frac{1}{(\sigma^{\mathrm{i}}_{\mathrm{stat}})^2}\,. \tag{5.25}$$

Note that if we included all the points, σ_{imp}would be artificially large because of the contributions from the points at the largest ρ_{s}. Thus we calculate the error on the ratio by including only the 5 inner most points in Eq. (5.23). Our best estimate for the value of the ratio is then given by

$$(R - 0.999\,421\,460\,7) \times 10^{12} = 188.2(71)\ \ (30)\,(34)\,(55)\,, \tag{5.26}$$

where the first number in parenthesis is the total error on the last two digits (σR), and the other three are σ_{stat},σ_{imp}, and σ_{ii}. This value is indicated in Fig. 5-10 as the solid horizontal line with the $1\,\sigma$ confidence interval denoted by dashed lines.

At this point, we have accounted for all the potential effects of ion-ion interactions, trapping field imperfections, and various other small effects described in Sect. 5.4 on the next page. The only effect that we have not discussed yet is the polarization force shift, which I very briefly mentioned in Sect. 3.5. This phenomenon is discussed in full detail in [19]. For the present measurement, there is the possibility that the $^{13}C_2H_2{}^+$ is bent and has a small dipole moment. However, the calculation of the molecular structure of $^{13}C_2H_2{}^+$ is complicated by the fact that it is not a simple diatomic molecule. We expect this correction to be small (10^{-11} range) but at the time of the submission of this thesis, the calculation has not been done and so we cannot report a final value for this mass ratio. We are confident that 7.1×10^{-12} is a conservative uncertainty for the cyclotron frequency ratio of $^{13}C_2H_2{}^+/{}^{14}N_2{}^+$. In the next chapter we will see that the data looked even better for the other two ratios we measured ($H^{32}S^+/{}^{33}S^+$ and $H^{28}Si^+/{}^{29}Si^+$), which further confirms our understanding of the system and the errors associated with it. However, because we have not performed an independent measurement of that ratio at a different m/q (see Sect. 5.5.4 below), and because of the uncertainty due to the effect on the polarization force shift on $^{13}C_2H_2{}^+$, we multiply our error bar by $\sqrt{2}$ to increase our final uncertainty to 10×10^{-12}.

Table 5.3: Error budget for all our measurements. The numbers quoted are the errors on R multiplied by 10^{12}. Others include the uncertainty from the polarization shift correction, and a "safety factor" we include to cover any effect we might have overlooked.

Source of error	Effect on $^{13}C_2H_2{}^+/^{14}N_2{}^+$	Effect on $H^{28}Si^+/^{29}Si^+$	Effect on $H^{32}S^+/^{33}S^+$
Statistics	3.0	3.3	4.1
Trap Imperfections	3.4	3.4	4.4
Ion-ion Interactions	5.5	4.4	4.2
Total Measurement Error	7.1	6.5	7.4
Others	7.0	2.6	10
Total Error	10	7.0	12

With the adjusted error bar, Eq. (5.26) becomes our premilinary value for R:

$$R = \frac{M[^{14}N_2{}^+]}{M[^{13}C_2H_2{}^+]} = 0.999\,421\,460\,888\,(10)^{\S}\,. \tag{5.27}$$

It is interesting to note that the value above is more than 10 times more accurate than the predicted ratio from the masses in [20] (and well within the old error bar as you can see in Table 7.1). Table 5.3 summarizes the various sources of error for this measurement.

It is generally more useful for the metrology community to express this result as a mass difference of neutral species. The procedure to do so has been described in Sect. 4.4. Using Eq. (5.27) and the numerical values in Table 4.3 on page 64, we find

$$M[^{14}N] - M[^{13}C] - M[H] = 0.008\,105\,862\,88\,(14) \qquad (1.7 \times 10^{-8})\,. \tag{5.28}$$

The uncertainty on the mass difference is completely dominated by the error on our measured ratio; the uncertainties on ΔE contribute less than 0.1×10^{-8} to the final relative error.

Note that we have been extremely conservative throughout this entire analysis. The agreement of all the data points for R as a function of ρ_s (especially the point at $1050\,\mu m$) is a striking demonstration that we know our trap field imperfections better than we have claimed in Table 2.4.

5.4 Minor Corrections

This section will discuss various frequency shifts we accounted for in calculating the ratio R. We corrected our measured frequencies for these effects, although the impact of these corrections on the ratio is much smaller than the estimated error.

[§]Preliminary value. Please refer to our future publications for the final value.

The effect of ion-ion interactions and trap field imperfections on the difference frequency $\omega_{\rm ct2}$ was discussed in the previous sections of this chapter. We never apply any correction to the measured $\omega_{\rm ct2}$ due to ion-ion interaction because our best estimate of the cyclotron radii imbalance $\delta_{\rm cyc}$ is 0. For trap imperfections, we usually optimize our trapping fields to experimentally cancel out any of these effects (by setting the guard ring voltage to $V_{\rm gr}^{\rm optct}$) and so no correction is necessary either. However, the other two ingredients in our calculation of the ratio from Eq. (4.8) (page 59), the two single ion's frequencies $\omega_{\rm cti}$ or $\omega_{\rm zi}$, are also subject to frequency shifts. Because we don't use the measured difference axial frequency, we have to apply a correction to the measured $\omega_{\rm cti}$ or $\omega_{\rm zi}$ to extract their values in the limit of zero mode amplitudes. The shifts due to trap imperfections can easily be calculated from the expressions given in Appendix A and using the numerical values from Table 2.4. The relativistic shift of $\omega_{\rm cti}$ was discussed in Sect. 2.5. The rms size of these shifts for all our ${}^{13}C_2H_2{}^+/{}^{14}N_2{}^+$data (for various terms of the expansion of our trapping fields) are given in Table 5.4. They are small shifts to start with, and their effect on the ratio is further reduced by a factor of $2\eta \simeq 5.8\times10^{-4}$ and $\omega_{\rm z1}/\omega_{\rm c1} \simeq 1/21.2$ and $2\eta(\omega_{\rm z1}/\omega_{\rm c1})^2 \simeq 1.3\times10^{-6}$ for $\omega_{\rm ct}$ and $\omega_{\rm z}$ respectively, as we have seen in Sect. 4.3.

The shift from D_2 accounts for the fact that we sometimes set the guard ring voltage to a different value during the evolution time than the one at which the axial frequency is measured (Sect. 4.1.6). Because the trap is not perfectly orthogonal, the axial frequency depends slightly on $V_{\rm gr}$. The main shift of the axial frequency that we need to account for is the part of the common shift of both axial frequencies due to ion-ion interactions which depends on axial amplitude (i.e. the difference between Eqs. (5.3) and (5.1)). The reason is that at the end of a simultaneous PNP, the axial amplitudes of both ions are fairly large ($\sim$350 µm) and essentially constant in time because the ions are far off-resonance (energy damping time $\sim$ 100 s). Finally, one might worry about the perturbation of the axial frequency because of its coupling to our detector ("frequency pulling effect"). Since the two ions are many coil's half-widths away from resonance ($\delta^* \approx 13$) this effect is very small. In addition, it has the opposite sign for each ion (because they are on either side of resonance) and so it should completely cancel out when we take the average of R_0 and R_1 as our final value of R. For this reason, no correction was applied for coil pulling.

For the cyclotron frequency, the last effect one might consider is the systematic shift due to the presence of the image charge induced in the ring electrode. In our trap, this shift has been calculated to be 92 µHz per charge, independent of mass (to first order) [12]. Since we used singly charged molecules for all our measurements, that shift is very small here. The conclusion from Table 5.4 is that all of these corrections change the ratio by less than 2×10^{-12} and therefore add no uncertainty to our final answer.

*... during the ringdown

Table 5.4: Table of all the frequency shifts for which a correction was applied. The rms shift (for all the $^{13}C_2H_2{}^+/^{14}N_2{}^+$data) expressed in mHz and as a fraction are given in columns 3 and 4. The maximum shift is given in column 2. The numbers for the effect on R (last column) are in 10^{-12}.

Source of error	$\Delta f_{\max}$ (mHz)	$\Delta f_{\rm rms}$ (mHz)	$\Delta f/f$	Effect on ratio
Δf_z from finite z^*	638	287	1.4×10^{-6}	1.76
Δf_z from C_4	-125	64.0	3.0×10^{-7}	0.39
Δf_z from C_6	22	13.0	6.1×10^{-8}	0.08
Δf_z from D_2	190	68.0	3.2×10^{-7}	0.42
Δf_z from coil pulling	6.3	6.1	2.9×10^{-8}	–
Δf_{ct} from C_4	11.6	5.0	1.1×10^{-9}	0.62
Δf_{ct} from C_6	-3.6	1.8	3.9×10^{-10}	0.22
Δf_{ct} from B_2	-4.7	2.9	6.2×10^{-10}	0.36
Δf_{ct} from B_4	0.0	0.0	2×10^{-12}	0.00
Δf_{ct} from relativity	-0.3	0.1	2.1×10^{-11}	0.01
Δf_{ct} from image charge	0.092	0.092	2.0×10^{-11}	0.01

5.5 Other Systematic and Experimental Checks

In this section, we briefly describe various checks that we have performed to build up confidence in our system and analysis machinery.

5.5.1 Two Different Pairs

After taking data with $^{13}C_2H_2{}^+/^{14}N_2{}^+$for 17 days, we expelled the ions from the trap and loaded a fresh pair of ions which we used to take the remaining data on that pair. We found no systematic difference in the measured ratio between the two pairs at the 10^{-11} level. We take great care to eliminate unwanted ions from our trap but this test further reduces the possibility that a third ion could be "hiding" in a very large orbit, and perturb the measured frequencies. Similarly, the fact that we could hold on to a pair for many weeks and observe it to behave very consistently on that time scale is also an indication that the pair was "clean", i. e., alone in the trap. This also indicates that the trap environment (charge patches, etc.) is not affected by making new ions.

5.5.2 R_0 vs R_1

As we have seen in Sect. 4.3, the ratio R can be calculated using the difference frequency ω_{ct2} and either ion 0's frequencies (ω_{ct0} and ω_{z0}), or ion 1's frequencies (ω_{ct1} and ω_{z1}). The two different answers R_0 and R_1 (obtained independently from Eqs. (4.7) and (4.8) on page 59) are usually averaged together but we can compare them and make sure they give the same result. The difference $R_1 - R_0$ is plotted in Fig. 5-11. The values agree well within

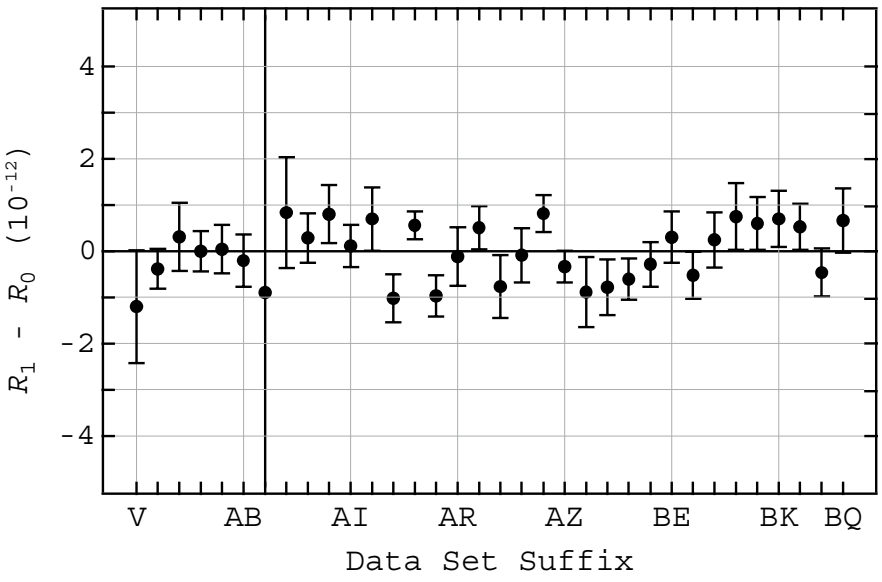

Figure 5-11: Relative difference between the value of R obtained from the frequencies of ion 1 (R_1 from Eq. (4.7)) and of ion 0 (R_0 from Eq. (4.8)) for each data set taken with ${}^{13}C_2H_2{}^+/{}^{14}N_2{}^+$. The same ω_{ct2} was obviously used in both R_1 and R_0, but the error bars plotted here represent only the uncorrelated errors from point to point, i. e., the contribution from ω_{ct} and ω_z to the error on the ratio.

the error bar; the largest difference is 1.2×10^{-12} and the χ^2_ν of the average difference is 1.15. Since ω_{ct1} and ω_{ct0} have been "phase unwrapped" independently (see Sect. 4.1.3) this lessens the chance that we missed an entire cyclotron cycle.

5.5.3 Phase Unwrapping Averages

The phase unwrapping procedure described in Sect. 4.1.3 extracts a value for ω_{ct2} for each PNP with the longest evolution time T_{evol}. That procedure involves averaging and interpolating the phases measured from PNPs with shorter T_{evol}. We then average all the values of ω_{ct2} together to obtain a final measurement of ω_{ct2} for that data set. We have checked that whether we take a weighted or unweighted average of these points does not affect the answer by more than 2×10^{-12}. We have also carried out a very different analysis in which we have averaged all the measured phases for a given T_{evol} together *before doing phase unwrapping*. This latter analysis is much simpler, and therefore less susceptible to mistakes, and serves as an independent analysis of each data set. The good agreement between the two analyses, shown in Fig. 5-12, is very reassuring. The reduced chi-squared of the difference between the two analyses is $\chi^2_\nu = 0.087$. Since the two analyses essentially give the same answer, one might be tempted to carry on only the simpler one (unwrapping the averages). The only motivation to phase unwrap each point individually is to reduce the final error by accounting for temporal drifts of the phase offsets (and the individual

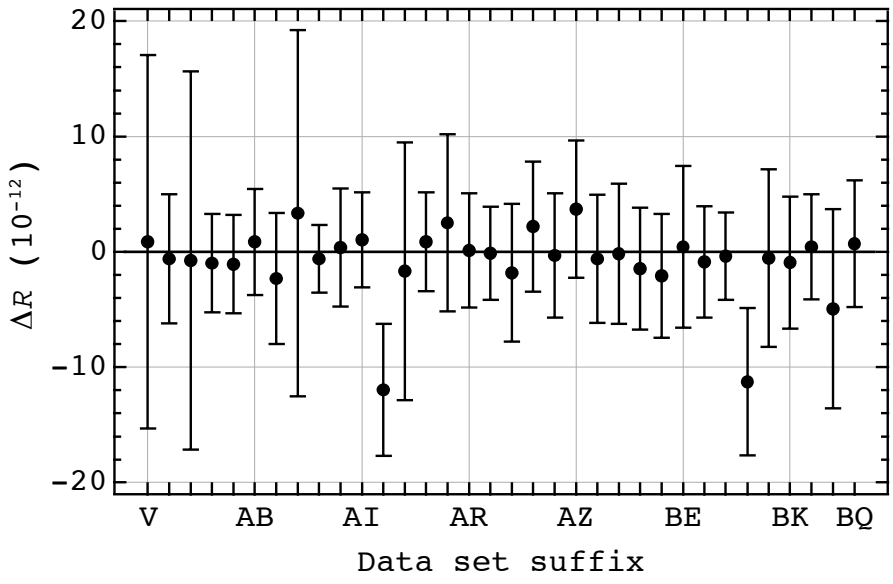

Figure 5-12: Difference between the ratio obtained from averaging all the measured phases at each $T_{\rm evol}$ and then phase unwrapping these averages, and the one obtained by the procedure described in Sect. 4.1.3 where we phase unwrapped each point individually and then take the average.

$\omega_{\rm ct2}$'s enable changes due to cyclotron frequency jumps, or other problems in the data to be monitored). But Fig. 5-13 shows that the error is essentially the same for both analyses; the average difference is $7.8(74) \times 10^{-13}$ (where we have eliminated the three early points with large errors). This indicates that temporal drifts were not a limiting factor in the final precision of our measurements.

5.5.4 Different m/q

For all the neutral masses previously measured by the MIT ICR Lab (like for example the alkali masses measured in 1999), we always had two independent routes to every mass as a check for systematic errors. For example to obtain the mass of ^{133}Cs, we measured $M[\mathrm{Cs}^{+++}]/M[\mathrm{CO_2}^{+}]$ and $M[\mathrm{Cs}^{++}]/M[\mathrm{C_5H_6}^{+}]$. These two ratios have very different mass/charge ratios (44 and 66), and that is why they are a powerful check for the presence of unknown systematic errors. Unfortunately, we don't have that kind of test for the measurements reported in this thesis. We had really hoped to measure the ratio $M[^{13}\mathrm{CH}^{+}]/M[^{14}\mathrm{N}^{+}]$ for that purpose, but we ran out of time. That would have been a measurement of the same mass difference as $^{13}\mathrm{C_2H_2}^{+}/^{14}\mathrm{N_2}^{+}$, but at $m/q = 14$ instead of 28, and a strong consistency check for our two-ion technique. Hopefully that ratio will be measured in the future. Nevertheless, given the number of self-consistency checks we have performed at $m/q = 28$ and the fact that the data turned out to look much better than expected, we feel confident the answer will agree with ours.

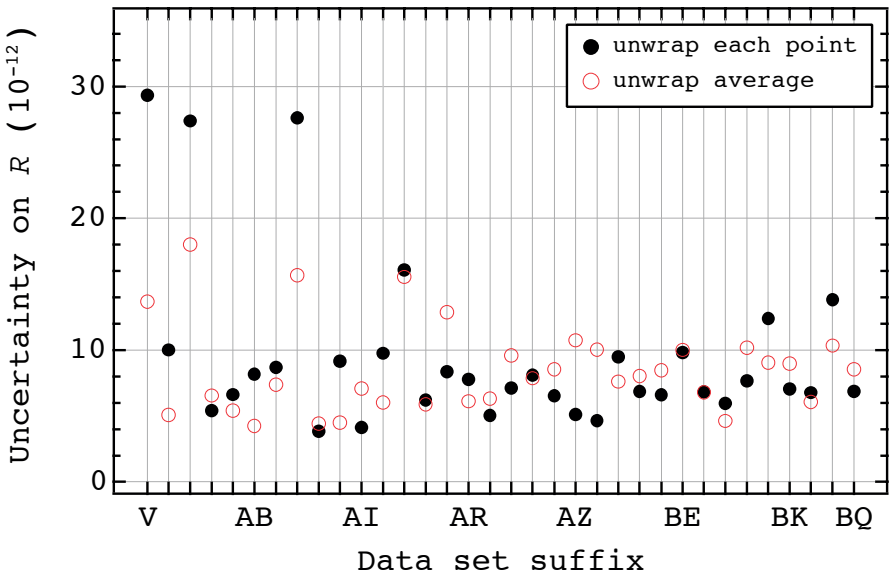

Figure 5-13: Comparison between the uncertainty in the ratio obtained from phase unwrapping the averages of all the measured phases at each T_{evol} (open circles), and the one obtained by the procedure described in Sect. 4.1.3 where we phase unwrapped each point individually and then took the average (solid points). On average, the difference between the resulting uncertainties (eliminating the first few points with large error) is less than 5×10^{-13}, indicating that temporal drifts are not a source of error.

5.6 Current Limitations

It is hoped that the reader is now convinced that our new two-ion technique has pushed state-of-the-art mass spectrometry below a relative accuracy of 10^{-11} by:

- Virtually eliminating the effect of magnetic field fluctuations on our measurement of the cyclotron frequency ratio by confining two different ions in our Penning trap and simultaneously measuring their cyclotron frequencies;
- Characterizing very carefully our trapping electric and magnetic fields and calibrating the absolute amplitude of motion of the ions in the trap. This allowed us to predict accurately the effect of imperfections on the mode frequencies of the ions and optimize the first order anharmonicity to cancel the effect of all other terms on the measured cyclotron frequency difference;
- Performing a series of powerful tests to experimentally verify our model of ion-ion interactions and put stringent limits on effects that we might have neglected.

A natural question to address at this point is: what limits the precision and accuracy of the two-ion technique ? The obvious answer from the above discussion is the potential systematic errors due to ion-ion interactions and field imperfections, as discussed in this

chapter. Clearly, on the road to 10^{-12} and below, one will need better knowledge of the field imperfections (C_6, $\widetilde{V}_{\rm gr}^{\circ}$, D_4, B_2, B_4) and a more accurate absolute amplitude calibration. Having control of C_6 experimentally would be tremendously helpful. All of these things would widen the window of $\rho_{\rm s}$ in which we can take precise data (see Fig. 5-10) and make it easier to study precisely the effect of ion-ion interactions on the ratio. Obviously the ions have to be chosen carefully to avoid atoms and molecules with large shifts of their ground state due to polarization forces. Alternately one can use ions for which this shift (the dipole moment) is known precisely enough. That might become a challenge, but it is not a fundamental limit inherent to our technique. Better calculations will be performed in the future, and in principle one could do the molecular spectroscopy of the ions in the trap and extract experimentally the needed parameters for this correction.

In terms of random fluctuations, let me reiterate that magnetic field fluctuations are no longer part of the picture. As we have seen in Sect. 4.3, the effect of an individual ion's cyclotron frequency on the ratio is multiplied by 2η ($\simeq 6\times10^{-4}$ for ${}^{13}C_2H_2{}^{+}/{}^{14}N_2{}^{+}$). Therefore, for a final precision on the ratio of 10^{-12}, we need the magnetic field to be constant to 1.7×10^{-9}. For our 8.5 T magnet, that corresponds to 0.14 mG. In Fig. 5-14, we show the value of our magnetic field computed from the free space cyclotron frequency $f_{\rm c}$ for all our ${}^{13}C_2H_2{}^{+}/{}^{14}N_2{}^{+}$, $H^{32}S^{+}/{}^{33}S^{+}$and $H^{28}Si^{+}/{}^{29}Si^{+}$data. The maximum slope is -0.84 mG/day, which corresponds to a long term drift in $f_{\rm c}$ of -46 mHz/day or 1×10^{-8}/day (at $m/q = 28$). The effect of that drift on the cyclotron frequency difference $\omega_{\rm ct2}$ is 6×10^{-12}/day. That confirms our previous conclusion that temporal drifts have not been a problem for us. The typical time scale for one measurement of the ratio is, say, 30 minutes and so long term magnetic field drifts will become a problem only in the 10^{-13} range. A more important effect is the short term magnetic field fluctuations that the Boston electrical subway and the elevator in our building induce in our laboratory. From Fig. 3-1 on page 39, we see that these are typically 4 mG during the day, which, since our magnet has a shielding factor of 10, correspond to fluctuations of the individual ion cyclotron frequencies of 5×10^{-9}. Therefore the short term magnetic field fluctuations induce shot to shot fluctuations of the ratio $R$of about 3×10^{-12}. In our measurements, that was about an order of magnitude smaller than the effect of the cyclotron amplitude fluctuations (see Sect. 5.6.1 below).

Now that our measurements are insensitive to the magnetic field fluctuations, the dominant source of random noise in our data is the shot-to-shot variation in the cyclotron radii of the ions. Before we describe our observations of this effect, we should say a few words about phase noise. As described in Sect. 4.1, the raw output of an experiment is an ion's signal (due to its axial motion) from which we extract an amplitude, a frequency, and most importantly a phase. Because we do things phase coherently (see Sect. 4.1.1), we expect to measure the same phase if we repeat a series of identical PNPs with short evolution time $T_{\rm evol}$ (typically 0.1 s). We call the standard deviation of the measured phases in this case the "short time phase noise", $\sigma_{\phi}^{\rm s}$. With a single ion in the trap $\sigma_{\phi}^{\rm s}$ is typically 8°, set by

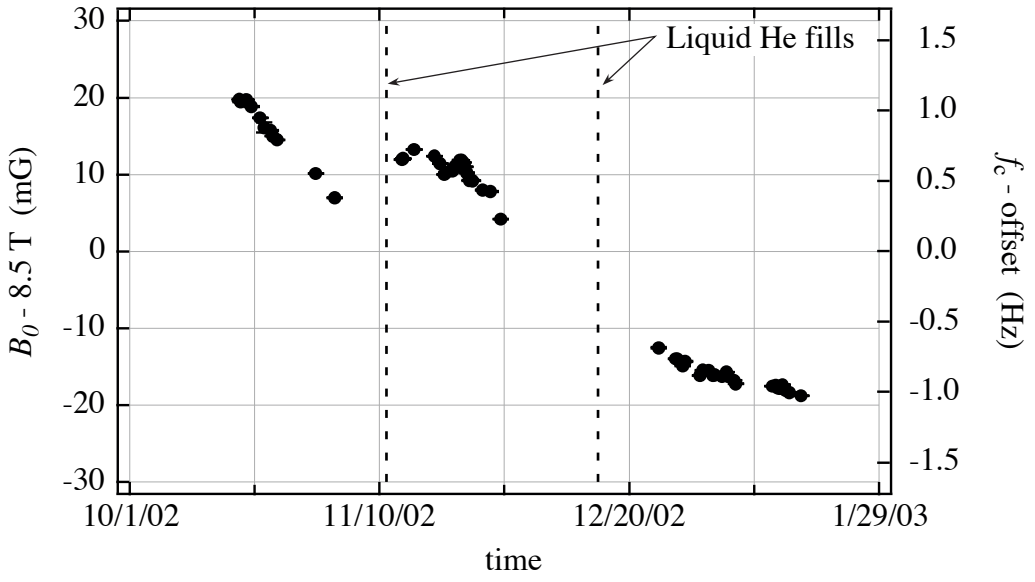

Figure 5-14: Magnetic field experienced by the ions as a function of time. This was extracted from the free space cyclotron frequencies for all our data sets at mass 28, 29, and 33. The right scale shows the corresponding effect on f_c at $m/q = 28$. The maximum slope is -0.84 mG/day, or -0.46 mHz/day, or 1×10^{-8}/day. The effect of such a drift on the frequency difference is 6×10^{-12}/day.

our signal-to-noise ratio. When we have two ions in the trap, we have to use smaller axial amplitudes and the reduced signal-to-noise lead to a σ_ϕ^s of about 15°. For simultaneous measurements on two ions we are interested in the difference phase between the two ions' signals which we determine simply by subtracting one from the other (see Sect. 4.1.2). We then expect the noise in the short time phase difference to be $\sqrt{2}$ higher, which is what we observe: $\sigma_{\phi 2}^s = 20 - 25°$ (confirming that it is measurement noise, not correlated for the two ions). Since that sets our starting point (things can only become worse from there), we have spent some time trying to make $\sigma_{\phi 2}^s$ as small as possible[†]. Figure 5-15 shows the dependence of $\sigma_{\phi 2}^s$ on two controllable parameters: the axial amplitude of oscillation z, and the duration of the axial signals we process.

The data show the somewhat obvious conclusion that for low axial amplitude, the noise goes up, but we can bring it back down by averaging for longer. For large axial amplitudes, the opposite is true since the noise goes up because of axial frequency chirping. If we process a shorter amount of data, the frequency is more stable and the noise comes back down. The axial amplitude at the end of a PNP is set by the cyclotron radius of the ion. We want to keep ρ_c as small as possible, while still getting a reasonable $\sigma_{\phi 2}^s$ in the least amount of time. From the data shown in Fig. 5-15 we chose to use a cyclotron radius of 66 μm and

[†]If a little genie gave me only one wish to improve the ICR experiment, I would pick a lower phase noise without any hesitation. Give me a detector that can do $\sigma_{\phi 2}^s \approx 1°$ and I will give you mass ratios with a precision below 10^{-12}

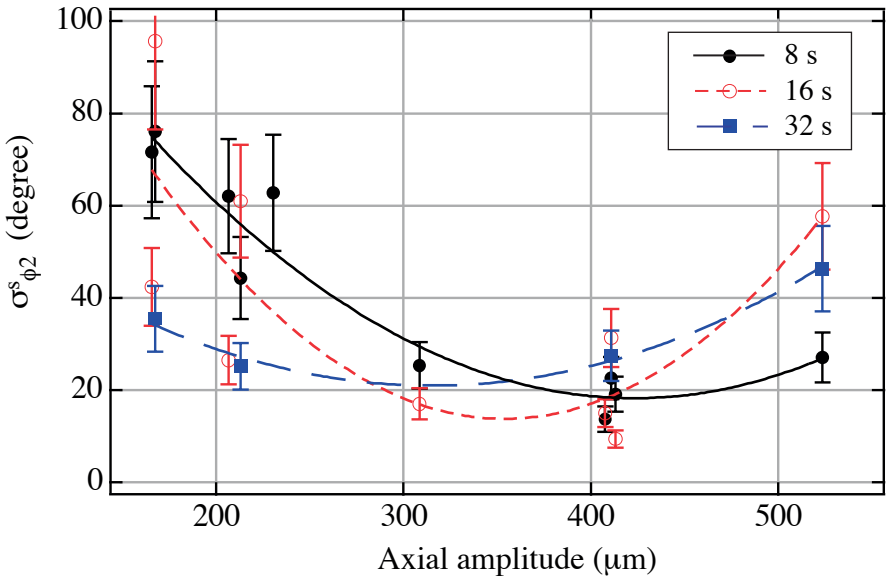

Figure 5-15: $\sigma^{\mathrm{s}}_{\phi 2}$ as a function of axial amplitude z. The short time phase noise $\sigma^{\mathrm{s}}_{\phi 2}$ is the standard deviation of the measured difference cyclotron phase after a series short PNP ($T_{\mathrm{evol}} = 0.1\,\mathrm{s}$) (using ${}^{13}C_2H_2{}^+/{}^{14}N_2{}^+$). After each PNP, we recorded the axial signals of the ions for 32/,s. The squares are obtained by processing the entire 32 s of data, whereas the open and closed circles are the result of processing only the first 16 and 8 s of the data. The lines are quadratic fits to the data. The precise mass comparison data were taken with $z \simeq 350\,\mu\mathrm{m}$ and 8 s of data.

record 8 s of data. That's what we used for all the data presented in this thesis (for the sulfur and silicon data, we used 76 and 71 μm respectively because of the mass dependence of the axial amplitude obtained from a given cyclotron radius after the π-pulse).

For a series of PNPs with longer (fixed) T_{evol}, we expect to see the measured phase noise (standard deviation of the phases) increase because of a contribution from the shot-to-shot cyclotron frequency noise σ_{f} (in Hz). Since $\sigma^{\mathrm{s}}_{\phi}$ and σ_{f} are independent, we add them in quadrature so that the total phase noise measured should be given by (for each ion)

$$\sigma_{\phi} = \sqrt{(\sigma^{\mathrm{s}}_{\phi})^2 + (360 \times T_{\mathrm{evol}} \times \sigma_{\mathrm{f}})^2}\,. \tag{5.29}$$

If σ_{ϕ} approaches 180°, it is impossible to assign unambiguously a phase to each point. Practically, we like to keep it below about 60° so that all our points fall in the same cycle. σ_{f} is dominated by magnetic field fluctuations and that is why in our previous single-ion measurements, we could not make T_{evol} much larger than about 60 s before loosing track of the total phase. When directly measuring the cyclotron phase difference, we are sensitive only to the differential frequency shift between the ions σ_{f2}, which is completely insensitive to the magnetic field. The dominant source of relative cyclotron frequency fluctuations is then the shot-to-shot variations in the cyclotron radii, as we will see below. (Note that for

simplicity, we did not use the electronic refrigeration technique described in Sect. 2.3 for the two-ion data.)

5.6.1 Cyclotron Amplitude Fluctuations

Figure 5-16 (a) shows the observed phase noise (with an $^{13}C_2H_2{}^+/^{14}N_2{}^+$ pair of ions) as a function of the PNP evolution time $T_{\rm evol}$ for various cyclotron radii ($\rho_{\rm c0} = \rho_{\rm c1} = \rho_{\rm c}$). Clearly, the phase noise increases as we make $T_{\rm evol}$ bigger, but note that thanks to the two-ion technique we can let the ions spin around at $\sim 5\,$MHz for 30 minutes, and still measure a reproducible phase difference at the end !! That is even more remarkable given the fact that after only a few minutes (at night) we have lost track of the number of cyclotron cycles for each ion due to magnetic field fluctuations. Putting an error bar on the measured standard deviation is slightly tricky and the topic is discussed in Appendix A4 of Frank DiFilippo's thesis and in [23]. To interpret the increase in phase noise with $T_{\rm evol}$, we write Eq. (5.29) for the noise in the difference phase between the two ions (in degree)

$$\sigma_{\phi 2} = \sqrt{(\sigma^{\rm s}_{\phi 2})^2 + (360 \times T_{\rm evol} \times \sigma_{\rm f2})^2}\ . \tag{5.30}$$

As we have seen above, $\sigma_{\rm f2}$ is independent of magnetic field fluctuations. From Sect. 5.1 and 5.2, we know that the difference frequency $\omega_{\rm ct2}$ is perturbed by trapping field imperfections and ion-ion interactions. From Eqs. (A.13), (5.6a) and also the relativistic shift (2.10), we obtain all the contributions to the shift of $\omega_{\rm ct2}$ to lowest order in $\rho_{\rm c}$:

$$\frac{\Delta f_{\rm ct2}}{\bar{f}_{\rm ct}} = \left(\frac{-1}{2}\,\frac{B_2}{B_0} - \frac{\bar{\omega_{\rm c}}^2}{2c^2} + \frac{3}{2}\,\frac{\bar{\omega_{\rm m}}}{\bar{\omega_{\rm ct}}}\,\frac{C_4}{d^2} - \frac{9}{16}\,\frac{\Omega_{\rm E}^2}{\bar{\omega_{\rm c}}^2 \rho_{\rm s}^2} \right) (\rho_{\rm c1}^2 - \rho_{\rm c0}^2)\ . \tag{5.31}$$

The frequency difference noise $\sigma_{\rm f2}$ arises from shot-to-shot fluctuation in the cyclotron radii. Indeed, before each PNP we cool the axial modes of each ion by allowing it to thermalize with our 4 K detector, and then transfer this "cold motion" into the cyclotron mode using a π-pulse (see Sect. 4.1.4). Since it is the classical action that is conserved during the π-pulse the effective temperature of the cyclotron is higher than 4 K:

$$T_{\rm c} = \frac{\omega_{\rm ct}}{\omega_{\rm z}}\,T_{\rm z}\ \simeq\ 22\,T_{\rm z}\ \simeq\ 90\,{\rm K}\ , \tag{5.32}$$

for $^{13}C_2H_2{}^+/^{14}N_2{}^+$. That temperature corresponds to a "thermal cyclotron radius" given by

$$\frac{1}{2} m \omega_{\rm ct}^2 \rho_{\rm cth}^2 = kT_{\rm c} \qquad \Rightarrow \qquad \rho_{\rm cth} = \sqrt{\frac{2}{m\omega_{\rm ct}\omega_{\rm z}} kT_{\rm z}} \approx 7.8\,\mu{\rm m}\ , \tag{5.33}$$

where k is the Boltzmann constant. (Note that $\rho_{\rm cth}$ is independent of mass if $\omega_{\rm z}$ is held constant.) When we initially drive the ions to a 66 μm orbit at the beginning of each PNP, $\rho_{\rm cth}$ adds vectorially to our drive with a random relative phase each time, and so we expect

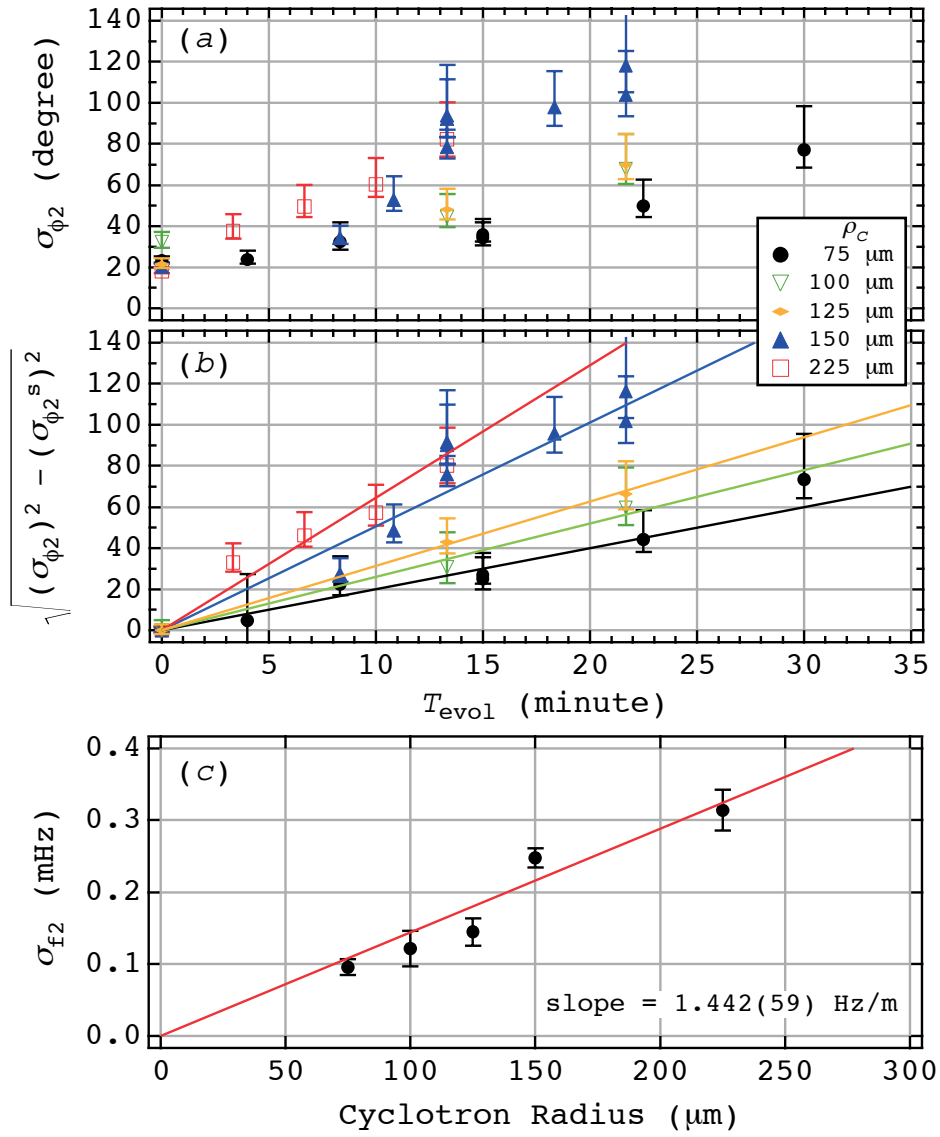

Figure 5-16: Cyclotron amplitude fluctuation data. (a) Measured difference phase noise (in degree) vs $T_{\rm evol}$ for various cyclotron radii, using a $^{13}C_2H_2{}^+/^{14}N_2{}^+$ pair separated by $\rho_s = 910\,\mu$m. The cyclotron radii of both ions are varied together, i. e., $\rho_{c0} = \rho_{c1} = \rho_c$. (b) Difference phase noise (in degree) with the short time phase noise $\sigma^s_{\phi 2}$ subtracted (in quadrature, using Eq. 5.30). The slope should correspond to the frequency noise σ_{f2} at that ρ_c. (c) Frequency noise σ_{f2} (in mHz) vs ρ_c. The observed linear dependence confirms our model (Eq. (5.34)). The slope, 1.442 (59) Hz/m corresponds to relative frequency noise of 2.3×10^{-11} at $\rho_c = 75\,\mu$m.

ρ_{c0} and ρ_{c1} to both fluctuate independently by an amount $\sigma_\rho \approx 7.8/\sqrt{2} \approx 5.5\,\mu\text{m}$. The magnitude of the frequency shift (Eq. (5.31)) therefore also varies from shot to shot. By differentiating Eq. (5.31), we obtain

$$\sigma_{f2} = \sqrt{2}\ \bar{f}_{ct}\,\rho_c\,\sigma_\rho \left| \frac{-B_2}{B_0} - \frac{\bar{\omega_c}^2}{c^2} + 3\,\frac{\bar{\omega_m}}{\bar{\omega_{ct}}}\,\frac{C_4}{d^2} - \frac{9}{8}\,\frac{\Omega_E^2}{\bar{\omega_c}^2\rho_s^2} \right| . \tag{5.34}$$

Figure 5-16 (b), shows the measured phase noise with σ_ϕ^s subtracted in quadrature. From Eq. (5.30), we expect this to scale linearly with T_{evol}, and it does. If one plots the fitted slope ($=\sigma_{f2}$) as a function of cyclotron radius, one again gets a straight line as expected (Fig. 5-16 (c)). The slope of that line equals σ_{f2}/ρ_c in our model and is measured to be $1.442(59)\,\text{Hz/m}$ ($\chi^2_\nu = 5.5^\dagger$.). That corresponds to a relative frequency noise $\sigma_{f2}/\,\bar{f}_{ct} \simeq 2.3 \times 10^{-11}$ at $\rho_c = 75\,\mu\text{m}$. By comparing the slope to Eq. (5.34), one finds an experimentally measured value for the rms cyclotron amplitude fluctuations of each ion of $10.0(13)\,\mu\text{m}$. The ratio of the contributions of the B_2, relativity, C_4 and ion-ion interaction terms is 40:63:27:68 respectively. (The data were taken at $\rho_s = 910\,\mu\text{m}$ ($\pm 5\,\%$) and $V_{gr}^t = -7.7(30)\,\text{mV}$.) The small disagreement between the measured rms cyclotron amplitude fluctuations and the predicted cyclotron thermal radius suggests that our cooling procedure was not optimal, or that our detector's effective temperature might be slightly higher than 4 K (due to extra electronic noise).

Note that the contribution from the ion-ion interaction scales like $1/\rho_s^5$ (Eq. 5.34) and is already dominant at $910\,\mu\text{m}$. This was confirmed experimentally by observing a dramatic increase in the phase noise as the ions were moved closer together (for $\rho_s < 800\,\mu\text{m}$) as shown in Fig. 5-17. The observed frequency noise σ_{f2} vs $1/\rho_s^5$ roughly exhibits the correct behavior. This is the main reason why we could not make precise measurement of the ratio below $600\,\mu\text{m}$.

So cyclotron amplitude fluctuations are clearly the dominant source of noise in the two-ion technique, introducing shot to shot fluctuations of $2-5\times10^{-11}$ in the measured cyclotron frequency difference. This is true even for ions with large m/q, and not just for light ions as was always assumed. To perform cyclotron frequency comparisons with a precision at the 10^{-12} level, it is therefore crucial to reduce the thermal amplitudes. Physically cooling our detector below 4 K is a sensible option, but would require some engineering. It would be limited by the fact that the SQUID won't work below 1 K, but it would also increase our signal-to-noise. The classical amplitude squeezing technique demonstrated by our group [7, 8] could reduce the amplitude noise, but at the expense of increased phase noise. The best approach (I think) is the electronic refrigeration technique described in Sect. 2.3 which can be used to cool the effective temperature of the detector and ion below the 4 K ambient temperature of the detector coil and trap environment.

Note that in order to simply our system, we did not use electronic refrigeration in

†Including the effect of C_6 would add a cubic term to the expected behavior of σ_{f2} vs ρ_c but that would not describe any better the data shown in Fig. 5-16

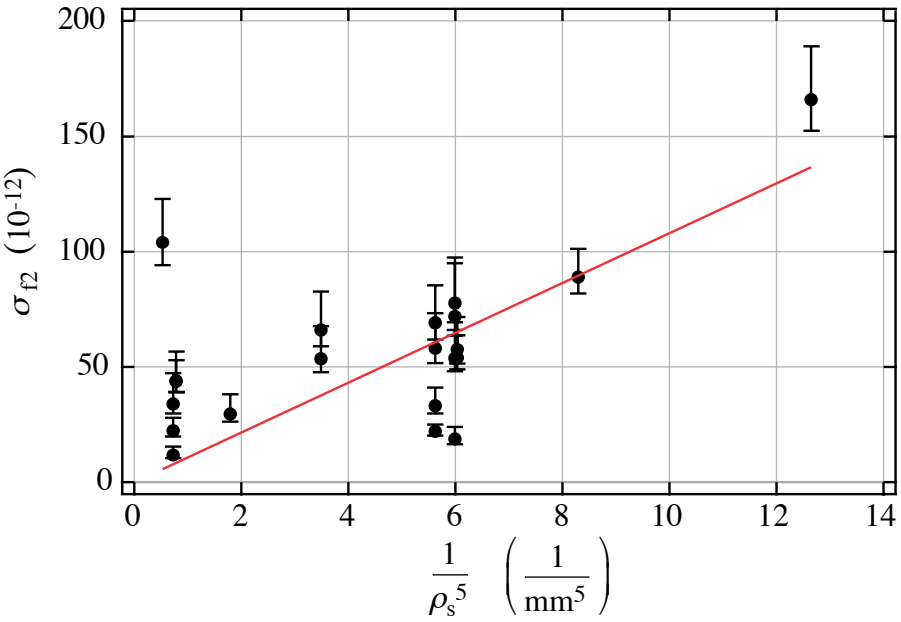

Figure 5-17: Observed frequency noise σ_{f2} as a function of $1/\rho_s^5$. The data exhibit the expected linear scaling at small separation (right hand side of the plot). At large separation, σ_{f2} levels off because relativity, and B_2 start to dominate. The straight line shown is a fit to the data constrained to go through the origin.

all the two-ion measurements reported in this thesis. Now that we have confidence in the two-ion technique, it should be easy to implement it again and potentially observe a large reduction in the fluctuations in our measurement. This would lead to even further improvement in precision, and especially allow us to move the ions closer to each other and better characterize the perturbations due to ion-ion interactions.

5.6.2 Optimizing T_{evol}

Based on our understanding of the source of the random fluctuations in our measurement, one can try to optimize the longest evolution time T_{evol} used to reach the maximum precision on ω_{ct2} in the shortest possible time. The simplest approach is to say that we want the contributions from both terms in Eq. (5.30) to be equal to each other. That would give an evolution time of about 500 s (8 minutes) for the small ρ_c that we use when we make our precision measurements of the ratio. We would rather stay on the smaller side of that limit just because, psychologically, it is preferable to have many less precise points than very few points that are in principle more precise. That is actually not just a psychological effect and can be quantified by considering the error on the estimate of the standard deviation of a finite series of measurements. Frank DiFilippo has a short appendix at the end of his Ph.D. thesis discussing this topic (see also [23] p.195 and 255). In developing a model for optimizing T_{evol}, I also studied this question.

To obtain a more complete model for optimizing $T_{\rm evol}$, we can include the fact that there is some "dead time" $T_{\rm dead}$ associated with each long time PNP — from the ringdown (typically 8 s), the cooling of the axial and cyclotron amplitudes (60 s), and all the other PNPs with shorter $T_{\rm evol}$ needed for phase unwrapping ($\sim$200 s). The goal is then to minimize the relative uncertainty of the measured cyclotron frequency difference which is given by the standard deviation of the mean of our measurements of $\omega_{\rm ct2}$:

$$\sigma_{\rm mean} \equiv \frac{\sigma f_{\rm ct2}}{\bar{f}_{\rm ct}} = \frac{1}{\sqrt{N}} \frac{\sigma_{\phi 2}}{360\, \bar{f}_{\rm ct} T_{\rm evol}} \qquad \text{where} \qquad N = \frac{t}{T_{\rm evol} + T_{\rm dead}} \tag{5.35}$$

is the number of long time points in the data set (which lasts for a total time t) and $\sigma_{\phi 2}$ is given by Eq. (5.30). The optimal $T_{\rm evol}$ is the solution of the cubic equation

$$(360\ \sigma_{\rm f2})^2 T_{\rm evol}^3 - (\sigma_{\phi 2}^{\rm s})^2 T - 2(\sigma_{\phi 2}^{\rm s})^2 T_{\rm dead} = 0\ . \tag{5.36}$$

In the limit where $T_{\rm dead} = 0$, one recovers our first order guess that the optimal $T_{\rm evol}$ is given by $\sigma_{\phi 2}^{\rm s}/(360\ \sigma_{\rm f2})$. Using the typical parameters for our ${}^{13}C_2H_2{}^+/{}^{14}N_2{}^+$ measurements, one predicts from this an optimum $T_{\rm evol}$ of 1060 s. However that would give us only ten points in 5 hours of data taking.

For a small number of points $N \lesssim 20$, the usual maximum likelyhood estimate of the standard deviation most often underestimates the true variations and so a better quantity to minimize would be the tip of the positive error bar on the standard deviation of the mean, which we call $\sigma_{\rm mean}^{\rm max}$. This has to be done numerically. In the calculation, we also changed the duration of the four longest PNPs so that the ratio from one $T_{\rm evol}$ to the next would be the same (that essentially makes $T_{\rm dead}$ a function of $T_{\rm evol}$). A typical list of $T_{\rm evol}$ would be 0.1; 0.15; 0.23; 0.7; 2; 7; 25; 90; 260; 600 s. The predicted precision on $\omega_{\rm ct2}$ ($\sigma_{\rm mean}$ and $\sigma_{\rm mean}^{\rm max}$) achieved after 5 hours of measurements as a function of $T_{\rm evol}^{\ell}$ is shown in Fig. 5-18. The result of the numerical optimization (minimizing $\sigma_{\rm mean}^{\rm max}$) is $T_{\rm evol} = 900$ s for a 5 hour data set. If one assumes a relative frequency noise ($\sigma_{\rm f2}/\ \bar{f}_{\rm ct}$) of 4.7×10^{-11} (twice the value from the data in the above section), then the same optimization leads to $T_{\rm evol} = 515$ s. At the end, we used all this fancy optimization only as a guide. We picked a list of $T_{\rm evol}$ that worked well and tended to keep it pretty constant. The most positive thing that came out of this work is that it motivated us to try longer $T_{\rm evol}$ than we intuitively would have done, and that led to some small gain in efficiency. From Fig. 5-18, we see that using $T_{\rm evol} = 800$ s instead of $T_{\rm evol} = 400$ s, should lead to an improvement of 3×10^{-12} in the precision for a 5 hour data set.

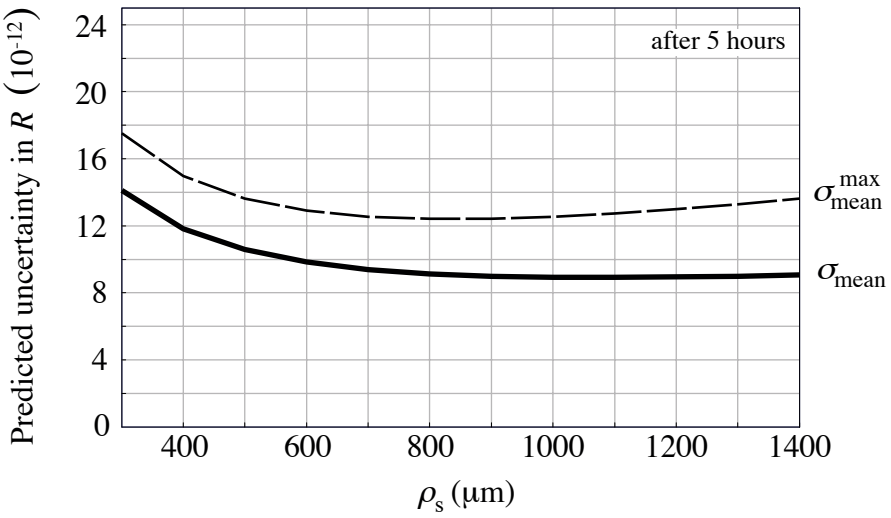

Figure 5-18: Predicted final error on R after 5 hours of data (with frequency noise of 2.3×10^{-11}). The solid curves represents the standard deviation of the mean $\sigma_{\rm mean}$ and it has a minimum at $T_{\rm evol} = 1066\,{\rm s}$. The dashed line shows $\sigma_{\rm mean}^{\rm max}$, the upper end of the error bar on $\sigma_{\rm mean}$. The minimum of $\sigma_{\rm mean}^{\rm max}$ is at $T_{\rm evol} = 900\,{\rm s}$.

Chapter 6

A direct test of $E = mc^2$

In this chapter we present two mass ratios measurements made with the two-ion technique to test $E = mc^2$ directly. It is presented as an expanded version of a Letter that will shortly be submitted to Physical Review Letters. More details are included here than the PRL format will allow us.

We report measurements of the two mass ratios $m[^{33}S^+]/m[^{32}SH^+]$ and $m[^{29}Si^+]/m[^{28}SiH^+]$ with a relative uncertainty of less than 10^{-11}, which makes them the best known mass ratios to date. These measurements were performed using our newly demonstrated technique for simultaneously comparing the cyclotron frequencies of two ions confined in a Penning trap. Combined with precise measurements of high-energy gamma-rays, these values provide a new laboratory test of special relativity which does not rely on the assumption of a preferred reference frame. The new bound we obtain is $1 - c_{\rm em}/c_{\rm m} < 2 \times 10^{-7}$. The uncertainty on the atomic mass of ^{29}Si is also reduced by more than an order of magnitude. The updated value is $M[^{29}\mathrm{Si}] = 28.976\,494\,662\,9\ (20)$ u.

6.1 Introduction

Precise mass measurements have a wide-ranging impact on both fundamental physics and metrology. By comparing the masses of single ions in a Penning trap, the MIT ICR group has measured a total of 13 neutral masses with fractional accuracies near or below 10^{-10} [24, 25]. Recently, we have demonstrated an ability to confine two different ions in a Penning trap and *simultaneously* measuring their cyclotron frequencies [26]. The mass ratio of the two ions can then be determined with a relative uncertainty of less than 10^{-11}. The two ratios reported here in conjunction with the related γ-ray energy measurements at NIST [27] enable a new test of special relativity. Before describing these measurements, we discuss the connection between mass ratio measurements, gamma-ray energies and the theory of special relativity.

6.2 Motivation

Over the last century, special relativity has established itself as one of the deepest principles in our understanding of modern physics. Lorentz invariance is deeply woven into the structure of quantum field theory; experiments in high-energy and atomic physics routinely confirm the predictions of special relativity; and even some "everyday" instruments (like the global positioning system) require a proper accounting of time dilation. This paper presents measurements that enable a direct test of one of the most significant consequences of special relativity: the mass-energy relationship, $E = mc^2$. By measuring the mass difference (this experiment) between two nuclear states that emit a γ-ray whose energy is also measured [28], we test it in the form

$$\Delta mc^2 = E_\gamma^* = \frac{hc}{\lambda^*} \, . \tag{6.1}$$

The prominent role of the theory has motivated many tests of its foundations and predictions; in fact the theory itself was motivated by the Michelson-Morley ether-drift experiment over a century ago. Added motivation has been provided by the discovery of the cosmic background radiation — a cosmological preferred frame of reference — and recent theoretical efforts to unify the forces of nature, which could lead to non-Lorentz-covariant Maxwell equations. The theoretical framework to describe a possible breakdown of Lorentz invariance and to interpret these tests has been developed by Robertson [29], Mansouri and Sexl [30], Haugan and Will [31], and recently Kostelecký and Mewes [32] .

In general, tests of special relativity can be divided in three categories according to which assumption they investigate: the isotropy of space (Michelson-Morley experiment, Hughes-Drever experiment); the independence of the speed of light from the velocity of the laboratory (Kennedy-Thorndike experiment); and the time dilation effect (Mössbauer-rotor experiments — Doppler spectroscopy).

The test performed here (proposed by Greene et al. [27]) is different from all of these in that it does not assume the existence of a preferred frame of reference. It can be compared to other tests by considering two distinct "speeds of light": the velocity of propagation of an electromagnetic wave in vacuum, denoted $c_{\rm em}$, and the limiting velocity of a massive particle $c_{\rm m}$. According to special relativity, $c_{\rm m} = c_{\rm em} = c$. One way to test this assumption is to measure the wavelength of a photon emitted in a transition where a mass Δm is converted into electromagnetic radiation. From energy conservation

$$\Delta mc_{\rm m}^2 = \frac{hc_{\rm em}}{\lambda} \, , \tag{6.2}$$

where λ is the photon wavelength and h is Planck constant. This test is most conveniently formulated in terms of two "fine structure constants"

$$\alpha_{\rm m} \equiv \frac{e^2}{\hbar c_{\rm m}} \quad \text{and} \quad \alpha_{\rm em} \equiv \frac{e^2}{\hbar c_{\rm em}} \,, \tag{6.3}$$

where e is the charge of the electron. It is shown in Ref. [27] that the value of α from the Compton wavelength of the electron is the currently most accurate determination of $\alpha_{\rm m}$. They also argue that the value derived from the quantum Hall effect [33] is $\alpha_{\rm em}$. Recently, a more precise value of $\alpha_{\rm em}$ was obtained by combining the recoil velocity $v_{\rm rec}$ of a Cs atom after absorbing a photon [34], the frequency of that photon $f_{\rm D1}$ [35], the atomic mass of Cs [25], and the atomic mass of the electron [36] as follows:

$$\alpha^2_{\rm Cs} = 2R_\infty \frac{h}{m[{\rm Cs}]} \frac{M[{\rm Cs}]}{M[{\rm e}]} = 2R_\infty \, \lambda_{\rm D1} \, v_{\rm rec} \, \frac{M[{\rm Cs}]}{M[{\rm e}]} \tag{6.4}$$

$$= 2R_\infty \left(\frac{c_{\rm em}}{f_{\rm D1}}\right) \left(\frac{f_{\rm rec} c_{\rm em}}{f_{\rm D1}}\right) \frac{M[{\rm Cs}]}{M[{\rm e}]} \,. \tag{6.5}$$

As discussed in [27], the c which appears in R_∞ arises from the relation between the photon energy and wavelength and is identified as $c_{\rm em}$. The same is true of the c relating $\lambda_{\rm D1}$ to $f_{\rm D1}$ (inside the first parentheses). Finally, to relate the experimentally measure frequency shift $f_{\rm rec}$ to $v_{\rm rec}$, one also needs $c_{\rm em}$ since the measurement of $v_{\rm rec}$ is essentially based on the first order Doppler shift of the laser light that the Cs atoms "perceive" while moving (non-relativistically). Thus we find that $\alpha_{\rm Cs}$ depends only on $c_{\rm em}$ and so corresponds to $\alpha_{\rm em}$. The preliminary value reported in [34] has an uncertainty of 7.3×10^{-9}.

To realize an experiment to test Eq. (6.2), we consider the non-resonant capture of cold neutrons in the reaction

$$^A{\rm X} + n \;\longrightarrow\; ^{A+1}{\rm X} + \gamma{\rm 's} \,. \tag{6.6}$$

From energy conservation (Eq. (6.2)), we obtain

$$M[^{\rm A}{\rm X}] + M[{\rm n}] - M[^{\rm A+1}{\rm X}] = \left(\frac{N_{\rm A} h}{c} 10^{-3}\right) \left(\frac{1}{\lambda^*_{\rm A+1}}\right) \,, \tag{6.7}$$

where $N_{\rm A}$ is the Avogadro constant, and all quantities are expressed in their respective SI units, except all the masses $M[{\rm X}]$, which are expressed in atomic mass units ($M[^{12}{\rm C}] \equiv 12\,{\rm u}$). ($\lambda^*$ includes a correction for the $^{A+1}$X recoil energy.) The mass measurements are performed with charged particles in a Penning trap and therefore the mass of the neutron has to be determined from the masses of deuterium and hydrogen along with $\lambda^*_{\rm D}$, the wavelength of the 2.2 MeV n–p capture gamma-ray corresponding to the deuteron binding energy (Eq. (6.7) with $A = 1$). We then obtain

$$M[^{\rm A}{\rm X}] - M[^{\rm A+1}{\rm X}] + M[{\rm D}] - M[{\rm H}] = \left(\frac{N_{\rm A} h}{c} 10^{-3}\right) \left(\frac{1}{\lambda^*_{\rm A+1}} - \frac{1}{\lambda^*_{\rm D}}\right) \,. \tag{6.8}$$

The most precise value for $N_A h$ (the molar Planck constant) is obtained by expressing the fine structure constant in terms of the Rydberg constant R_∞ as follows

$$\alpha^2 = \frac{2R_\infty}{M[\mathrm{e}]} \left(\frac{N_A h}{c} 10^{-3} \right) . \tag{6.9}$$

The wavelength λ_D^* in Eq. (6.8) has been measured by a group from NIST (Gaithersburg) using crystal diffraction at the GAMS4 facility at the Institut Laue-Langevin [37]. Recently, they have performed similar measurements for ^{29}Si, ^{33}S, and ^{36}Cl which are reported in another Letter in this issue [28]. In the next section we will describe our measurement of the mass difference on the left-hand side of Eq. (6.8) for A=28 (Si) and A=32 (S). The results can be interpreted two different ways: if we extract the value of $N_A h$ from the most precise α_{em} using Eq. (6.9), and substitute it in Eq. (6.8), we obtain a new limit on the quantity $1 - c_{\mathrm{m}}/c_{\mathrm{em}}$. Conversely, if we assume $c_{\mathrm{em}} = c_{\mathrm{m}}$, Eq. (6.8) gives us a new determination of $N_A h$ and hence α_{m}. Both interpretations will be discussed in Sect. 6.4.

6.3 Mass Measurements

To measure atomic masses we compare the cyclotron frequencies of single ions in a Penning Trap. A strong magnetic field (8.5 T) is provided by a stable superconducting magnet and the corresponding cyclotron frequency is simply given by $2\pi f_{\mathrm{c}} = qB/m$ (typically 5 MHz). By measuring the ratio of the cyclotron frequencies of two different ions, we obtain their mass ratio, which can then be converted into a mass difference (we choose ions whose $\Delta m/m < 10^{-3}$ so that $R \approx 1$). The ions are confined along the magnetic field axis by a quadrupole electric field produced by hyperbolic electrodes (orthogonally compensated, characteristic dimension $d \simeq 0.55$ cm [2]), which generates harmonic oscillations of the ions along that axis (axial motion with $f_{\mathrm{z}} \approx 210$ kHz). The electrostatic field modifies the cyclotron frequency and results in a third mode of motion of an ion in the trap, called the magnetron mode, which corresponds to a slow $E \times B$ drift of the ion's position around the trap center ($f_{\mathrm{m}} \approx 5$ kHz). The free space cyclotron frequency can be recovered using the invariance theorem demonstrated in [2]:

$$f_{\mathrm{c}}^2 = f_{\mathrm{ct}}^2 + f_{\mathrm{z}}^2 + f_{\mathrm{m}}^2 , \tag{6.10}$$

where f_{ct} is the (trap) cyclotron frequency measured experimentally. Only the axial motion is detected (and damped to 4 K). This is done by coupling the image current the ion's motion induces across the trap to a dc SQUID via a superconducting resonant transformer ($Q \sim 47\,000$). To measure the cyclotron and magnetron frequencies and also to cool these radial modes, we use rf coupling to the detected axial mode [4].

To make our measurement insensitive to magnetic field fluctuations, we load two different ions in our trap and measure their cyclotron frequencies *simultaneously*. To minimize

frequency perturbations due to ion-ion interactions, we keep the distance between the ions $\rho_s \approx$700–800 μm. The dynamics of two ions in a Penning trap and the details of how we load a pair of ions and control their trajectories have been described in [13] and [26].

Because f_m is to first order independent of mass, the Coulomb force between the ions is strong enough to couple the two individual magnetron modes. The dynamics of the two ions is then described by new magnetron normal modes: the center-of-mass mode and the difference mode. We have developed techniques to damp the center-of-mass mode amplitude, which effectively "park" the two ions on a common magnetron orbit on opposite sides of the trap. The distance between the ions is constant in time and can be controlled experimentally. This is the ideal configuration in which we perform precise simultaneous measurements of the cyclotron frequencies of both ions f_{ct0} and f_{ct1}. Note that the differences between both the axial and cyclotron frequencies are large enough to keep these modes uncoupled although their frequencies are perturbed.

A particular challenge for these measurements was to introduce in our trap the rare isotopes ^{29}Si, and especially ^{33}S. To directly measure the mass difference on the left-hand side of Eq. (6.8), we originally wanted to compare $m[^{32}SD^+]$ with $m[^{33}SH^+]$. However, we did not succeed in having enriched hydrogen sulfide-33 synthesized in time for the measurement. We resorted to rely on the 0.4 % natural abundance of ^{33}S in a regular $^{32}SH_2$ gas bottle. After $\sim$ 40 unsuccesful attempts, we trapped a $^{33}S^+$ ion and performed our entire measurement (over three weeks) with that single $^{33}S^+$. (We could never make a $^{33}SH^+$ ion). The same procedure was repeated for $^{29}Si^+$(natural abundance: 4 %). This dramatically illustrates a very powerful aspect of our new two-ion technique: the need for only a single atom or molecule to perform a measurement.

Once a pair is loaded in the trap and placed in the ideal configuration described above, we can perform simultaneous measurements of the two trap cyclotron frequencies f_{ct0} and f_{ct1} using the same coupling techniques we have developed for single-ion alternating measurements [24, 25]. Figure 6-1 shows the measured difference frequency $f_{ct2} \equiv f_{ct1} - f_{ct0}$ vs time for a typical data set (5–15 hours). The common mode rejection of the magnetic field noise is striking. The standard deviation of the measurements is 7×10^{-11}, and the whole 17 hours of data therefore determines f_{ct2} with a relative precision 10^{-11}. Since $\Delta m/m < 10^{-3}$, f_{ct2} is the only frequency we need to measure precisely. As described in [13, 26], the mass ratio $R \equiv f_{ct0}/f_{ct1}$ is determined from f_{ct2}, combined with the measured frequecies f_{ct} and f_z of one ion. To obtain a relative precision of 10^{-11} on the ratio, we only need to know f_{ct} to 4×10^{-8} (or 0.16 Hz) and f_z to 1.4×10^{-5} (or 2.9 Hz).

6.3.1 Systematic Errors

The tremendous increase in precision of the two-ion technique seen above comes at the price of a more complex system, and is limited by systematic errors: Coulomb interaction when the ions are close together and imperfections in the trapping fields when the ions are far

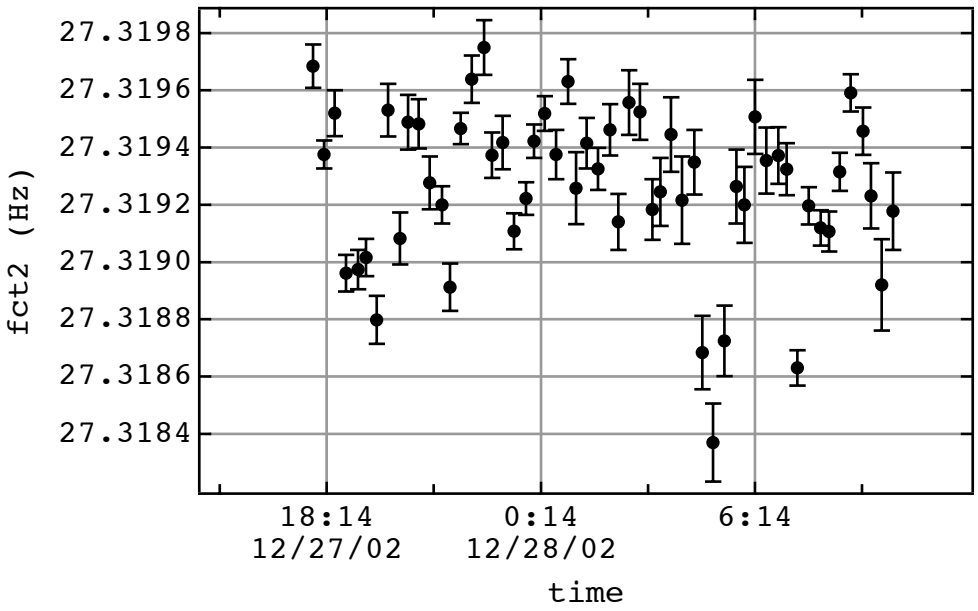

Figure 6-1: Typical sequence of measured cyclotron frequency difference vs time. The standard deviation of the points is 7×10^{-11} and the total data set determines the difference frequency with a relative precision of 1×10^{-11}.

apart. For the $H^{32}S^+/^{33}S^+$ pair, we calculate that the ion-ion interaction should perturb the individual cyclotron frequencies by about 5×10^{-8} when the ions are at a distance $\rho_s = 750\,\mu m$ from each other. However the shift of the all-important *difference* should only be 5×10^{-13}, if the radii of the two cyclotron orbits are equal ($\rho_{c0} = \rho_{c1}$). If they are not, it has been shown in Ref. [13] that the non-linear interaction between the ions gives a shift of f_{ct2} proportional to ρ_c^2, $\delta_{cyc} = (\rho_{c1} - \rho_{c0})/(\rho_{c1} + \rho_{c0})$, and ρ_s^{-5}. The main concern is therefore the possibility of a systematic imbalance between the two cyclotron radii. From our knowledge of the frequency dependence of the electronics between our cyclotron drive synthesizers and the trap, and by directly comparing the outputs of the synthesizers, we estimate that $|\delta_{cyc}| \lesssim 0.005$. Experimentally we have performed three types of two-ion measurements to directly confirm our model for the ion-ion interactions and put limits on δ_{cyc} (see [26] for more details):

1. Direct measurement of the shift in f_{ct2} when δ_{cyc} is made purposely large, i. e., measure the difference between $f_{ct2}(\delta_{cyc}$=+0.1) and $f_{ct2}(\delta_{cyc}$=-0.1).

2. Direct measurement of the shift in f_{ct2} when the average ρ_c of both ions are made bigger by $\sqrt{2}$.

3. Verification that the measured ratio does not vary when the role of the two cyclotron drive synthesizers are interchanged.

In the first experiment, we compared the observed shift with the predicted shift from our model. The difference between the observed and predicted shifts was $+21(22) \times 10^{-12}$ and $-29(11) \times 10^{-12}$ at $\rho_s = 775\,\mu m$ and $1000\,\mu m$ respectively. As was the case for our ${}^{13}C_2H_2{}^+/{}^{14}N_2{}^+$ measurement (see [26]), the agreement at small distances confirms our model of the effect of a mismatch in cyclotron orbit sizes from ion-ion interactions. Again, there is some discrepancy at $\rho_s = 1000\,\mu m$, but our measurements put an upper limit of 3.5×10^{-12} for the effect of any phenomenon unaccounted for when we take precise measurement data (and $|\delta_{cyc}| < 0.013$ as we will see below). In experiments #2 and #3, we drive both ions to nominally the same cyclotron radii and the comparison between the measured shifts and the expressions from our model leads to an upper limit on δ_{cyc}. The resulting measurements of δ_{cyc} are +0.010(18) and -0.001(13) for the sulfur and silicon data sets respectively. Even though we have independent reasons (mentioned above) to believe that $|\delta_{cyc}| \lesssim 0.005$, we take $\delta_{cyc} = 0.000(13)$ for all data sets to be conservative and account for any unknown systematic error related to ion-ion interactions. The uncertainty in the cyclotron radius imbalance leads to an "uncertainty band" shown on the left of Fig. 6-3 and 6-4.

The potential systematic error from ion-ion interactions depends very strongly on ρ_s, and the obvious solution is to move the ions further apart. However, as we do so, we also move the ions further away from the trap center. Our measurements then become more sensitive to frequency shifts due to electric field anharmonicities and magnetic field inhomogeneities. Field imperfections affect f_{ct2} due to the fact that the two ions' magnetron radii are systematically different from each other (by a few percent) due to their finite mass difference [13]. In order to control this problem, we have had to characterize our trapping fields very well (with a single ion in the trap), and optimize the one electrostatic term we can control, C_4, to cancel out the effect of all the other perturbations. But our uncertainties in the various terms in the expansions of our fields (10 % on D_4, C_6, B_2, and 44 % on B_4 — see [2]) limit our ability to do so perfectly. This leads to a potential systematic error which grows very quickly with ρ_s (at least as ρ_s^5), as indicated by the gray band on the right-hand side of Fig. 6-3 and 6-4. To make sure that we understand the effect of field imperfections on our measurements, we have measured the slope $\partial f_{ct2}/\partial C_4$ and found that it agrees very well with our prediction, as shown in Fig. 6-2 (χ^2_ν(measured-predicted) ~ 0.15).

The ultimate test for probing possible systematic errors is to measure the ratio R as a function of the distance between the ions. The fact that all the data points fall within our uncertainty bands is a very powerful check for the presence of unknown systematic errors, because the size of each contribution has changed by at least a factor of 30 between $\rho_s = 600$ and $1200\,\mu m$. In fact, the lack of a sharp change in the data toward the ends of the range of measured ρ_s strongly suggests that we have overestimated our errors. Our final values of the measured mass ratios (taking into account the correlated errors between points) are

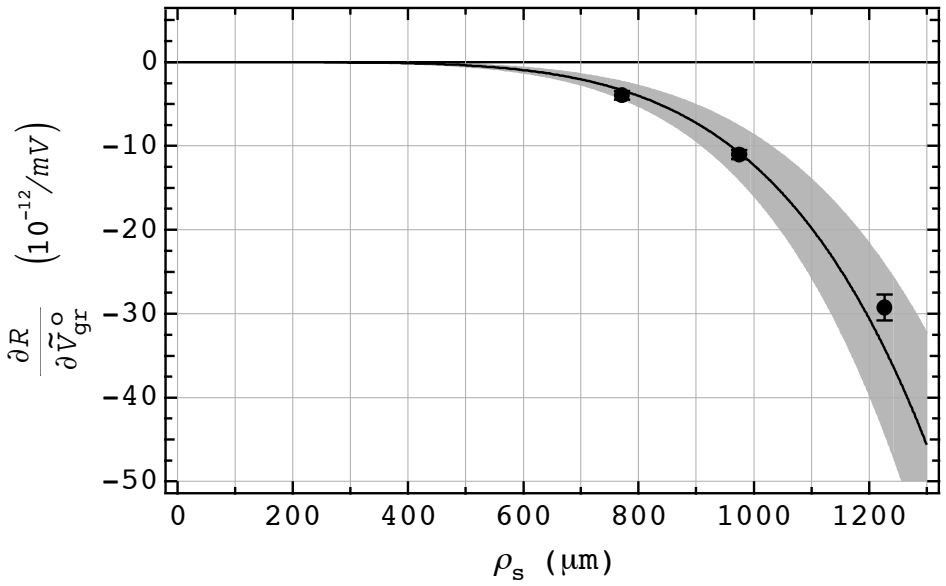

Figure 6-2: Measured slope $\partial R/\partial V_{\mathrm{gr}}^{\mathrm{t}}$ using $\mathrm{H}^{32}\mathrm{S}^{+}/{}^{33}\mathrm{S}^{+}$ compared to the expected slope from our independent measurements of the trap field imperfections (and uncertainty). $V_{\mathrm{gr}}^{\mathrm{t}}$ is related to the voltage applied to one of the electrodes of our trap (guard ring) which affects C_4. These results show that we understand the effect of field imperfections on our measured ratio.

$$\frac{m[^{33}\mathrm{S}^{+}]}{m[^{32}\mathrm{SH}^{+}]} = 0.999\,744\,166\,300\,0(74) \tag{6.11a}$$

$$\frac{m[^{29}\mathrm{Si}^{+}]}{m[^{28}\mathrm{SiH}^{+}]} = 0.999\,715\,124\,173\,9(65)\,. \tag{6.11b}$$

Table 5.3 shows the error budget for these measurements. Note that we will have to apply a correction of about $+50\times10^{-12}$ and $+7\times10^{-12}$ to the measured ratios to account for the polarization energies of the $^{32}\mathrm{SH}^{+}$and $^{28}\mathrm{SiH}^{+}$molecules. (The mass ratios including this correction are given in Table 7.1.) The corrections mentioned above are only preliminary estimates and complete calculations will be performed shortly. Please refer to our future publications for the final values (and a complete explanation of the cyclotron frequency shift of a cold polarizable molecule in a Penning trap). To account for our uncertainty in that correction, we increase here the relative uncertainties of the two measured ratios to 12 and 7×10^{-12} for sulfur and silicon respectively. But even with these increased error bars our ratios are still 425 and 200 times more accurate than previous values. By accounting for the mass of the missing electron and the chemical binding energies (from [22]), the mass ratios (Eq. (6.11)) can be converted into the following neutral mass differences

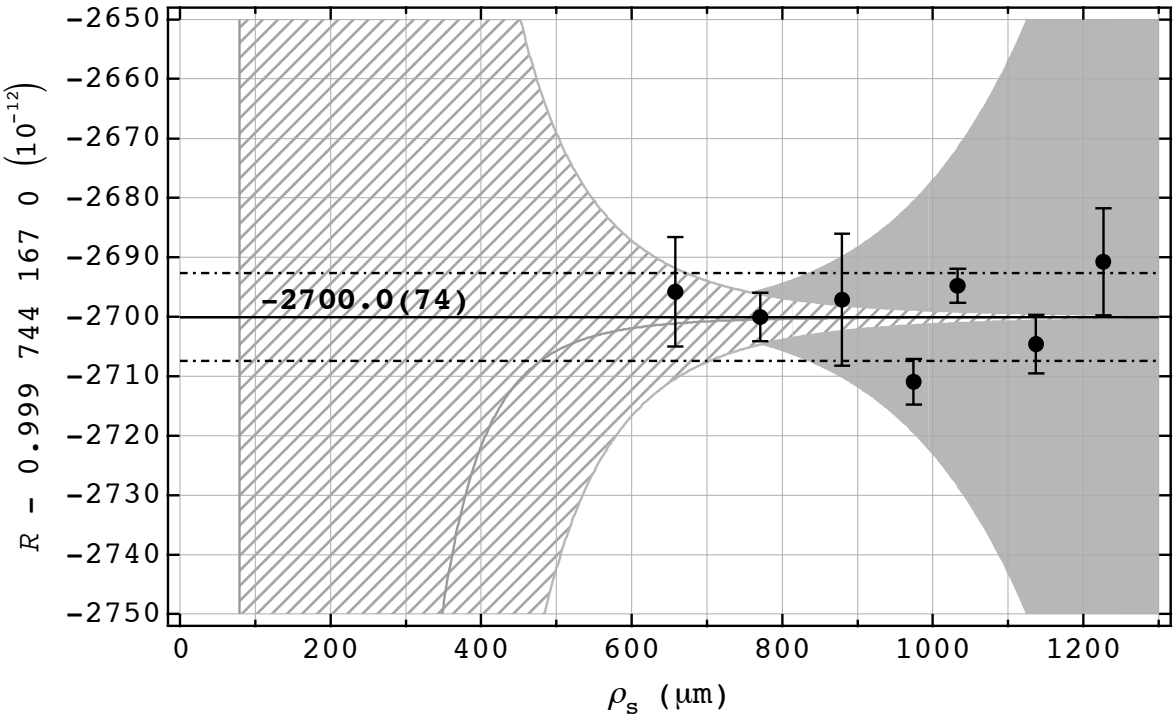

Figure 6-3: Summary of the measured ratio $m[^{33}S^{+}]/m[^{32}SH^{+}]$ as a function of ion-ion separation distance. The substracted offset is the ratio predicted from the masses in [20].The shaded areas represent the possible systematic error from ion-ion interactions (left) and field imperfections (right). The solid horizontal line indicates our best estimate of the cyclotron frequency ratio, with the $1\,\sigma$ confidence interval denoted by dashed lines.

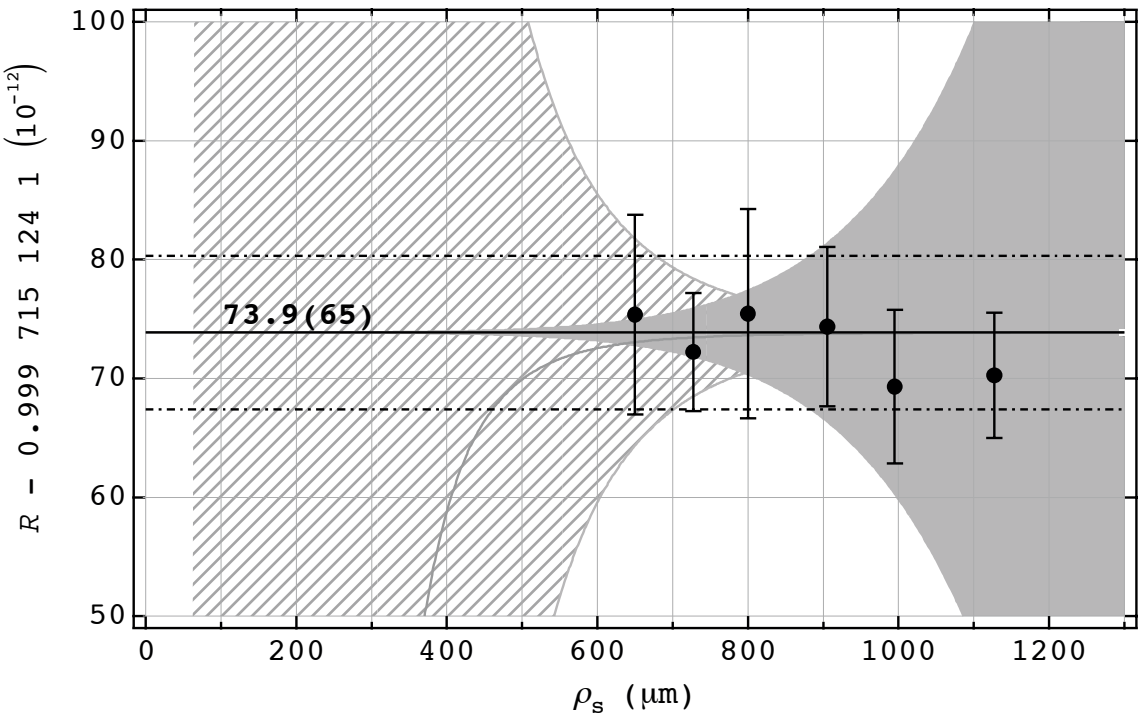

Figure 6-4: Summary of the measured ratio $m[^{29}\mathrm{Si}^+]/m[^{28}\mathrm{SiH}^+]$ as a function of ion-ion separation distance. See caption of Fig. 6-3.

$$M[^{32}\mathrm{S}] + M[\mathrm{H}] - M[^{33}\mathrm{S}] = 0.008\,437\,296\,58\,(40)\,, \tag{6.12a}$$

$$M[^{28}\mathrm{Si}] + M[\mathrm{H}] - M[^{29}\mathrm{Si}] = 0.008\,256\,901\,99\,(24)\,^{\dagger}. \tag{6.12b}$$

The relative precisions of these mass differences are 4.7 and 2.9×10^{-8} respectively. Note that the uncertainties on the heat of formation of SiH^+ and Si^+ (from [21]) contribute an error of 1.7×10^{-8} to the silicon mass difference.

6.4 Conclusion

Unfortunately, the measured mass differences (Eq. (6.12)) are not quite what appear in Eq. (6.8) and so we need to add to each of them $M[\mathrm{D}]$ - $2M[\mathrm{H}]$. That mass difference can be calculated from the most current values of $M[\mathrm{D}]$ and $M[\mathrm{H}]$ from [22] with a relative precision of 2.7×10^{-7}. Since $M[\mathrm{D}]$ - $2M[\mathrm{H}]$ is about 5 times smaller than the mass differences we measured, its contribution to the uncertainty of the total mass difference should be slightly above the uncertainty from our measurements (about 5×10^{-8}). Using the values of λ^*_{D}, λ^*_{S}, and λ^*_{Si} from the GAMS4 group, and α_{em} from [34], we will obtain two independent tests of the famous relationship $E = mc^2$ with an uncertainty of about 2×10^{-7} (dominated by

Table 6.1: Comparison with other tests of special relativity that we are aware of.

Type of experiment	$1 - c_{\mathrm{m}}/c_{\mathrm{em}}$	References
Michelson-Morley (anisotropy)*	10^{-9}	[39]
Hughes-Drever (anisotropy) *	3×10^{-22}	[41, 42]
Mössbauer-rotor*†	10^{-6}	[43]
Eötvös*†‡	10^{-9}	[44]
High-energy tests	1×10^{-23}	[45, 38]
Mass - Wavelength measurements†	2×10^{-7}	(this work)

the wavelength measurements). These will be the most precise *direct* tests of $E = mc^2$ by about two orders of magnitude. As described in Sect. 6.2, these results also correspond to two new limits on $1 - c_{\mathrm{em}}/c_{\mathrm{m}}$, also with a precision of 2×10^{-7}.

For comparison, the limits on this quantity that can be extracted from other tests of special relativity are shown in Table 6.1. Even though our new limit will not be as stringent as most of the other tests, it is unique in that it does not rely on any assumption of a preferred reference frame [27]. Haugan and Will have also noted that most of the very precise tests of special relativity are sensitive only to the tensor contribution of any Lorentz-invariance violating coupling [31]. The Mössbauer-rotor and the Eötvös experiments are two exceptions, as is our test of $E = mc^2$. However, in contrast to our limit, the Eötvös experiments is also be sensitive to a coupling violating local position invariance [31], and so they have to assume that there is no fortuitous cancellation between these two anomalies. Finally, Coleman and Glashow have obtained very stringent limits based on the observation of primary cosmic-ray photons and protons with very high energies [38].

Alternatively, if we set $c_{\mathrm{em}} = c_{\mathrm{m}}$, we will obtain a new value of the molar Planck constant $N_{\mathrm{A}}h$, and the most accurate determination of the mechanical fine structure constant. The previous best was the value of α_{m} from the Compton wavelength of the electron with an uncertainty of 1.2×10^{-5}. However, it is still about 55 times less precise than the current best value of α [46]. Finally, Eq. (6.12b) combined with $M[^{28}\mathrm{Si}]$ and $M[\mathrm{H}]$ from [20] lead to an new value of $M[^{29}\mathrm{Si}]$ with an uncertainty reduced by an order of magnitude from the current most precise value [47] (dominated by the error on $M[^{28}\mathrm{Si}]$):

$$M[^{29}\mathrm{Si}] = 28.976\,494\,662\,6(20)\,\mathrm{u}\,. \tag{6.13}$$

In the future, the same test could be carried out with ^{15}N, ^{36}Cl and ^{49}TiThe λ^*_{Cl} and λ^*_{Ti} have been measured but ^{36}Cl is slightly radioactive and ^{49}Ti is heavier than most masses we have measured. ^{15}N would be best from the mass measurement aspect but the intensities of the γ-rays are low and it is not clear whether a precise measurement of λ^*_{N} will be possible.

*Assumes preferred frame (cosmic microwave background)

†Tests scalar contribution (the others test the tensor contribution).

‡Assumes no fortuitous cancellation between local Lorentz invariance and local position invariance.

Chapter 7

Conclusion and Outlook

Starting in 1983, seven graduate students, four post-docs, and many undergraduate students have constructed the world's most accurate and versatile mass spectrometer, and used it to perform many interesting mass comparisons with fractional accuracies near or below 10^{-10}. Over the last four years, James Thompson and I have improved the apparatus and demonstrated a qualitatively new technique to further improve its accuracy by about an order of magnitude. By simultaneously confining two different ions in our Penning trap and directly measuring the difference in their cyclotron frequencies, we have measured three mass ratios with a relative uncertainty at or below 10^{-11}. The measured ratios are summarized in Table 7.1, and Table 7.2 gives the mass differences that can be extracted from them.

There were many challenges in the development of the two-ion technique, but thanks to the great legacy of all the previous members of the group and a good dose of perseverance (maybe some luck too!), we were able to succeed. The first one was to control the trajectories of the two ions in the trap to "park" them in an ideal configuration where they both move on nearly the same magnetron orbit, on opposite sides of the trap. That required the development of completely new experimental tools to precisely characterize and control all

Table 7.1: Best values for the measured mass ratios. These are preliminary values; they include only an estimate of the polarization shift correction. Please refer to our future publications for the final value. Also shown are the differences between our measured ratio and the predicted values from the masses in [20] (and binding energies), and the factor of improvement in the uncertainty.

Ratio	Measured value	$(R - R_{95}) \times 10^{12}$	$\sigma R_{95}/\sigma R$
$\frac{M[^{14}N_2{}^+]}{M[^{13}C_2H_2{}^+]}$	0.999 421 460 888 (10)	+130 (110)	11
$\frac{m[^{29}Si^+]}{m[^{28}SiH^+]}$	0.999 715 124 181 (7)	-1 900 (1 400)	200
$\frac{m[^{33}S^+]}{m[^{32}SH^+]}$	0.999 744 164 350 (12)	-1 950 (5 100)	425

Table 7.2: Mass differences obtained from the preliminary measured mass ratios given in Table 7.1. These are NOT our final values since they include only an estimate of the polarization shift correction. Please refer to our future publications for the final numbers.

Mass difference	Measured value (u)	Relative accuracy
$M[^{14}\mathrm{N}]$-$M[^{13}\mathrm{C}]$-$M[\mathrm{H}]$	0.008 105 862 88 (14)	1.7×10^{-8}
$M[^{28}\mathrm{Si}]$+$M[\mathrm{H}]$-$M[^{29}\mathrm{Si}]$	0.008 256 901 99 (24)	2.9×10^{-8}
$M[^{32}\mathrm{S}]$+$M[\mathrm{H}]$-$M[^{33}\mathrm{S}]$	0.008 437 296 58 (40)	4.7×10^{-8}

three normal modes of motion of each ion, including the two strongly coupled magnetron modes. The other big challenge was to quantify and minimize the systematic shifts of the ion frequencies due to the Coulomb interaction between the ions and the trapping field imperfections. The effect of ion-ion interactions on the measured ratio was kept below 10^{-11} by separating the ions about 800 µm from each other. We then had to characterize our trapping fields very well, and optimize the one source of anharmonicity we have experimental control of to cancel the effect of all other sources of frequency shifts. We empirically demonstrated (in several independent ways) our understanding of the effects of trap imperfections on the measured ratio. We have also established our understanding of the effect of a systematic mismatch between the cyclotron orbit size (ion-ion interaction) at the 20 % level in a regime where they were at least 10 times larger than they were when we took the measurements.

The uncertainties on the measured cyclotron frequency ratios have approximately equal contributions from statistics, ion-ion interactions, and trap imperfections ($\sim 4 \times 10^{-12}$). However, we need to apply a correction to the measured ratios due to the polarization force shift of the cyclotron frequencies of some molecules we have used. At the time of the submission of this thesis, we have not completed the final calculations for these corrections, but we estimate this correction to be about 0.7 and 5×10^{-11} for the sulfur and silicon ratios respectively. These estimates have been included in the numbers given in Tables 7.1 and 7.2. Since we take the uncertainty in this correction to be 20 %, the reported final uncertainty for $\mathrm{H}^{32}\mathrm{S}^{+}/^{33}\mathrm{S}^{+}$ is dominated by the uncertainty on that correction. The correction of the $^{13}\mathrm{C}_2\mathrm{H}_2{}^{+}/^{14}\mathrm{N}_2{}^{+}$ ratio is a lot less understood at this time so no correction was applied, and the uncertainty was multiplied by $\sqrt{2}$.

Still our reported values are clearly the most accurate mass measurements in the world to date. We have been very conservative in our estimate of errors and are confident in the reported values. The $^{13}\mathrm{C}_2\mathrm{H}_2{}^{+}/^{14}\mathrm{N}_2{}^{+}$ mass ratio measurement was performed for a demonstration of the technique, with no specific applications in mind. The other two ratios can be combined with precise γ-ray measurements performed by a group from NIST at the Institut Laue-Langevin to perform a direct test of the famous relation $E = mc^2$. It will also

allows us to obtain a new limit on possible deviations of the limiting velocity of massive particles from the speed of propagation of an electromagnetic wave in vacuum. The γ-ray measurements have been performed, but the final results not available yet [28]. The relative uncertainty on the measured wavelengths are expected to be 2×10^{-7} so that our limit is expected to look like:

$$1 - \frac{c_{\rm m}}{c_{\rm em}} < 2 \times 10^{-7} \ ^{*}. \tag{7.1}$$

This tests one of the basic assumptions of the theory of special relativity. Even though this limit is not nearly as stringent as the one obtained from kinematical tests of special relativity (e. g., Michelson-Morley, Kennedy-Thorndike, and Hughes-Drever experiments), it is unique in that it does not rely on the assumption of a preferred frame of reference. Also, unlike most of the very precise tests of SR, it is sensitive to the scalar contribution of any Lorentz-invariance violating coupling, and not the tensor contribution. The Mössbauer-rotor and the Eötvös experiments also constrain the scalar inertial anomaly, but the later relies on an extra assumption: that there is no fortuitous cancellation between a coupling violating local position invariance, with one violating Lorentz invariance.

Alternately, if one assumes that $E = mc^2$ is correct, our mass ratio and the γ-ray wavelengths measurements will lead to a new value of the fine structure constant with a relative precision of 2×10^{-7}. This is 50 times less accurate than the current best value of alpha from the $g - 2$ of the electron, but it improves the value of the "mechanical fine structure constant" by a factor of 5. Finally, because the mass of ^{29}Si was not known as precisely as the mass of ^{28}Si, our measured mass ratio involving these isotopes has reduced the uncertainty on the mass of ^{29}Si by an order of magnitude.

7.1 Future Directions

Unfortunately, we only had a few months at the end of our graduate careers to measure mass ratios and we left a lot of interesting measurements behind. With just a few more ratios, we could have built a short MIT mass table with ^{13}C, ^{14}N, ^{15}N, ^{16}O, ^{32}S, ^{33}S, and ^{34}S at or below 10^{-11}. By comparing $CD_2{}^+$ with $CH_4{}^+$, we also could have obtained the D/H mass ratio to about 3×10^{-11}. But the next ratio on our list was $^{13}CH^+$ vs N^+ which measures the same mass difference as our $^{13}C_2H_2{}^+/{}^{14}N_2{}^+$ ratio but at half the m/q. That would provide a nice independent check on systematic errors. It turns out not to be too difficult to find pairs with mass differences in the range $10^{-4} < \Delta m/m < 10^{-3}$ where the two-ion technique works well, but the correction required when using polarizable molecules will probably be a concern below 10^{-11}. We don't see this as a fundamental limitation of our technique however; more precise calculations of the dipole moments of ions and their molecular structure should be available in the future.

*preliminary estimate

Scientifically, the most interesting measurement to perform now would be to compare the masses of ^{3}He and ^{3}H to help place a limit on the mass of the electron neutrino. The very low mass would bring a new challenges for our apparatus, but the two-ion technique seems to be ideally suited for this measurement: much lower systematic effects and very small amount of radioactive tritium needed. Eventually it could also be interesting to broaden even further the use of our setup to work with highly-charged ions, or explore the potential applications in molecular spectroscopy that our discovery of the polarization force might have opened up.

So the future looks very promising for the MIT ICR experiment, or I should say the FSU ICR experiment. Indeed, the apparatus is now being moved to Florida State University where Edmund Myers will carry on our work.

Appendix A

Effect of Field Imperfections on an Ion's Frequencies

This appendix describes how to calculate the effect of the trapping field imperfections on the three normal mode frequencies of an ion in a Penning trap. The expressions for the effect of C_4, C_6, and B_2 have been given in previous ICR theses (and in [2]) but they are not always consistent with each other. The fact is that in the past nobody in this lab ever worried about the effect of any term beyond C_4 and B_2 quantitatively and there has never been a need for getting the right expression within a factor of two (and the correct sign). However that changed when we obtained an absolute amplitude calibration for the motion of an ion in our trap with an uncertainty of a few percent (by measuring relativistic frequency shifts – see Sect. 2.4). Also the new computer control system opened the possibility of taking a lot more data, a lot more systematically, and therefore we could measure C_6 in our trap with unprecedented precision ($\sim$10 %) (see Sect. 2.5). Finally, getting the correct expressions for these frequency shifts has been absolutely crucial to controlling the systematic errors in our two-ion technique. Since we now make precise frequency measurements with the ions away from the center of the trap, the effects of field imperfections are much more important. We will begin by describing the effect of electric field anharmonicities and then we will tackle magnetic field inhomogeneities.

A.1 Electric Field Anharmonicities

Following the convention of [2] (and all ICR theses), we expand the electric potential near the center of our trap in terms of Legendre polynomials:

$$\Phi(\vec{r}) = \frac{V_\mathrm{r}}{2} \sum_{n=2}^{\mathrm{even}} C_\mathrm{n} \left(\frac{r}{d}\right)^n P_\mathrm{n}(\cos\theta) \;, \tag{A.1}$$

where V_r is the voltage on the ring electrode (taken to be positive) and d is the characteristic

Table A.1: Explicit expressions for $r^n P_{\rm n}(\cos\theta)$

n	$r^n P_{\rm n}(\cos\theta)$
2	$z^2 - \frac{\rho^2}{2}$
4	$z^4 - 3z^2\rho^2 + \frac{3}{8}\rho^4$
6	$z^6 - \frac{15}{2}z^4\rho^2 + \frac{45}{8}z^2\rho^4 - \frac{5}{16}\rho^6$
8	$z^8 - 14z^6\rho^2 + \frac{105}{4}z^4\rho^4 - \frac{35}{4}z^2\rho^6 + \frac{35}{1128}\rho^8$

trap size. Our trap electrodes are very carefully machined to be cylindrically symmetric and invariant under the reflection $z \to -z$ so we need only to consider the even terms. To first order, the odd terms do not induce any frequency shift and the second order contribution is heavily suppressed, as is shown in James Thompson's thesis. The first term ($n = 2$) with $C_2 = 1$ represents the axial harmonic potential which is responsible for the axial motion (Eq. (2.2)). The leading anharmonic correction is the $n = 4$ term over which we have control by adjusting the voltage on our Guard Ring electrode. Table A.1 gives the explicit expressions for $r^n P_{\rm n}(\cos\theta)$ using $r^2 = \rho^2 + z^2$ and $\cos\theta = z/r$. The equation of motion of an ion in our trap is then

$$m\vec{a} = q\vec{v} \times \vec{B} - q\nabla\Phi \tag{A.2}$$

$$\Rightarrow \quad \ddot{\vec{r}} = \omega_{\rm c}\,\dot{\vec{\rho}} \times \hat{z} - \frac{\omega_{\rm z}^2 d^2}{2}\nabla\left(\sum C_{\rm n}\left(\frac{r}{d}\right)^n P_{\rm n}(\cos\theta)\right)\,, \tag{A.3}$$

where we have used $\vec{B} = B_0\hat{z}$, $\omega_{\rm c} = qB/m$, and $\omega_{\rm z}^2 = (qV_{\rm r})/(md^2)$. To calculate the shift of the axial frequency, we write the $\hat{z}$ component of (A.3) as

$$\ddot{z} = -\frac{\omega_{\rm z}^2 d^2}{2}\frac{\partial}{\partial z}\left(\sum C_{\rm n}\left(\frac{r}{d}\right)^n P_{\rm n}(\cos\theta)\right) \equiv -\omega_{\rm z}^2(1 + 2\sum\alpha_n)z\,, \tag{A.4}$$

so that the relative shift of the axial frequency due to the term of order n is given by

$$\left.\frac{\Delta\omega_{\rm z}}{\omega_{\rm z}}\right|_n = \alpha_n = \frac{d^2}{4z_0}\frac{\partial}{\partial z}\left(C_{\rm n}\left(\frac{r}{d}\right)^n P_{\rm n}(\cos\theta)\right) = \frac{C_{\rm n}}{z_0 d^{n-2}}\frac{\partial}{\partial z}\left(r^n P_{\rm n}(\cos\theta)\right)\Big|_{\text{at }\omega_{\rm z}}\,. \tag{A.5}$$

To evaluate the above expression, we substitute $r^n P_{\rm n}(\cos\theta)$ from Table A.1 and, after taking the derivative, we substitute $z = z_0\cos(\omega_{\rm z}t)$. The factors z^n need to be expanded in a Fourier series and only the term proportional to $\cos(\omega_{\rm z}t)$ is kept. Finally, one must calculate ρ^n by expanding $((\vec{\rho}_{\rm c} + \vec{\rho}_{\rm m})\cdot(\vec{\rho}_{\rm c} + \vec{\rho}_{\rm m}))^{n/2}$ and extracting the dc component, i. e., the terms with no frequency dependence. (Use $\vec{\rho}_{\rm c} = \rho_{\rm c}\,\Re\left\{e^{i\omega_{\rm ct}t}\right\}$ and a similar expression for $\vec{\rho}_{\rm m}$.) The algebra becomes quickly overwhelming for $n > 6$ and so Mathematica was used to

generate all the expressions below.

To calculate the frequency shifts of the radial modes, we write the radial component of the equation of motion (A.3) as

$$\ddot{\vec{\rho}} = \omega_{\rm c}\,\dot{\vec{\rho}} \times \hat{z} - \frac{\omega_{\rm z}^2 d^2}{2}\frac{\partial}{\partial\rho}\left(\sum C_{\rm n}\left(\frac{r}{d}\right)^n P_{\rm n}(\cos\theta)\right)\,\hat{\rho} \tag{A.6}$$

$$\equiv \omega_{\rm c}\,\dot{\vec{\rho}} \times \hat{z} - \frac{\omega_{\rm z}^2}{2}(1+\beta)\,\vec{\rho}\;. \tag{A.7}$$

For the cyclotron motion, we substitute $\vec{\rho} = \rho_{\rm c}\,\Re\left\{(\hat{x}+{\rm i}\hat{y}){\rm e}^{{\rm i}\omega_{\rm ct}t(1+\delta)}\right\}$ in (A.7) and, neglecting δ^2, we solve for the relative shift in the trap cyclotron frequency:

$$\frac{\Delta\omega_{\rm ct}}{\omega_{\rm ct}} = \delta = \frac{\omega_{\rm z}^2\beta_{\rm c}/2}{\omega_{\rm ct}(2\omega_{\rm ct}-\omega_{\rm c})} \approx \frac{\omega_{\rm m}\beta_{\rm c}}{\omega_{\rm c}}\;. \tag{A.8}$$

The last expression is an approximation to simplify the results below, which introduces an error of order $\omega_{\rm m}/\omega_{\rm c}$. From (A.6) and (A.7) we get an expression for $\beta_{\rm c}$ that we can then use to write the relative shift in the trap cyclotron frequency due to $C_{\rm n}$:

$$\left.\frac{\Delta\omega_{\rm ct}}{\omega_{\rm ct}}\right|_n = \frac{\omega_{\rm m}}{\omega_{\rm c}}\frac{d^2}{\rho_{\rm c}}\frac{\partial}{\partial\rho}\left(C_{\rm n}\left(\frac{r}{d}\right)^n P_{\rm n}(\cos\theta)\right) = \frac{\omega_{\rm m}}{\omega_{\rm c}}\frac{C_{\rm n}}{\rho_{\rm c}d^{n-2}}\frac{\partial}{\partial\rho}\left(r^n P_{\rm n}(\cos\theta)\right)\;. \tag{A.9}$$

Using a very similar procedure we find for the magnetron frequency

$$\frac{\Delta\omega_{\rm m}}{\omega_{\rm m}} = \frac{\omega_{\rm z}^2\beta_{\rm m}/2}{\omega_{\rm m}(2\omega_{\rm m}-\omega_{\rm c})} \approx -\beta_{\rm m}\;, \tag{A.10}$$

from which we obtain the relative shift in the magnetron frequency due to $C_{\rm n}$:

$$\left.\frac{\Delta\omega_{\rm m}}{\omega_{\rm m}}\right|_n = -\frac{d^2}{\rho_{\rm m}}\frac{\partial}{\partial\rho}\left(C_{\rm n}\left(\frac{r}{d}\right)^n P_{\rm n}(\cos\theta)\right) = \frac{-C_{\rm n}}{\rho_{\rm m}d^{n-2}}\frac{\partial}{\partial\rho}\left(r^n P_{\rm n}(\cos\theta)\right)\;. \tag{A.11}$$

Once again, to evaluate (A.9) and (A.11), we need to be a little careful. We substitute $r^n P_{\rm n}(\cos\theta)$ from Table A.1 and then $z = z_0\cos(\omega_{\rm z}t)$. Here however to calculate z^n, we compute the time average $\langle\cos(\omega_{\rm z}t)^n\rangle$. Finally, we have to explicitly calculate ρ^{n+1} by expanding $((\vec{\rho}_{\rm c}+\vec{\rho}_{\rm m})\cdot(\vec{\rho}_{\rm c}+\vec{\rho}_{\rm m}))^{n/2}\,(\vec{\rho}_{\rm c}+\vec{\rho}_{\rm m})$ and picking the Fourier component at $\omega_{\rm ct}$ in the case of the cyclotron frequency (A.13), and at $\omega_{\rm m}$ in the case of the magnetron frequency (A.13). The resulting expression from (A.5), (A.9), and (A.11) calculated up to C_8 are given below. These expression have been checked and rechecked, and calculated independently by James Thompson (using a slightly different approach) so we are very confident that they are correct.

$$\begin{aligned}\frac{\Delta\omega_{\rm z}}{\omega_{\rm z}} &= \frac{3}{4}\frac{C_4}{d^2}\left(z^2-2\rho_{\rm c}^2-2\rho_{\rm m}^2\right)\\ &+\frac{15}{16}\frac{C_6}{d^4}\left(z^4-6\,z^2\rho_{\rm c}^2+3\,\rho_{\rm c}^4-6\,z^2\rho_{\rm m}^2+12\,\rho_{\rm c}^2\rho_{\rm m}^2+3\,\rho_{\rm m}^4\right)\\ &+\frac{35}{32}\frac{C_8}{d^6}\left(z^6-12\,z^4\rho_{\rm c}^2+18\,z^2\rho_{\rm c}^4-4\,\rho_{\rm c}^6-12\,z^4\rho_{\rm m}^2+72\,z^2\rho_{\rm c}^2\rho_{\rm m}^2\right.\\ &\qquad\left.-36\,\rho_{\rm c}^4\rho_{\rm m}^2+18\,z^2\rho_{\rm m}^4-36\,\rho_{\rm c}^2\rho_{\rm m}^4-4\,\rho_{\rm m}^6\right)\end{aligned}\tag{A.12}$$

$$\begin{aligned}\frac{\Delta\omega_{\rm ct}}{\omega_{\rm ct}} &= \frac{-3}{2}\frac{\omega_{\rm m}}{\omega_{\rm c}}\frac{C_4}{d^2}\left(2z^2-\rho_{\rm c}^2-2\,\rho_{\rm m}^2\right)\\ &-\frac{15}{8}\frac{\omega_{\rm m}}{\omega_{\rm c}}\frac{C_6}{d^4}\left(3\,z^4-6\,z^2\rho_{\rm c}^2+\rho_{\rm c}^4-12\,z^2\rho_{\rm m}^2+6\,\rho_{\rm c}^2\rho_{\rm m}^2+3\,\rho_{\rm m}^4\right)\\ &-\frac{35}{16}\frac{\omega_{\rm m}}{\omega_{\rm c}}\frac{C_8}{d^6}\left(4\,z^6-18\,z^4\rho_{\rm c}^2+12\,z^2\rho_{\rm c}^4-\rho_{\rm c}^6-36\,z^4\rho_{\rm m}^2+72\,z^2\rho_{\rm c}^2\rho_{\rm m}^2\right.\\ &\qquad\left.-12\,\rho_{\rm c}^4\rho_{\rm m}^2+36\,z^2\rho_{\rm m}^4-18\,\rho_{\rm c}^2\rho_{\rm m}^4-4\,\rho_{\rm m}^6\right)\end{aligned}\tag{A.13}$$

$$\begin{aligned}\frac{\Delta\omega_{\rm m}}{\omega_{\rm m}} &= \frac{3}{2}\frac{C_4}{d^2}\left(2\,z^2-2\,\rho_{\rm c}^2-\rho_{\rm m}^2\right)\\ &+\frac{15}{8}\frac{C_6}{d^4}\left(3\,z^4-12\,z^2\rho_{\rm c}^2+3\,\rho_{\rm c}^4-6\,z^2\rho_{\rm m}^2+6\,\rho_{\rm c}^2\rho_{\rm m}^2+\rho_{\rm m}^4\right)\\ &+\frac{35}{16}\frac{C_8}{d^6}\left(4\,z^6-36\,z^4\rho_{\rm c}^2+36\,z^2\rho_{\rm c}^4-4\,\rho_{\rm c}^6-18\,z^4\rho_{\rm m}^2+72\,z^2\rho_{\rm c}^2\rho_{\rm m}^2\right.\\ &\qquad\left.-18\,\rho_{\rm c}^4\rho_{\rm m}^2+12\,z^2\rho_{\rm m}^4-12\,\rho_{\rm c}^2\rho_{\rm m}^4-\rho_{\rm m}^6\right)\end{aligned}\tag{A.14}$$

If one were concerned about precision to better than $\omega_{\rm m}/\omega_{\rm c}$, one should use the full expressions in (A.8) and (A.10), which corresponds to multiplying the expressions above for $\Delta\omega_{\rm ct}/\omega_{\rm ct}$ and $\Delta\omega_{\rm m}/\omega_{\rm m}$ by

$$\frac{\omega_{\rm c}}{\omega_{\rm m}}\frac{\omega_{\rm z}^2/2}{\omega_{\rm ct}(2\omega_{\rm ct}-\omega_{\rm c})}\quad\text{and}\quad\frac{-\omega_{\rm z}^2/2}{\omega_{\rm m}(2\omega_{\rm m}-\omega_{\rm c})}\qquad\text{respectively.}\tag{A.15}$$

A.2 Magnetic Field Inhomogeneities

We now turn to the effect of magnetic field inhomogeneities on the three normal mode frequencies of an ion in our Penning trap. The calculation of these expressions is very similar to what was done in Sect. A.1 for the electric field anharmonicities. We follow again the convention of [2] and express the magnetic field as the gradient of a scalar potential $\vec{B}=-\nabla\Psi$ with

$$\Psi(\vec{r})=-\sum_{n=0}^{\infty}\frac{B_{\rm n}}{n+1}\,r^{n+1}\,P_{\rm n+1}(\cos\theta)\equiv\sum_{n=0}^{\infty}\Psi_{\rm n}\;.\tag{A.16}$$

The first few terms of the expansion are

$$\vec{B}(\vec{r}) = B_0\hat{z} + B_2\left(\frac{1}{2}\left(2\,z^2-\rho^2\right)\hat{z} - (z\,\rho)\,\hat{\rho}\right) + B_4\left(\frac{1}{8}\left(8\,z^4-24\,z^2\,\rho^2+3\,\rho^4\right)\hat{z} - \frac{1}{2}\left(4\,z^3\,\rho-3\,z\,\rho^3\right)\hat{\rho}\right)+\dots\,. \tag{A.17}$$

Again, from symmetry arguments, we need only to consider the even terms[†]. From each $n \neq 0$ term, we get an extra force in the equation of motion (A.2) of the form

$$\vec{F_{\rm n}} = -\frac{m\omega_{\rm c}}{B_0}\vec{v}\times\nabla\Psi_{\rm n}\,. \tag{A.18}$$

To calculate the effect of that extra force on the cyclotron frequency, we suppose again that $\vec{\rho} = \rho_{\rm c}\,\Re\left\{(\hat{x}+{\rm i}\hat{y}){\rm e}^{{\rm i}\omega_{\rm ct}t(1+\delta)}\right\}$ and we find

$$\left.\frac{\Delta\omega_{\rm ct}}{\omega_{\rm ct}}\right|_n = \frac{1}{\omega_{\rm ct}(\omega_{\rm c}-2\omega_{\rm ct})}\,\frac{F_{\rm n}^{\rm cyc}}{\rho_{\rm c}} \approx -\frac{1}{\omega_{\rm c}^2}\frac{F_{\rm n}^{\rm cyc}}{\rho_{\rm c}}\,, \tag{A.19}$$

where $F_{\rm n}^{\rm cyc}$ is the Fourier component of $\vec{F_{\rm n}}$ at $\omega_{\rm ct}$ along the $\hat{\rho}$ direction. Similarly, the relative frequency shift of the magnetron and axial frequencies are given by

$$\left.\frac{\Delta\omega_{\rm m}}{\omega_{\rm m}}\right|_n = \frac{1}{\omega_{\rm m}(\omega_{\rm c}-2\omega_{\rm m})}\,\frac{F_{\rm n}^{\rm mag}}{\rho_{\rm m}} \approx \frac{2}{\omega_{\rm z}^2}\frac{F_{\rm n}^{\rm mag}}{\rho_{\rm m}} \tag{A.20}$$

$$\left.\frac{\Delta\omega_{\rm z}}{\omega_{\rm z}}\right|_n = -\frac{1}{2\omega_{\rm z}^2}\,\frac{F_{\rm n}^{\rm z}}{z}\,, \tag{A.21}$$

where $F_{\rm n}^{\rm mag}$ is the Fourier component of $\vec{F_{\rm n}}$ at $\omega_{\rm m}$ along the $\hat{\rho}$ direction and $F_{\rm n}^{\rm z}$ is the Fourier component of $\vec{F_{\rm n}}$ at $\omega_{\rm z}$ along the $\hat{z}$ direction. When the dust settles, we find the following expressions for the various frequency shifts due to magnetic field imperfections:

[†]The effect of B_1 and B_3 are discussed in Weisskoff's thesis [5] p.33

$$\frac{\Delta\omega_z}{\omega_z} = \frac{1}{4}\frac{B_2}{B_0}\left({\rho_m}^2 + \frac{\omega_c}{\omega_m}{\rho_c}^2\right) + \frac{3}{8}\frac{B_4}{B_0}\left(z^2{\rho_m}^2 - {\rho_m}^4 + \frac{\omega_c}{\omega_m}z^2{\rho_c}^2 - \frac{\omega_c}{\omega_m}{\rho_c}^4 - \frac{\omega_c}{\omega_m}2{\rho_c}^2{\rho_m}^2\right) \tag{A.22}$$

$$\frac{\Delta\omega_{ct}}{\omega_{ct}} = \frac{1}{2}\frac{B_2}{B_0}\left(z^2 - {\rho_c}^2 - {\rho_m}^2\right) + \frac{3}{8}\frac{B_4}{B_0}\left(z^4 - 4z^2{\rho_c}^2 + {\rho_c}^4 - 4z^2{\rho_m}^2 + 4{\rho_c}^2{\rho_m}^2 + {\rho_m}^4\right) \tag{A.23}$$

$$\frac{\Delta\omega_m}{\omega_m} = \frac{1}{2}\frac{B_2}{B_0}\left(-z^2 + {\rho_m}^2 + \frac{\omega_c}{\omega_m}{\rho_c}^2\right) - \frac{3}{8}\frac{B_4}{B_0}\left(z^4 - 4z^2{\rho_m}^2 + {\rho_m}^4 - \frac{\omega_c}{\omega_m}4z^2{\rho_c}^2 + \frac{\omega_c}{\omega_m}2{\rho_c}^4 + \frac{\omega_c}{\omega_m}2{\rho_c}^2{\rho_m}^2\right) \tag{A.24}$$

Bibliography

[1] D. Kuchnir, B.sc. thesis, Massachusetts Intitute of Technology, 1989.

[2] L. S. Brown and G. Gabrielse, "Geonium Theory - Physics of a Single Electron or Ion in a Penning Trap," Rev. Mod. Phys. **58**, 233 (1986).

[3] R. M. Weisskoff, G. P. Lafyatis, K. R. Boyce, E. A. Cornell, R. W. Flanagan, and D. E. Pritchard, "Rf Squid Detector for Single-Ion Trapping Experiments," J. Appl. Phys. **63**, 4599 (1988).

[4] E. A. Cornell, R. M. Weisskoff, K. R. Boyce, and D. E. Pritchard, "Mode-Coupling in a Penning Trap - Pi-Pulses and a Classical Avoided Crossing," Phys. Rev. A **41**, 312 (1990).

[5] R. M. Weisskoff, Ph.D. thesis, Massachusetts Institute of Technology, 1988.

[6] E. A. Cornell, R. M. Weisskoff, K. R. Boyce, R. W. Flanagan, G. P. Lafyatis, and D. E. Pritchard, "Single-Ion Cyclotron-Resonance Measurement of $M(CO^+)/M(N_2^+)$," Phys. Rev. Lett. **63**, 1674 (1989).

[7] F. Difilippo, V. Natarajan, K. R. Boyce, and D. E. Pritchard, "Classical Amplitude Squeezing for Precision-Measurements," Phys. Rev. Lett. **68**, 2859 (1992).

[8] V. Natarajan, F. Difilippo, and D. E. Pritchard, "Classical Squeezing of an Oscillator for Subthermal Noise Operation," Phys. Rev. Lett. **74**, 2855 (1995).

[9] R. Forward, "Electronic cooling of resonant gravity gradiometers," J. Appl. Phys. **50**, 1 (1979).

[10] B. D'Urso, B. Odom, and G. Gabrielse, "Feedback cooling of a one-electron oscillator," Phys. Rev. Lett. **90**, art. no. (2003).

[11] M. Bradley, Ph.D. thesis, Massachusetts Institute of Technology, 2000.

[12] J. V. Porto, "Series solution for the image charge fields in arbitrary cylindrically symmetric Penning traps," Phys. Rev. A **64**, 023403 (2001).

[13] E. A. Cornell, K. R. Boyce, D. L. K. Fygenson, and D. E. Pritchard, "Two Ions in a Penning Trap - Implications for Precision Mass-Spectroscopy," Phys. Rev. A **45**, 3049 (1992).

[14] V. Natarajan, Ph.D. thesis, Massachusetts Institute of Technology, 1993.

[15] S. Rusinkiewicz, B.sc. thesis, Massachusetts Institute of Technology, 1995.

[16] S. Rainville, J. K. Thompson, and D. E. Pritchard, "Single-ion mass spectrometry at 100 ppt and beyond," Can. J. Phys. **80**, 1329 (2002).

[17] R. S. Van Dyck, D. L. Farnham, S. L. Zafonte, and P. B. Schwinberg, "Ultrastable superconducting magnet system for a penning trap mass spectrometer," Rev. Sci. Instrum. **70**, 1665 (1999).

[18] G. Gabrielse, A. Khabbaz, D. S. Hall, C. Heimann, H. Kalinowsky, and W. Jhe, "Precision mass spectroscopy of the antiproton and proton using simultaneously trapped particles," Phys. Rev. Lett. **82**, 3198 (1999).

[19] J. K. Thompson, Ph.D. thesis, Massachusetts Institute of Technology, 2003, in preparation.

[20] G. Audi and A. H. Wapstra, "The 1995 update to the atomic mass evaluation," Nucl. Phys. A **595**, 409 (1995).

[21] M. W. Chase, "NIST-JANAF Thermochemical Tables, Fourth Edition," J. Phys. Chem. Ref. Data **9**, 1 (1998).

[22] P. Linstrom and W. Mallard, eds., NIST Chemistry WebBook, NIST Standard Reference Database Number 69, March 2003, National Institute of Standards and Technology, Gaithersburg MD, 20899 (http://webbook.nist.gov).

[23] P. Bevington and D. Robinson, *Data Reduction and Error Analysis for the Physical Sciences*, 2nd ed. (McGraw-Hill, Boston, 1992).

[24] F. Difilippo, V. Natarajan, K. R. Boyce, and D. E. Pritchard, "Accurate Atomic Masses for Fundamental Metrology," Phys. Rev. Lett. **73**, 1481 (1994).

[25] M. P. Bradley, J. V. Porto, S. Rainville, J. K. Thompson, and D. E. Pritchard, "Penning trap measurements of the masses of ^{133}Cs, ^{87}Rb, ^{85}Rb, and ^{23}Na with uncertainties $\leq$ 0.2 ppb," Phys. Rev. Lett. **83**, 4510 (1999).

[26] S. Rainville, J. K. Thompson, and D. E. Pritchard, manuscript in preparation.

[27] G. L. Greene, M. S. Dewey, E. G. Kessler, and E. Fischbach, "Test of Special Relativity by a Determination of the Lorentz Limiting Velocity - Does E = mc^2," Phys. Rev. D **44**, R2216 (1991).

[28] M. S. Dewey, private communication.

[29] H. Robertson, Rev. Mod. Phys. **21**, 378 (1949).

[30] R. Mansouri and R. U. Sexl, "Test Theory of Special Relativity," Gen. Relativ. Gravit. **8**, 497 (1977); **8**, 515 (1977); **8**, 809 (1977).

[31] M. P. Haugan and C. M. Will, "Modern Tests of Special Relativity," Phys. Today **40**, 69 (1987).

[32] V. A. Kostelecky and M. Mewes, "Signals for Lorentz violation in electrodynamics," Phys. Rev. D **66**, 056005 (2002).

[33] M. E. Cage, R. F. Dziuba, R. E. Elmquist, B. F. Field, G. R. Jones, P. T. Olsen, W. D. Phillips, J. Q. Shields, R. L. Steiner, B. N. Taylor, and E. R. Williams, "Nbs Determination of the Fine-Structure Constant, and of the Quantized Hall Resistance and Josephson Frequency-to-Voltage Quotient in Si Units," IEEE Trans. Instrum. Meas. **38**, 284 (1989).

[34] A. Wicht, J. M. Hensley, E. Sarajlic, and S. Chu, "A preliminary measurement of the fine structure constant based on atom interferometry," Phys. Scr. **T102**, 82 (2002).

[35] T. Udem, J. Reichert, R. Holzwarth, and T. W. Hansch, "Absolute optical frequency measurement of the cesium D-1 line with a mode-locked laser," Phys. Rev. Lett. **82**, 3568 (1999).

[36] T. Beier, H. Haffner, N. Hermanspahn, S. Karshenboim, H. J. Kluge, W. Quint, S. Stahl, J. Verdu, and G. Werth, "New Determination of the Electron's Mass," Phys. Rev. Lett. **88**, 011603 (2002).

[37] E. G. Kessler, M. S. Dewey, R. D. Deslattes, A. Henins, H. G. Borner, M. Jentschel, C. Doll, and H. Lehmann, "The deuteron binding energy and the neutron mass," Phys. Lett. A **255**, 221 (1999).

[38] S. Coleman and S. L. Glashow, "High-energy tests of Lorentz invariance," Phys. Rev. D **5911**, art. no. (1999).

[39] A. Brillet and J. L. Hall, "Improved Laser Test of the Isotropy of Space," Phys. Rev. Lett. **42**, 549 (1979).

[40] C. Braxmaier, H. Muller, O. Pradl, J. Mlynek, A. Peters, and S. Schiller, "Tests of relativity using a cryogenic optical resonator," Phys. Rev. Lett. **88**, 010401 (2002).

[41] S. K. Lamoreaux, J. P. Jacobs, B. R. Heckel, F. J. Raab, and E. N. Fortson, "New Limits on Spatial Anisotropy from Optically Pumped Hg-201 and Hg-199," Phys. Rev. Lett. **57**, 3125 (1986).

[42] C. J. Berglund, L. R. Hunter, D. Krause, E. O. Prigge, M. S. Ronfeldt, and S. K. Lamoreaux, "New Limits on Local Lorentz Invariance from Hg and Cs Magnetometers," Phys. Rev. Lett. **75**, 1879 (1995).

[43] G. Isaak, Phys. Bull. **21**, 255 (1970).

[44] V. Braginsky and V. Panov, Sov. Phys. JETP **34**, 464 (1971).

[45] S. Coleman and S. L. Glashow, "Cosmic ray and neutrino tests of special relativity," Phys. Lett. B **405**, 249 (1997).

[46] P. Mohr and B. Taylor, "CODATA recommended values of the fundamental physical constants: 1998," Rev. Mod. Phys. **72**, 351 (2000).

[47] A. Paul, S. Rottger, A. Zimbal, and U. Keyser, "Prompt (n,gamma) mass measurements for the AVOGADRO project," Hyperfine Interact. **132**, 189 (2001).